

**LINEAR AND NON LINEAR VIBRATION RESPONSE OF THIN
ROTATING DISKS**

by

Ramin MohammadHasani Khorasany

B.Sc., Sharif University of Technology, Iran, 2002

M.Sc., Sharif University of Technology, Iran, 2004

A THESIS SUBMITTED IN PARTIAL FULFILMENT OF
THE REQUIREMENTS FOR THE DEGREE OF
DOCTOR OF PHILOSOPHY

in

THE FACULTY OF GRADUATE STUDIES

(Mechanical Engineering)

THE UNIVERSITY OF BRITISH COLUMBIA

(Vancouver)

September 2010

© Ramin MohammadHasani Khorasany

Abstract

Spinning disks have substantial applications in today's industries (e.g., saw mill industries). Developing a greater understanding the dynamics of spinning disks is a central topic for this thesis. Specifically, this thesis investigates the linear and nonlinear vibrations of spinning disks.

In some of the spinning disk applications, the disks may experience a rigid body translational degree of freedom. Having this degree of freedom can change the stability characteristics of spinning disks. Using analytical techniques and a two-mode approximation, the stability characteristics of elastically guided spinning disks having a rigid body translational degree of freedom are thus studied.

The effect of axisymmetric non-flatness on the frequency behaviour of spinning disks is also studied. The equations of motion are based on Von Karman plate theory. Assuming that the shape of initial runout is in the form of mode shapes with zero nodal diameters, the equations of motion are then discretized. Neglecting higher order terms, the equations are linearized and the effects of different levels of initial runout on the dynamics of spinning disks are thus studied.

Using experimental measurements, the effects of large deformations on the frequency behaviour and amplitude of response for the spinning disks are investigated. Disks with different thicknesses are used in this study. The disks were under the application of a space fixed external force which can produce different levels of nonlinearity. By measuring the disk displacement and conducting FFT analyses, the frequencies were measured for different levels of initial deflection.

In order to see how the geometrical nonlinear terms affect the frequency behaviour of spinning disks, the nonlinear governing equations are discretized and then solved to find the equilibrium solutions. By assuming a small perturbation around the equilibrium solution, the nonlinear equations of motion are linearized. Using the linearized form of the equations of motion, the effect of large deformations of the frequency characteristics of spinning disks is analyzed. The analytical results are then compared with the experimentally obtained results.

Table of Contents

Abstract.....	ii
Table of Contents	iii
List of Tables	vi
List of Figures.....	vii
List of Symbols	x
Acknowledgments	xiii
Dedication	xiv
Statement of Co-Authorship	xv
Chapter 1- Introduction	1
1.1. Background.....	1
1.2. Linear Theory of Vibration.....	2
1.2.1. Clamped Disks	3
1.2.2. Elastically Constrained Spinning Disks	7
1.2.3. Effects of Rigid Body Translation on the Dynamics of Spinning Disks	9
1.3. Nonlinear Theory of Vibration	10
1.3.1. Nonlinear Analysis and Basic Assumptions	10
1.3.2. Disk Initial Runout.....	12
1.3.3. Experimental Investigations on the Effects of Large Deformations	13
1.3.4. Numerical Investigations on the Effects of Large Deformations.....	14
1.4. Objective and Scope.....	16
1.5. References.....	19
Chapter 2- On the Effects of Rigid Body Translational Mode	25
2.1. Introduction.....	25
2.2. Linear Equations of Motion	26
2.3. Interaction Between a Backward Traveling Wave and Its Complex Conjugate with Rigid Body Translational Mode.....	28
2.4. Interaction Between a Forward or Backward or Reflected Traveling Wave with Rigid Body Translational Mode.....	32

2.5.	Conclusions.....	39
2.6.	References.....	40
Chapter 3- On the Effects of Initial Runout.....		42
3.1.	Introduction.....	42
3.2.	Formulation.....	43
3.3.	Solution Method.....	47
3.4.	Numerical Simulations.....	51
3.5.	Conclusions.....	62
3.6.	References.....	63
Chapter 4- Experimental Investigations on the Nonlinear Frequency Behavior		65
4.1.	Introduction.....	65
4.2.	Experimental Setup.....	66
4.3.	Experimental Results	68
4.3.1.	Disk #1 – 0.050” Thickness	68
4.3.2.	Disk #2 – 0.040” Thickness	75
4.3.3.	Disk #3 – 0.030” Thickness	78
4.4.	Conclusions.....	81
4.5.	References.....	83
Chapter 5- Analytical Investigations on the Nonlinear Frequency Behavior		85
5.1.	Introduction.....	85
5.2.	Formulation.....	87
5.3.	Linearization	91
5.4.	Numerical Analysis.....	95
5.4.1.	Stationary Disk.....	96
5.4.2.	Spinning Disk.....	98
5.5.	Conclusions.....	105
5.6.	References.....	107

Chapter 6- Summary and Conclusions	109
6.1. Summary and Conclusions.....	109
6.2. Recommendations for Future Work.....	113
6.3. References.....	114
Appendix A.	115

List of Tables

Table 3. 1. Ratio of disk deflection to its thickness at the outer rim when $W_{i0}^R = 100$	51
Table 3. 2. Comparison between the results of the proposed analysis and those predicted by ANSYS.....	52
Table 3. 3. Level of runout by which the frequencies of the oscillations of the (0,0) mode exceed those of the (0,2) and (0,3) modes	58
Table 3. 4. a_{mm}^ϕ for different modes and different forms of initial runout when $W_{i0}^R = 100$	59
Table 4. 1. Disk Dimensions and Flatness Indicators (inches)	67
Table 4. 2. Estimated Frequencies at Zero Speed (Hz); (0,2) Mode.....	72

List of Figures

Figure 1.1. Guided saw blade.....	1
Figure 1.2. Natural frequencies versus rotation speed	4
Figure 1.3. The (a) natural frequencies and (b) real part of the eigenvalues of an elastically constrained disk	8
Figure 1.4. The (a) natural frequencies and (b) real part of the eigenvalues of an elastically constrained disk having rigid body translational degree of freedom	9
Figure 1.5. Linear and nonlinear response of the blade at 1850 RPM for w/h when (a) $F=1$ N and (b) $F=10$ N	12
Figure 2. 1. A guided rotating disk with rigid body degrees of freedom.....	27
Figure 2. 2. Normalized natural frequencies of the guided disk (shown with the broken lines) versus normalized speed when (a) $k = 0.057$ and (b) $k = 2.85$. The solid lines show the normalized natural frequencies of the unguided disk..	32
Figure 2. 3. A general shape for $f(\omega, k)$ using the characteristics of a backward or forward traveling wave	34
Figure 2. 4. A typical plot of $f_1(\omega, k)$ (solid line) and $f_2(\omega, k)$ for a relatively small (dotted line) and large (dashed line) value of k when the discriminant of $f_2(\omega, k)$ is positive.....	36
Figure 2. 5. A typical plot of $f_1(\omega, k)$ (solid line) and $f_2(\omega, k)$ for a relatively small (dotted line) and large (dashed line) value of k when the discriminant of $f_2(\omega, k)$ is negative.....	37
Figure 2. 6. The interaction between the (0,2) mode of the clamped disk with rigid body translational mode when (a) $k = 1$, (b) $k = 2$, (c) $k = 5$, (d) $k = 10$, (e) $k = 10^4$ and (f) $k = 10^6$	38
Figure 3. 1. Non-dimensionalized oscillation frequencies versus non-dimensionalized rotation speed when the runout is zero (solid lines) and when $W_{00}^R = 100$ (broken lines).....	53

Figure 3. 2. Non-dimensionalized oscillation frequencies versus non-dimensionalized rotation speed when the runout is zero (solid lines) and when $W_{10}^R = 100$ (broken lines).....	54
Figure 3. 3. Non-dimensionalized oscillation frequencies of the stationary disk when the non-flatness is assumed to be in the shape of the (0,0) mode	55
Figure 3. 4. Non-dimensionalized oscillation frequencies of the stationary disk when the non-flatness is assumed to be in the shape of the (1,0) mode	56
Figure 3. 5. Non-dimensionalized oscillation frequencies of the stationary disk when the non-flatness is assumed to be in the shape of the (2,0) mode	56
Figure 3. 6. Non-dimensionalized oscillation frequencies of the stationary disk when the non-flatness is assumed to be in the shape of the (3,0) mode	57
Figure 3. 7. Change in the critical speed of the (0,2) Mode, assuming different shapes of runout (the legends show the shape of initial non-flatness).....	61
Figure 3. 8. Change in the critical speed of the (0,3) Mode, assuming different shapes of runout (the legends show the shape of initial non-flatness).....	61
Figure 3. 9. Change in the critical speed of the (0,4) Mode, assuming different shapes of runout	62
Figure 4. 1. The Experimental Setup	68
Figure 4. 2. Frequency Response of Disk #1 for Different Force Levels	73
Figure 4. 3. Disk 1- DC Displacement versus Speed (probe 3)	74
Figure 4. 4. Disk 1- Waterfall plot with white noise magnetic excitation ($w_0/h = 0.0$) in the run-up case	74
Figure 4. 5. Disk 1- DC amplitude at 3600 RPM at the location of four probes (shown with stars) and the (0,3) mode curve fitting (solid lines) when $w_0/h = 0.6$	75
Figure 4. 6. Frequency Response of Disk #2 for Different Force Levels	77
Figure 4. 7. Disk 2- DC Displacement versus Speed (probe 3)	78
Figure 4. 8. DC displacement of disk #3, when $w_0/h = 0.5$ at all probes	79
Figure 4. 9. Frequency Response of Disk #3 for Different Force Levels	80
Figure 4. 10. Disk 3- DC Displacement versus Speed (probe 3)	81
Figure 5. 1. Linear natural frequencies of the disk versus rotation speed.....	95

Figure 5. 2. The nonlinear frequencies of the backward (solid lines) and forward (broken lines) traveling waves of (a) (0,2), (b) (0,3), and (c) (0,4) modes of the stationary disk 97

Figure 5. 3. (a) The particular part of the stress function, (b) the nonlinear radial stress and (c) the nonlinear hoop stress along the normalized radial direction for three different angular directions when $w_0/h = 4$ 98

Figure 5. 4. Nonlinear frequencies of the spinning 0.05 in.-thick disk when $w_0/h = 0.1$, (a) numerical results (broken and solid lines show the linear and nonlinear results, respectively), (b) experimental results (run-up case) 101

Figure 5. 5. A comparison between the numerical and experimental results (run-up case) for the dc amplitude of oscillations when $w_0/h = 0.1$ at the location of the applied external force..... 101

Figure 5. 6. Nonlinear frequencies of the spinning disk when $w_0/h = 0.6$, (a) numerical results 102

Figure 5. 7. A comparison between the numerical and experimental results (run-up case) for the dc amplitude of oscillations when $w_0/h = 0.6$ 103

Figure 5. 8. Calculated linear (broken lines) and nonlinear frequencies (solid lines) of the spinning disk when $w_0/h = 2.0$ 104

Figure 5. 9. Dc amplitude of oscillation when $w_0/h = 2.0$ 104

List of Symbols

a	Inner radius of the disc
b	Outer radius of the disc
A_D	Disk area
c_1, c_2	Coefficients in the homogenous part of the stress function
C_1, C_2, C_3 and C_4	Coefficients of the in-plane stresses terms
C_{rr}, C_r, C_θ	Coefficients of the in-plane stresses terms in normalized equation
$C_{mn}^w, S_{mn}^w, c_1^w, c_2^w$	Time dependent generalized coordinates of the disc for the transverse deflection of the disk
D	Disk bending rigidity ($Eh^3/[12(1-\nu^2)]$)
E	Young's modulus
F	Applied external point force
G_w	Gyroscopic matrix
h	Disc thickness
i	Imaginary unit ($\sqrt{-1}$)
k	Stiffness of the spring
K_w	Stiffness matrix
m	Number of nodal diameters
M	Maximum number of nodal diameter in approximation function
n	Number of nodal circles
(n,m)	A mode with n and m nodal circles and diameters, respectively
N	Maximum number of nodal circles in approximation function
N_R	The number of axisymmetric modes with which the runout of the disk can be approximated
$p(r, \theta, t)$	External pressure acting on the disk surface
(r, θ, z)	Space-fixed polar coordinate system
(r_F, θ_F)	Radial and angular position of the external point force

(r^k, θ^k)	Radial and angular position of spring
$R_{mn}^w(r), \tilde{R}_{mn}^w(r)$	Mode shape in the radial direction for the disk deflection
R_{mn}^ϕ	Eigenfunctions of the stress function in the radial direction
S_{mn}^{ew}, C_{mn}^{ew}	Equilibrium solutions for the amplitude of the sin and cos waves of the transverse displacement
S_{mn}^ϕ, C_{mn}^ϕ	Amplitudes of the sin and cos waves in the stress function
$S_{mn}^{e\phi}, C_{mn}^{e\phi}$	Equilibrium solutions for the amplitude of the sin and cos waves of the stress function
S	Disk domain
t	Time
u	The net deflection of a non-flat disk
w	Displacement in z direction
w ₀	The maximum deflection of the stationary disk at the outer rim caused by the application of air jet
\tilde{w}	The disk deflection at around its critical speed
w ₀ ^R	The initial deformation (non-flatness) of the disk
W _{mn}	Eigenfunctions for the transverse displacement
W _{i0} ^R	The amplitude of runout corresponding to (i,0) mode
Z ₀	Rigid body displacement in the z direction
$\alpha_1, \alpha_2, \alpha_3, \alpha_4$	Constants in the characteristics equation
$\delta(\cdot)$	Dirac delta function
δ_{ij}	Kronecker delta
$\delta()$	Dirac delta
Δ	Discriminant of the characteristics equation
$\phi(r, \theta, t)$	Stress function
ϕ^h	The homogenous part of the stress function
ϕ^p	The particular part of the stress function

ϕ_{mn}	Eigenfunctions for the stress function
η	The ratio of inner radius to outer radius of the disk (a/b)
λ, λ_{mn}^w	Eigenvalues for the transverse displacement
λ_{mn}^ϕ	Eigenvalues for the stress function
ν	Poisson's ratio
$\Theta_{mn}(\theta)$	Mode shape in the θ direction
ρ	Density
σ_r, σ_θ	Radial and hoop stress due to rotation
ω	Imaginary part of the eigenvalue
$\tilde{\omega}_{mn}$	The natural frequency of the disk in the inertial frame
Ω	Rotation speed

Acknowledgments

First and foremost I would like to pay special tribute to my supervisor, Prof Stanley Hutton for his technical guidance and support during research. I also would like to thank Prof Mohamed Gadala who has provided me with lots of helps during my PhD studies.

I am also grateful to my PhD committee members: Prof Farokh Sassani, Prof Carlos Ventura and Dr Bruce Lehmann for their helpful inputs and valuable discussions.

The supports from the University of British Columbia Graduate Fellowships are highly appreciated.

I also would to thank all of my friends all around the world who have helped and motivated me during my PhD studies.

Last, but not least, I would like to thank my parents, brothers and sisters for their invaluable supports. My special thanks go to my lovely wife, Sara, for her unlimited patience, love and encouragements that have made this work possible.

Dedication

To:

Endless supports and encouragements of my parents, brothers and sisters

To:

My wife, Sara

Statement of Co-Authorship

Ramin MohammadHasani Khorasany is the primary author of papers presented in this work. For all these works Mr Khorasany identified and proposed the research topic, performed the literature survey and research, analyzed the data, performed the simulations and prepared the manuscript under the supervision and direction of Prof Stanley Hutton.

All this work has been done completely during Mr Khorasany's PhD program. None of the papers presented in this work have received credit or presented in any other thesis work.

Chapter 1- Introduction

1.1. Background

Spinning thin disks can be found in many engineering applications. Common industrial applications include circular saws (Figure 1.1), turbine rotors, brake systems, fans, precision gyroscopes, and computer storage devices. Spinning disks may experience severe vibration which could lead to fatigue failure of the system.

A disk is usually defined as a thin, flat, circular plate. Hence, the analysis of spinning disks involves the theory of thin plates. The first step in investigating the vibrations of the spinning disk is to set up a mathematical model of the system. The aim is to set up a model that captures the essential physics of the problem.

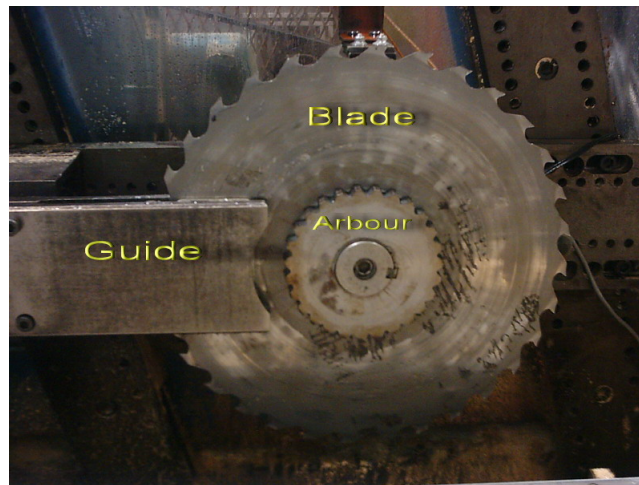


Figure 1.1. Guided saw blade

One of the most common applications of the rotating disks is in the saw mill industry. For several years, the blade that was used in this industry had a fixed inner boundary condition and free outer boundary condition. These types of saws are called “clamped” saws. Later on, less and less guided clamped saws were used in the saw mill industry. In the splined guided saw blades, the guide is composed of two flat pads in a space fixed point, and the blade rotates between the pads. The clearance between the pads and the blade is in the order of several thousandths of an inch. A combination of water and air is used to keep the blade cool and also to lubricate the blade. The splined saw blades have a rigid body translational degree of freedom. This degree of freedom can

substantially change the stability characteristics of spinning disks. Therefore, there is the need to study the effect of the rigid body translational degree of freedom on the dynamic behaviour of saw blades.

Saw blades in the mill industry have different sources of imperfections including those imperfections due to the initial non-flatness of the disk. The initial lack of flatness may change the frequency and critical speed behaviours of saw blades. Therefore in order to see how a non-flat saw blade performs at very high speeds, the effect of initial runout on the dynamics of spinning disks should be studied.

When saw blades are in the cutting modes, they experience external forces in the radial, tangential, and lateral directions. The lateral forces cause lateral deflections where, in some cases, these lateral deflections may change the dynamics of spinning disks at critical speed ranges. The effect of large deformations on the dynamics of spinning disks can be looked at both numerically and experimentally. Here, it will be determined how the frequency behaviour of spinning disks changes with regard to large deformations.

In the theory of vibrations for spinning disks, two different approaches have been taken. The first one utilizes linear theory where the effects of nonlinear terms are neglected; the second approach, nonlinear theory, instead takes those effects into account. The following sections introduce and discuss these two theories in detail.

1.2. Linear Theory of Vibration

In the approach based on the linear theory of vibration, the effect of higher order terms in the strain-displacement relations is neglected. Thus the resulting equations of motion are solely linear. The governing equation of transverse vibration of a spinning disk in terms of lateral displacement $w(r, \theta, t)$, with respect to a space fixed polar coordinate system shown with (r, θ) , can be written as [36]:

$$\rho h (w_{,tt} + 2\Omega w_{,t\theta} + \Omega^2 w_{,\theta\theta}) + D \nabla^4 w - \frac{h}{r} (\sigma_r r w_{,r})_{,r} - \frac{h}{r^2} \sigma_{,\theta} w_{,\theta\theta} = F(t) \quad (1.1)$$

Where D and ρ are the flexural rigidity and mass density of the plate respectively, $F(t)$ is the applied external load, a is the inner radius, b is the outer radius, h is its thickness, and Ω represents the angular velocity. σ_r and σ_θ the radial and tangential stresses, respectively, can be obtained through:

$$\sigma_r = \rho\Omega^2 \left(C_1 + \frac{C_2}{r^2} + C_3 r^2 \right) \quad (1.2a)$$

$$\sigma_\theta = \rho\Omega^2 \left(C_1 - \frac{C_2}{r^2} + C_4 r^2 \right) \quad (1.2b)$$

Two different disks with different boundary conditions are considered in this research work: the clamped disk and the splined disk. As mentioned above, for a clamped disk it is assumed that the inner boundary is fixed and the outer boundary is free. For the splined disk it is assumed that both of the boundaries are free. In the above equations C_1, C_2, C_3 and C_4 are constants that can be determined from the boundary conditions. For disks clamped at in the inner rim and free at the outer rim, the following equations can be used:

$$C_1 = \frac{1+\nu}{8} \frac{(\nu-1)a^4 - (3+\nu)b^4}{(\nu-1)a^2 - (1+\nu)b^2},$$

$$C_2 = \frac{1-\nu}{8} a^2 b^2 \frac{(\nu+1)a^2 - (3+\nu)b^2}{(\nu-1)a^2 - (1+\nu)b^2},$$

$$C_3 = -(3+\nu)/8,$$

$$C_4 = -(1+3\nu)/8.$$

For a splined disk with an idealized free-free boundary condition for both inner and outer rims C_3 and C_4 remain unchanged and C_1 and C_2 are:

$$C_1 = \frac{3+\nu}{8} (a^2 + b^2)$$

$$C_2 = -\frac{3+\nu}{8} a^2 b^2$$

The main focus of this work is to study the dynamics characteristics of the clamped disks. At first, brief discussions regarding the dynamical characteristics of clamped disks are presented. Following that considerations and discussions will be made of the effect of elastic constraints and the effects of elastic constraints and rigid body modes on the vibration characteristics of the spinning disks.

1.2.1. Clamped Disks

Figure 1.2 shows the natural frequencies of a disk calculated with respect to stationary coordinates with the inner and outer diameters of 6" and 17", respectively, and a thickness of 0.05". In this graph the modes are distinguished from each other by the

number of their nodal circles $-n-$ and also the number of their nodal diameters $-m-$ and shown as mode (n,m) . Corresponding to each mode there are two waves travelling around the disk. One travels in the direction of rotation (forward travelling wave) and the other travels in the opposite direction (backward travelling wave). It can be seen that natural frequencies of the backward and forward travelling waves of a mode are the same when the disk is stationary. Once the disk starts to spin, the natural frequency of the forward travelling wave increases and that of the backward travelling wave decreases as the rotation speed increases. It can be seen that for the modes having more than one nodal diameter a speed is reached at which the natural frequency of its backward travelling wave is zero. This speed is called the disk “critical speed.”

There has been a large body of research work concerning the dynamic characteristics of clamped spinning disks. Lamb et. al. [1] investigated the transverse vibration of a circular disk of uniform thickness rotating about its axis with constant velocity. Tian and Hutton [2] developed an analytical model for wood cutting of circular saws in order to understand the washboarding mechanism.

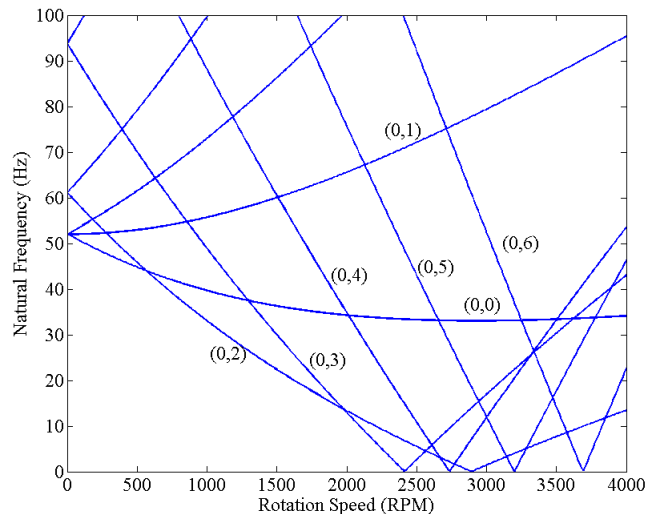


Figure 1.2. Natural frequencies versus rotation speed

Yu [3] presented a generalized Hamilton’s principle and the associated equation of motion for finite elastic deformation. By means of the generalized variational equation of motion, it is possible to deduce immediately the nonlinear equation of motion. He then employed the generalized variational equation of motion for the derivation of plate equations for both flexural and extensional motions. Mote [4] analyzed the free vibration

characteristics of centrally clamped, variable thickness disks by the Rayleigh-Ritz technique. Natural frequencies of transverse vibration were computed, taking into consideration rotational and thermal in-plane stress as well as purposely induced initial stress. Based on his analysis initial stresses can significantly raise the minimum disk natural frequency throughout a prescribed rotational and thermal environment. Vogel [5] derived the frequency determinants for various combinations of boundary conditions associated with the transverse vibrations of uniform annular plates. From these equations, he calculated the values of the resonant frequencies for various normal modes.

Chen [6] analyzed the forced response of a spinning disk under space fixed couples analytically using the eigenfunction expansion method. He considered a general couple on the disk surface as a superposition of two components. One of the components was pitching which was in the radial direction and the other one is a rolling component which is in the circumferential direction. He investigated the transient and steady state deflection of the disk. Nishio [7] investigated variations of the lateral vibration mode, the natural frequency, and the critical rotational speed of a slotted circular saw blade through both experiment and by numerical calculations.

J.-S. Chen performed numerous studies in the linear region of the rotating elastically constrained rotating disks. He [8] used the orthogonality properties that govern the modes to determine the certain derivative of modes with respect to a specified parameter. He then found the derivative of the natural frequencies of the system with respect to constraint parameters such as mass, damper, and stiffness. He [9] also used a series approximation to show that stress distribution induced by the friction effect from a fixed space source cannot affect the stability of the system. In other works ([10], [11] and [12]) he studied the effect of edge loads on the stability characteristics of a rotating disk.

DasGupta and Hagedorn [13] modelled the dynamics of spinning ring with a variable thickness external ring attached to it. They used von Karman plate theory to develop the equation of motion for the rotating disk with a ring attached to it. They found that a considerable change in the critical speed was achieved by designing an appropriate external ring. Kim and Renshaw [14] studied the effect of asymmetry of a spinning disk, using the finite element method. They investigated the effect of asymmetry on the natural frequencies of a rotating disk. Shen and Song [15] studied the effect of asymmetric

membrane stresses resulting from stationary in-plane edge loads. They used the method of multiple scales to study the stability of the disk subjected to stationary in-plane edge loads. Gupta et. al. [16] studied the asymmetric vibration of polar orthotropic circular plates. Adams [17] studied the effect of an elastic foundation on the critical speeds of a spinning disk. Eid et. al. [18] used Mindlin plate theory, which includes shear deformation and rotational inertia, to find the critical speeds of a spinning disk.

Parker and Mote [19] proposed a method for initially stressing the disk that can increase the natural frequencies of some of the modes simultaneously. In another work Parker and Mote [20] used a perturbation solution to analytically determine the eigensolutions of an annular plate. Young and Wu [21] studied the dynamic instability of a spinning disk with a periodically varying speed, subjected to a stationary in plane edge load. They used perturbation method to analyze the effect of varying speed on the vibration characteristics of the disk. Tian and Hutton [22] introduces a general approach which predicts the physical instability mechanism that take place when the rotating disk is in interaction with a fixed space constraint. They used a physical energy flux equation for the disk to explain its instability. Then they investigated the effect of conservative and non-conservative forces on the stability of the disk.

Shahab [23] used the Ritz method to investigate the transverse vibration of a disk with variable thickness. He developed a thick three dimensional element that includes the effect of rotary inertia and shear deformation for this purpose. Chung et. al. [24] investigated the effects of misalignment on the natural frequencies of a spinning disk. Huang, Wang, and Yap [25] studied feedback control of a rotating disk in an enclosure at flutter instability speed. They studied the effect of different gains on suppressing the transverse vibration of the disk. Gabrielson [26] presented the natural frequency of a disk with different boundary conditions and also different ratios of outer to inner diameter. Chen and Jhu [27] investigated the inplane vibrations of rotating disks. They studied the effect of clamping ration on the natural frequencies and critical speed of a rotating disk. Lee and Kim [28] developed direction frequency response functions for rotating disks. They then used this method to separate backward and forward travelling waves. Leissa, Laura, and Gutierrez [29] studied the free vibration of circular plates having non-uniform edge loads. They studied edge supports having translational and rotational flexibilities

which both vary in an arbitrary manner around the boundary of the disk. Gutierrez and Laura [30] studied the transverse vibration of a circular plate with a concentric circular support. Tandon, Rao, and Agrawal [31] performed experimental studies on vibration and noise generated by computer hard disk drives. Irie, Yamada, and Aomura [32] studied vibration and stability of radially stiffened annular plates subjected to in plane forces uniformly distributed at the edges by means of the energy method. Huang and Chou [33] studied the vibration feedback control of rotating disks. They used the root locus approach for an infinite number of poles and zeroes. By means of one sensor and one actuator they designed a feedback control algorithm for suppressing vibration in rotating disks. Chen [34] used a transfer function model to design a feedback control algorithm for suppressing vibration of rotating disks at sub- and super-critical speeds. He used one sensor and one actuator to implement his feedback control algorithm.

1.2.2. Elastically Constrained Spinning Disks

There are some applications for spinning disks such as in saw mill industry where they are elastically constrained. The constraint is generally modelled with a mass-spring-damper system. In this research work, only the spring component is considered. Figure 1.3 shows the natural frequencies and the real parts of eigenvalues of the elastically constrained spinning disk with the aforementioned dimensions. It is assumed that the spring stiffness is $4kN/m$ and that it is acting at the outer rim of the disk. It can be seen that the frequency characteristics of the spinning disk is different from the unconstrained disk.

Chen et. al. [35] studied the interaction of the mode at sub- and super-critical speeds. He categorized modal interactions to be four and he studied the effect of each of the constraint parameters on the stability of the system at sub- and super-critical speeds. He concluded that the interaction between the natural frequencies of backward and reflected travelling waves causes flutter type instability for an elastically constrained disk as shown in Figure 1.3.

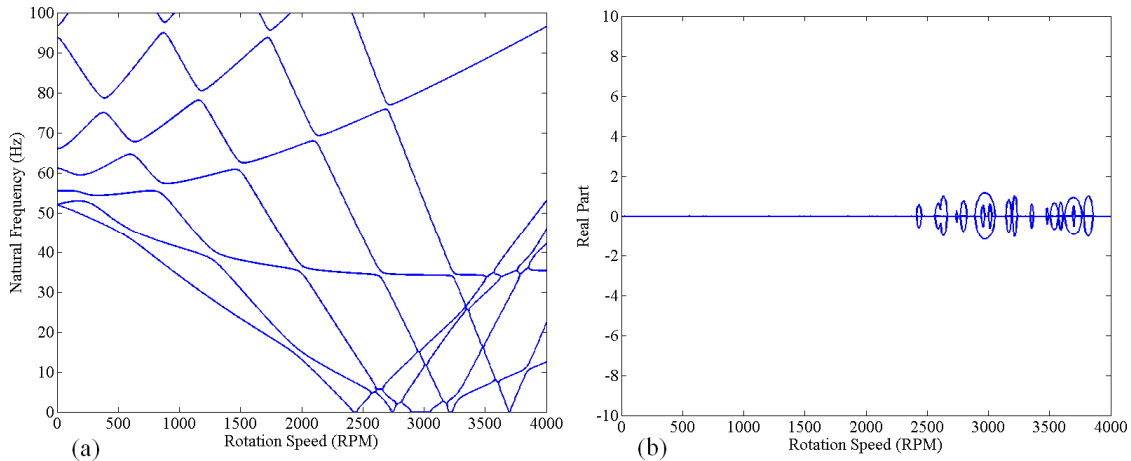


Figure 1.3. The (a) natural frequencies and (b) real part of the eigenvalues of an elastically constrained disk

When flutter instability happens, the real parts of eigenvalues have positive parts. Another source of instability for an elastically constrained disk is at the location of critical speed. This type of instability is called “divergence instability.” When the divergence instability occurs, there is one eigenvalue for the system with a zero imaginary part and a positive real part.

There are some works in the literature that studied the dynamics of elastically constrained spinning disks. Hutton, Chonan, and Lehmann [36] studied the dynamic response characteristics of rotating circular disks when subjected to the effect of forces produced by stationary spring guides. Young et al. [37] studied the free vibration of a rotation clamped disk under the constraint of an elastically fixed space oscillating unit. The unit he considered was composed of two parallel combinations of springs and dampers attached above and under a mass. He studied the flutter type instabilities imposed by these two units.

Ouyang and Mottershead [38] studied the instability of a transverse vibration of a disk excited by two sliders on each side of the disk. He modeled the sliders with a mass-spring-damper system. He considered the effect of friction due to movement of these two sliders on the disk which produces a fluctuating couple on the disk.

1.2.3. Effects of Rigid Body Translation on the Dynamics of Spinning Disks

Some of the spinning disk applications may have the rigid body translational degree of freedom along the axis of rotations. In this case, Eq. (1.1) should be modified such that it takes into account the effect of the rigid body translational degree of freedom.

When the rigid body translational degree of freedom is taken into account, the dynamic response of the disk will be different. Figure 1.4 shows the frequencies of the guided disk having the rigid body translational degree of freedom. Here it is also assumed that the spring stiffness is $4kN/m$ and it is acting at the outer rim of the disk.

Through comparison of Figure 1.4 with Figure 1.3 it can be seen that when the disk is elastically constrained with one spring the divergence instability does not occur at the location of critical speeds. Thus, the speed ranges at which the disk is stable are changed when the disk has a rigid body translational degree of freedom. It may be also noted that at sub-critical speeds there is a natural frequency which is constant and does not change with the speed. This natural frequency corresponds to rigid body motion. The interaction of this natural frequency with other natural frequencies may produce flutter instability.

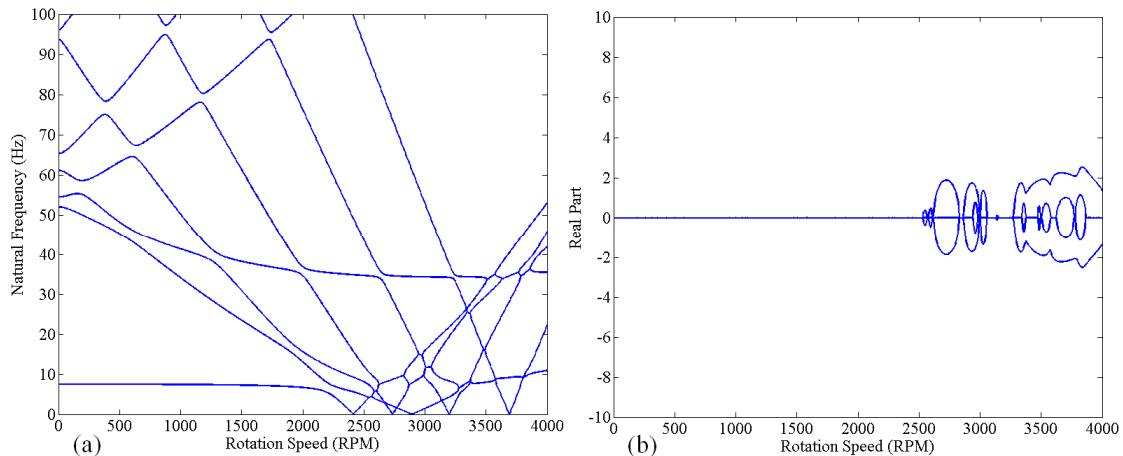


Figure 1.4. The (a) natural frequencies and (b) real part of the eigenvalues of an elastically constrained disk having rigid body translational degree of freedom

There has been a limited number of works that studied the effects of the rigid body translational degree of freedom on the stability characteristics of spinning disks. Yang [39] studied the vibration of spinning disks with translational and rotational rigid body motion. He considered the coupling effect between the rigid body motion and the annular

disk modal function. He showed that there is a stability region above the critical speed due to the coupling effect.

Mote [40] studied the effect of a collar (which was allowed to move freely on the arbor) on the stability of a guided rotating disk. Price [41] studied the dynamics of the plates with clamped-free boundary conditions and studied the effect of a rigid body translational mode on the dynamic response of rotating plates. Chen and Wong [42] used finite element analysis to study the effect of evenly fixed spaced springs on the divergence instability of a rotating disk having translational degrees of freedom. Chen [43] studied the effect of rigid body tilting on the natural frequencies of a rotating disk.

1.3. Nonlinear Theory of Vibration

In the nonlinear theory of vibration, the effect of higher order stress terms in strain-displacement relations are taken into account. Based on the linear theory of oscillations for spinning disks, disk deflection is unbounded at speeds corresponding to flutter or divergence instabilities. In fact, in these very cases, the disk deflection is beyond the validity range of linear equations of motion and it is necessary to use nonlinear equations for better predictions of the dynamics of spinning disks.

1.3.1. Nonlinear Analysis and Basic Assumptions

Nowinski [44] was amongst the first researchers to develop the nonlinear equations of motion for a spinning disk. He assumed the disk thickness to be much less than the outer radius. He also assumed that the disk is perfectly flat and is made of an isotropic material. He also assumed that the disk is free of any initial stress and that the effect of in-plane vibrations and rotary inertia are negligible. Based on these assumptions, he developed the nonlinear equations of motion of a spinning disk with speed Ω in the space-fixed polar coordinate system $((r, \theta))$ as:

$$\rho h \left(\frac{\partial^2 w}{\partial t^2} + 2\Omega \frac{\partial^2 w}{\partial \theta \partial t} + \Omega^2 \frac{\partial^2 w}{\partial \theta^2} \right) + D \nabla^4 w = L(w, \phi) + p(r, \theta, t) - \frac{1}{2} \rho h \Omega^2 r^2 \nabla^2 w - \rho h \Omega^2 r \frac{\partial w}{\partial r}, \quad (1.3)$$

$$\nabla^4 \phi = -\frac{1}{2} EhL(w, w) + 2\rho h(1-\nu)\Omega^2, \quad (1.4)$$

$$\nabla^4 = \left(\frac{\partial^2}{\partial r^2} + \frac{1}{r} \frac{\partial}{\partial r} + \frac{1}{r^2} \frac{\partial^2}{\partial \theta^2} \right)^2,$$

where $p(r, \theta, t)$ is an external surface pressure, ϕ is the stress function and $L(w, \phi)$ is the operator that includes nonlinearities arising from the strain-displacement relations

$$L(w, \phi) = \frac{\partial^2 w}{\partial r^2} \left(\frac{1}{r} \frac{\partial \phi}{\partial r} + \frac{1}{r^2} \frac{\partial^2 \phi}{\partial \theta^2} \right) + \frac{\partial^2 \phi}{\partial r^2} \left(\frac{1}{r} \frac{\partial w}{\partial r} + \frac{1}{r^2} \frac{\partial^2 w}{\partial \theta^2} \right) - 2 \left(\frac{1}{r} \frac{\partial^2 \phi}{\partial r \partial \theta} - \frac{1}{r^2} \frac{\partial \phi}{\partial \theta} \right) \left(\frac{1}{r} \frac{\partial^2 w}{\partial r \partial \theta} - \frac{1}{r^2} \frac{\partial w}{\partial \theta} \right).$$

Later on, Baddour et. al. [45] developed a full model of the nonlinear governing equations of motions considering the effects of in-plane displacements. The predicted responses based on the linear and nonlinear theories could be dramatically different. For instance, Figure 1.5 compares the linear and nonlinear analyses for a spinning disk with free-free boundary conditions at 1850 RPM. The rigid body degrees of freedom are taken into account in this analysis. The dimensions of the disk are the ones that are indicated previously. The disk was assumed to be elastically constrained by four linear springs at the radial locations: $0.58b, 0.88b$ and the angular positions $\theta_j = \pm 0.65, \pm 0.41 \text{ Rad}$. It can be seen that when the disk deflection is relatively small, e.g. $w/h < 1$, there is no significant difference in the amplitude of disk oscillations. It may be noted that in this case, there is a small difference in the oscillation frequencies. When the level of nonlinearity is high enough (e.g., $w/h > 1$), the predicted amplitudes of oscillations and their frequencies through nonlinear analyses are very different compared to those predicted by the linear analysis. Therefore, there is a need to investigate the effect of large deformations on the dynamical behavior of spinning disks. The effect of large deformations can either be investigated experimentally or analytically. Both of these methods are discussed in this work. Also, through the nonlinear form of the equations of motion, one can study the effect of initial disk runout on the frequency behaviour of the spinning disks.

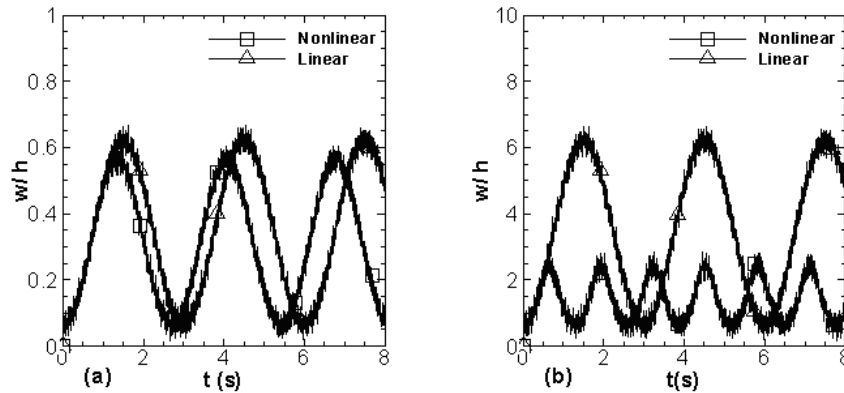


Figure 1.5. Linear and nonlinear response of the blade at 1850 RPM for w/h when (a) $F= 1 \text{ N}$ and (b) $F=10\text{N}$

1.3.2. Disk Initial Runout

Initial disk non-flatness can change the frequency characteristics of spinning disks. It also can change the critical speeds of spinning disks. To have a better understanding of the performance of spinning disks in real life applications, we have to know how the frequency and critical speed characteristics of spinning disks change when assuming the initial runout for them.

In order to study the effect of initial runout on spinning disk natural frequencies, one must use the governing equations of motion for initially non-flat spinning disks.

There have been a few studies in the literature that focus on the dynamics of non-flat disks. Jia [46] used the linear equation of motion to investigate the effect of runout on the vibration of a rotating disk. He approximated the runout of the blade with the summation of some modes having different nodal diameter numbers and then determined the deflection of the disk analytically. Since he used linear equations of motion, he could not study the effect of initial non-flatness on the frequency characteristics of spinning disks. Benson et al. [47] studied the effect of initial runout on the amplitude of oscillations, using both numerical and experimental techniques. At the same time, Carpino [48] investigated the effect of initial curvature of the dynamics of a disk rotating near a rigid surface.

While the aforementioned studies employed linearized equations of motion, other literature studies have considered the effect of geometrical nonlinear terms on the response of a non-flat spinning disk. Chen et al. [49] used the nonlinear governing

equations of motion to investigate the impact of symmetrical initial runout on the amplitude of spinning disk deflection. He concluded that depending on the shape and level of initial non-flatness, the disk may snap from one side to another. To verify his results, he used a warped disk with an initial level of non-flatness almost eight times higher than the disk thickness. In another work, Chen et al. [50] used the nonlinear equations of motion to consider an unsymmetrical initial non-flatness for the disk. In this paper, he studied the effect of unsymmetrical terms on the snapping speed while the disk was spinning.

1.3.3. Experimental Investigations on the Effects of Large Deformations

As it was mentioned earlier, large deformations may substantially change the vibration characteristics of spinning disks. Large deformations can change the amplitude of disk oscillations and they can also modify the frequency characteristics of spinning disks. In most of the experimental research work available in the literature, the amplitude response of spinning disks has been investigated experimentally.

Tobias and Arnold [51] investigated the effect of disk imperfections on the dynamic behavior of spinning disks. In their studies, they conducted experiments on the amplitude response of a spinning disk in the region of its critical speeds while subjected to a space fixed external force. They observed that a stationary wave develops in the region of a critical speed and collapses sometime after the critical speed. They did not consider the effect of large deformations on the frequency response characteristics of the disks that were tested. In another work [52], Tobias studied the large vibrations of stationary disks. He was able to record phase and amplitude jumps while the disk was being excited with a frequency close to one of its natural frequencies.

Thomas et. al. [53] measured the amplitude response of an imperfect stationary disk. Due to the presence of imperfections, there were two different configurations associated with each mode. He was able to measure the amplitude response of each configuration and compare them with analytical predictions. Raman and Mote [54] conducted experiments to study the behaviour of an imperfect spinning disk near its critical speeds. In their experimental work they were able to observe the existence of a critical speed for very small disk deflections.

In all of the aforementioned studies, the amplitude response of spinning disks has been studied. There are a few investigations in the literature that are concerned with the effect of large deformations on the frequency behaviour of spinning disks. D'Angelo and Mote [55] were amongst the first researchers to measure the oscillation frequencies of a spinning disk having large deformations. They noted that at supercritical speeds, the measured frequency of backward travelling waves maintain a constant level.

Raman et. al. [56] investigated experimentally the post-flutter frequency response of spinning disks. They recorded sudden jump and drops in the frequency response of the disks tested. Also, they noticed that the frequency response of the backward travelling wave of one of the modes was nearly constant over a specific speed region.

Namchelo and Raman [57] studied the vibrations of a spinning disk in a gas-filled enclosure. More recently, Jana et. al. [58] conducted experiments to investigate the aeroelastic phenomena of a disk rotating in air. They measured the amplitude and frequency responses of a spinning disk and noticed jumps and drops in the frequency response. They also reported that, in some supercritical speed ranges, a frequency lock-in phenomenon occurred.

1.3.4. Numerical Investigations on the Effects of Large Deformations

There has been an exhaustive amount of research work that explore the effects of geometrical nonlinear terms on the dynamics of spinning disks.

Jana and Raman [59] investigated the nonlinear dynamics of a flexible spinning disk coupled to a precompressed spring. They studied large amplitude wave motions and their stability using the averaging method. Chen [60] also studied the steady-state deflection of a rotating disk in the neighbourhood of its critical speed and found that after surpassing the critical speed there are three steady state solutions to the nonlinear equation of motion and only one of them is stable in the presence of space-fixed damping.

Nayfeh, Jilani, and Manzione [61] used the method of multiple scales to investigate the transverse nonlinear vibrations of a centrally clamped rotating circular disk. Chen [62] used the multiple scales method to investigate the internal resonance between a pair of forward and backward modes of a spinning disk under space fixed pulsating edge loads. Touze et al. [63] studied the nonlinear oscillations of a stationary disk with

imperfections. They also examined the coupling between preferential configurations and investigated its effect on the travelling wave components in the response.

Yang and Hutton [64] used polynomial expansion functions as the approximation function in Galerkin's method to solve the nonlinear equations of motion for thin rotating disks. Luo and Mote [65] used a new plate theory to study the effect of large amplitude displacements on the frequency behaviour of spinning disks. Based on energy principles they calculated the frequencies of a spinning disk with consideration of the effect of nonlinear terms.

Arafat, Nayfeh, and Faris [66] studied the behaviour of an annular disk subjected to axisymmetric in-plane thermal load with a clamped-clamped boundary condition. They investigated the effect of thermal loads on the natural frequencies of a stationary disk and found that, depending on the thermal load, there may be a three-to-one combination internal resonance between the modes having the same number of nodal diameters.

Arafat and Nayfeh [67] studied a three-to-one internal resonance between the first and second axisymmetric modes of an annular disk with a clamped-clamped boundary condition, which was subjected to an external force and a thermal load. They used multiple scales to find the governing equations for the amplitudes and phases of the responses. Arafat and Nayfeh [68] used von Karman plate theory to study the combination of internal resonance for a thermally loaded annular plate subjected to harmonic excitation near primary resonance of one of the modes with a clamped-clamped boundary condition. Chen, Hua, and Sun [69] used von Karman's plate theory to investigate the secondary resonance of a rotating disk under space fixed force. Heo, Chung, and Choi [70] used a finite element method to study the time domain response of a rotating disk misaligned from its axis of symmetry. In their analysis they considered both inplane and out of plane deformations of the disk. Raman and Mote [71] studied the large amplitude vibration of a rotating disk with imperfections near the critical speed.

Manziona and Nayfeh [72] studied the transverse vibrations of a circular spinning disk with uniform thickness subjected to a space fixed spring-mass-dashpot system. They used the method of multiple scales to find the nonlinear coupled governing equations of the motion and they studied the stability of the equilibrium solutions. Jalali and Angoshtari [73] used a Hamiltonian formulation to study the dynamics of forced spinning

disks. Using a Poincare map, they showed that a one mode approximation of rotating disks may have chaotic behaviour. Also they studied the effect of structural damping and showed the existence of asymptotically stable limit cycles for the damped system.

1.4. Objective and Scope

In this thesis, the vibration characteristics of spinning disks are investigated. This research work aims to examine the linear and nonlinear vibration characteristics of spinning disks with applications to the saw mill industry.

As was mentioned above, for some of the saw mills industries saw blades are not constrained in the inner rim and may have a rigid body translational degree of freedom. Thus, it is important to determine how the rigid body translational degree of freedom might affect the dynamics stability of saw blades at supercritical speeds.

There are several sources of imperfections in real saw blades. One such source is the imperfection due to a lack of flatness. These types of imperfections can change the modal stiffness characteristic of a saw blade. As such, they can change the frequency and critical speed behaviour of saw blades. Therefore, in order to have a better understanding of the dynamics of real saws, there will be a discussion on the effect of imperfections on the frequency and critical speed behaviour of spinning disks. Runouts can be axisymmetric or unsymmetrical. As a first step, the axisymmetric case is investigated in this work.

Real saw blades in cutting modes experience the application of radial, tangential, and lateral cutting forces. The lateral forces produce lateral deflections and when the lateral deflection is large compared to its thickness (e.g., greater than 0.3 of its thickness) the frequency and critical speed behaviour of saw blades change. This change is especially more noticeable at supercritical speeds. Therefore, the objective of this research work is to first study the effects of the rigid body translational degree of freedom, initial non-flatness, and large deformations on the dynamics of spinning disks. To meet these general objectives, the approach taken in this thesis consists of the following sub-objectives:

To understand the stability mechanics of a guided rotating disk with rigid body translational mode. The linear theory will be used to study the effect of rigid body modes on the stability characteristics of an elastically constrained rotating disk.

To study the effect of symmetrical non flatness on the frequency response of an elastically constrained disk. Also the effect of such these imperfections on the critical speeds of different modes are of major concern.

To experimentally investigate the amplitude and frequency characteristics of spinning disks under the application of a space fixed external force.

To analytically investigate the effect of nonlinear terms on the frequency response of a rotating disk using a linearization method. The aim is to study the effect of the level of nonlinearity on the forced frequencies of a rotating disk.

This thesis is presented in six chapters. In Chapter 2 a discussion on the linear model prediction for the stability of the disk is made. The linear equations of motion coupled with the rigid body translational mode are used to investigate the stability characteristics of an elastically constrained disk. The effect of the rigid body mode on the stability characteristics of a spinning disk is studied. Generally there are three types of interaction between the rigid body translational mode and bending modes: the rigid body translational mode may have interactions with a forward, backward, or reflected wave. The stability characteristics of the disk at the speeds corresponding to these types of interactions are studied. Also, a one mode approximation model around the critical speed is utilized to study the effect of the rigid body translational mode on the divergence instability of the disk.

Chapter 3 is concerned with the effect of non-flatness on the frequency response of a spinning disk assuming symmetric non-flatness. Since the non-flatness is assumed to be axisymmetric, the equations of motion can be expressed in an inertial frame. The non-flatness is assumed to be expressed as a summation of the eigenfunctions of the modes with a zero number of nodal diameters. As an approximation, the effect of higher order terms in the nonlinear equations of motion is neglected. Using this assumption the particular solution for the stress function is found from the compatibility relation. Substituting the stress function into the governing equation of motion and utilizing Galerkin's method while neglecting higher order terms, a linearized system of equations is found. Using the obtained linear system, the effect of symmetrical non-flatness on the frequency response of an elastically constrained spinning disk is investigated.

Chapter 4 is concerned with the effects of large deformations on the amplitude and frequency characteristics of spinning disks. This chapter describes attempts made to experimentally study the effects of nonlinear terms on the dynamics of spinning disks under the applications of space fixed external forces. Three disks with the same inner and outer radii and different thicknesses were used. Different levels of force are applied to these three disks and their amplitudes of oscillation and frequencies were measured.

Chapter 5 is primarily concerned with the effect of nonlinear terms on the forced frequency response of a disk using the linearization method. Using Galerkin's method, the nonlinear equations of motion are discretized. The equilibrium solution for a spinning disk under the application of a space fixed external force is found. Then, the nonlinear equations of motion are linearized around that equilibrium solution to obtain a linearized system of equations of motion. These linearized equations of motion are used to study the effect of different levels of nonlinearity on the frequency response of a rotating disk.

Finally, Chapter 6 presents the conclusions and suggestions for future investigations on this subject.

1.5. References

- [1] Lamb, H., and Southwell, R.V., 1921, "The Vibration of Spinning Disk," Proc R Soc Lond 99, pp. 272-280.
- [2] Tian, J.F., and Hutton, S.G., 2001, "Cutting-Induced Vibration in Circular Saws," Journal of Sound and Vibration, 242(5), pp. 907-922.
- [3] Yu, Y.Y., 1964, "Generalized Hamilton's Principle and Variational Equation of Motion in Nonlinear Elasticity Theory," Journal of the Acoustical Society of America, 36, pp. 111-120.
- [4] Mote, C.D., 1965, "Free Vibration of Initially Stressed Circular Plates," Journal of Engineering for Industry, 87, pp. 258-264.
- [5] Vogel, S.M., and Skinner, D.W., 1965, "Natural Frequencies of Transversely Vibrating Uniform Annular Plates", ASME Journal of Applied Mechanics, 32, pp. 926-931.
- [6] Chen, J.S., Hsu, C.M. , 1997, "Forced Response of a Spinning Disk Under Space-Fixed Couples," Journal of Sound and Vibration, 206(5), pp. 627-639.
- [7] Nishio, S., and Marui, E., 1996, "Effect of Slots on the Lateral Vibration of a Circular Saw Blade," International Journal of Machine Tools and Manufacture, 36(7), pp. 771-787.
- [8] Chen, J.S., and Bogy, D.B., 1992, "Effects of Load Parameters on the Natural Frequencies and Stability of a Flexible Spinning Disk With a Stationary Load System," Journal of Applied Mechanics, 59, pp. S230-S235.
- [9] Chen, J.S., and Bogy, D. B., 1993, "The Effects of a Spaced-Fixed Friction Force on the In-Plane Stress and Stability of Transverse Vibrations of a Spinning Disk," ASME Journal of Applied Mechanics, 60(3), pp. 646-648.
- [10] Chen, J.S., 1994, "Stability Analysis of a Spinning Elastic Disk Under a Stationary Concentrated Edge Load," ASME Journal of Applied Mechanics, 61, pp. 788-792.
- [11] Chen, J.S., 1996, "Vibration And Stability of a Spinning Disk Under Stationary Distributed Edge Loads," ASME Journal of Applied Mechanics, 63, pp. 439-444.
- [12] Chen, J.S., 1997, "Parametric Response of a Spinning Disk Under Space-Fixed Pulsating Edge Loads," ASME Journal of Applied Mechanics, 64, pp. 139-143.

- [13] DasGupta, A., and Hagedorn, P., 2005, "Critical Speeds of a Spinning Thin Disk With an External Ring," *Journal of Sound and Vibration*, 283, pp. 765-779.
- [14] Kim, H.R., and Renshaw, A.A., 1998, "Asymmetric, Speed Dependent Tensioning of Circular Rotating Disks," *Journal of Sound and Vibration*, 218, pp. 65-80.
- [15] Shen, I. Y., and Song, Y., 1996, "Stability and Vibration of a Rotating Circular Plate Subjected to Stationary In-Plane Edge Loads," *ASME Journal of Applied Mechanics*, 63, pp. 121-127.
- [16] Gupta. U.S., and Ansari, A.H., 1998, "Asymmetric vibrations and elastic stability of polar orthotropic circular plates of linearly varying profile," *Journal of Sound and vibration*, 215, pp. 231-250.
- [17] Adams, G., 1987, "Critical Speeds for a Flexible Spinning Disk," *International Journal of Mechanical Sciences*, 29 (8), pp. 525-531.
- [18] Eid, H., Adams, G.G., 2006, "Critical speeds and the response of a spinning disk to a stationary load using Mindlin plate theory," *Journal of Sound and Vibration*, 290, pp. 209-222.
- [19] Parker. R.G., and Mote, C.D., 1991, "Tuning of the Natural Frequency Spectrum of a Circular Plate by In-plane Stress," *Journal of Sound and Vibration*, 145, pp. 95-110.
- [20] Parker. R.G., and Mote, C.D., 1996, "Exact Perturbation for the Vibration of Almost Annular or Circular Plates," *Journal of Vibration and Acoustics*, 118, pp. 436-445.
- [21] Young, T. H., and Wu, M. Y., 2004, "Dynamic Stability of Disks with Periodically Varying Spin Rates Subjected to Stationary In-Plane Edge Loads," *Journal of Applied Mechanics*, 71, pp. 450-458.
- [22] Tian, J., and Hutton, S.G., 1999, "Self Excited Vibration in Flexible Rotating Discs Subjected to Transverse Interaction Forces – A General Approach," *ASME Journal of Applied Mechanics*, 66, pp. 800-805.
- [23] Shahab, A.A.S., 1993, "Finite Element Analysis for the Vibration of Variable Thickness Discs," *Journal of Sound and Vibration*, 162, pp. 67-88.

- [24] Chung, J.T., Heo, J.W., and Han, C.S., 2003, "Natural frequencies of a flexible spinning disk misaligned with the axis of rotation," *Journal of Sound and Vibration*, 260, pp. 763-775.
- [25] Huang, X.Y., Wang, X., and Yap, F.F., 2004, "Feedback Control of Rotating Disk Flutter in an Enclosure," *Journal of Fluids and Structures*, 19, pp. 917-932.
- [26] Gabrielson, T.B., 1999, "Frequency Constants for Transverse Vibration of Annular Disks," *Journal of Acoustical Society of America*, 105 (6) , pp. 3311-3317.
- [27] Chen, J.S., and Jhu, J.L., 1996, "On the In-Plane Vibration and Stability of a Spinning Annular Disk," *Journal of Sound and Vibration*, 195(4), pp. 585-593.
- [28] Lee, C.-W., and Kim, M.-E., 1995, "Separation and Identification of Travelling Wave Modes in Rotating Disk via Directional Spectral Analysis," *Journal of Sound and Vibration*, 187, pp. 851-864.
- [29] Leissa, A.W., Laura, P.A., and Guiterez, R.H., 1979, "Transverse Vibrations of Circular Plates Having Nonuniform Edge Constraints," *Journal of the Acoustical Society of America*, 66(1), pp. 180-184.
- [30] Gutierrez, R. H., and Laura, P. A. A., 2000, "Transverse Vibrations of a Circular Plate Polar Anisotropy with a Concentric Circular Support," *Journal of Sound and Vibration*, 231, pp. 1175-1178.
- [31] Tandon, N., Rao, V.V.P., and Agrawal, V.P., 2006, "Vibration and Noise Analysis of Computer Hard Disk Drives," *Journal of the International Measurement Confederation*, 39, pp. 16-25.
- [32] Irie, T., Yamada, G., and Aomura, S., 1982, "Vibration And Stability Of Stiffened Annular Plates," *Journal of Acoustical Society of America*, 72, pp. 466-471.
- [33] Huang, C.C., and Chou, R.J., 2000, "Vibration Control of a Rotating Disk," *Mechanical Systems and Signal Processing*, 14, pp. 151-165.
- [34] Chen, J.S., 2003, "Vibration Control of a Spinning Disk," *International Journal of Mechanical Sciences*, 45, pp. 1269-1282.
- [35] Chen, J. S., and Bogy, D.B., 1992, "Mathematical Structure of Modal Interactions in a Spinning Disk-Stationary Load System," *American Society of Mechanical Engineers Journal of Applied mechanics*, 59, pp. 390-397.

- [36] Hutton, S.G., Chonan, S., and Lehmann, B.F., 1987, "Dynamic Response of a Guided Circular Saw," *Journal of Sound and Vibration*, 112, pp. 527-539.
- [37] Young, T.H., and Lin, C.Y., 2006, "Stability of a Spinning Disk Under a Stationary Oscillating Unit," *Journal of Sound and Vibration*, 298, pp 307-18.
- [38] Ouyang, H., and Mottershead, J. E. , 2003, "A Moving-Load Model for Disc-Brake Stability Analysis," *Journal of Vibration and Acoustics*, 125, pp. 753-758.
- [39] Yang, S.M., 1993, "Vibration of a Spinning Annular Disk with Coupled Rigid-Body Motion," *Journal of Vibration, Acoustics*, 115, pp. 159-164.
- [40] Mote, C.D., 1977, "Moving Load Stability of a Circular Plate on a Floating Central Collar," *Journal of Acoustical Society of America*, 61, pp. 439-447.
- [41] Price, K.B., 1987, "Analysis of the Dynamics of Guided Rotating Free Center Plates," Ph.D. Dissertation, University of California, Berkeley.
- [42] Chen, J.S., and Wong, C.C., 1995, "Divergence Instability of a Spinning Disk with Axial Spindle Displacement in Contact with Evenly Spaced Stationary Springs," *Journal of Applied Mechanics*, 62, pp. 544-547.
- [43] Chen, J.S., and Bogy, D.B., 1993, "Natural Frequencies and Stability of a Flexible Spinning Disk-Stationary Load System With Rigid Body Tilting," *Journal of Applied Mechanics*, 60, pp. 470-477.
- [44] Nowinski, J.L., 1964, "Nonlinear Transverse Vibrations of a Spinning disk," *Journal of Applied Mechanics*, 31, pp. 72-78.
- [45] Baddour, N., Zu, J.W, 2001, "A revisit of spinning disk models. Part I: Derivation of equations of motion," *Applied Mathematical Modelling*, 25, 7, pp. 541-559
- [46] Jia, H. S., 2000, "Analysis of Transverse Runout in Rotating Flexible Disks by Using Galerkin's Method", *International Journal of Mechanical Sciences*, 42, pp. 237-248.
- [47] Benson, R.C., and Cole, K. A., 1991, "Transverse Runout of a Nonflat Spinning Disk," *Tribology Transactions*, 34, pp. 545-552.
- [48] Carpino, M., 1991, "The Effect of Initial Curvature in a Flexible Disk Rotating Near a Flat Plate," *ASME Journal of Tribology*, 113, pp. 355-360.
- [49] Chen, J.S. and Lin, C., 2005, "Axisymmetrical Snapping of a Spinning Nonflat Disk," *Journal of Applied Mechanics*, 72(6), pp. 879-886.

- [50] Chen, J.S. and Chang, Y., 2007, "On the Unsymmetrical Deformation and Reverse Snapping of a Spinning Non-Flat Disk," *International Journal of Non-Linear Mechanics*, 42(8), pp. 1000-1009.
- [51] Tobias, S.A., and Arnold, R.N., 1957, "The Influence of Dynamical Imperfections on Vibration of Rotating Disks," *Institution of Mechanical Engineers, Proceedings* 171, pp. 669-690.
- [52] Tobias, S.A., 1958, "Non-Linear Forced Vibrations of Circular Discs: an Experimental Investigation," *Engineering*, 186, pp. 51-56.
- [53] Thomas, O., Touze, C., and Chaigne, A., 2003, "Asymmetric Non-Linear Forced Vibrations of Free-Edge Circular Plates. Part II: Experiments," *Journal of Sound and Vibration*, 265, pp. 1075-1101.
- [54] Raman, A., and Mote, C.D., 2001, "Experimental Studies on the Non-Linear Oscillations of Imperfect Circular Disks Spinning Near Critical Speed," *International Journal of Non-Linear Mechanics*, 36, pp. 291-305.
- [55] D'Angelo, C., and Mote, C.D., 1993, "Aerodynamically Excited Vibration and Flutter of a Thin Disk Rotating at Supercritical Speed," *Journal of Sound and Vibration*, 168, pp. 15-30.
- [56] Raman, A., Hansen, M.H., and Mote, C.D., 2002, "A Note on the Post-Flutter Dynamics of a Rotating Disk," *Journal of Applied Mechanics*, 69, pp. 864-866 .
- [57] Kang, N, and Raman, A., 2006, "Vibrations and Stability of a Flexible Disk Rotating in a Gas-Filled Enclosure-Part 2: Experimental Study," *Journal of Sound and Vibration*, 296, pp. 676-68.
- [58] Jana, A., and Raman, A., 2005, "Nonlinear Aeroelastic Flutter Phenomena of a Flexible Disk Rotating in an Unbounded Fluid," *Journal of Fluids and Structures*, 20, pp. 993-1006
- [59] Jana, A., and Raman, A., 2005, "Nonlinear Dynamics of a Flexible Spinning Disc Coupled to a Precompressed Spring," *Nonlinear Dynamics*, 40, pp. 1-20.
- [60] Chen, J.S., 1999, "Steady State Deflection of a Circular Plate Rotating Near its Critical Speed," *Journal of Applied Mechanics*, 66, pp. 1015-1017.
- [61] Nayfeh, A. H., Jilani, A., and Manzione, P., 2001, "Transverse Vibrations of a Centrally Clamped Rotating Circular Disk," *Nonlinear Dynamics*, 26, pp. 163-178.

- [62] Chen, J.S., 2001, "On the Internal Resonance of a Spinning Disk Under Space-Fixed Pulsating Edge Loads," *Journal of Applied Mechanics*, 68, pp. 854-859.
- [63] Touze, C., Thomas, O., and Chaigne, A., 2002, "Asymmetric Non-linear Forced Vibrations of Free-Edge Circular Plates. Part 1: Theory," *Journal of Sound and Vibration*, 258, pp. 649-676.
- [64] Yang, L., and Hutton, S.G., 1998, "Nonlinear Vibrations of Elastically-Constrained Rotating Discs," *Journal of Vibration and Acoustics*, 120, pp. 475-483.
- [65] Luo, A.C.J., and Mote, C.D., 2000, "Nonlinear Vibration of Rotating Thin Disks", *Journal of Vibration and Acoustics*," 122, pp. 376-383.
- [66] Arafat, H.N., and Nayfeh, A.H., 2004, "Natural Frequencies of Heated Annular and Circular Plates," *International Journal of Solids and Structures*, 41, pp. 3031-3051.
- [67] Arafat, H. N. and Nayfeh, A. H., 2004, "Modal Interactions in the Vibrations of a Heated Annular Plate," *International Journal of Non-Linear Mechanics*, 39(10), pp. 1671-1685.
- [68] Arafat, H.N., and Nayfeh, A.H., 2004, "Combination Internal Resonances in Heated Annular Plates," *Nonlinear Dynamics*, 37, pp. 285-306.
- [69] Chen, J., and Hua, C., 2004, "On the Secondary Resonance of a Spinning Disk Under Space-Fixed Excitations," *ASME Journal of Vibration and Acoustics*, 126, pp. 422-429.
- [70] Heo, J.W., Chung, J., and Choi, K., 2003, "Dynamic Time Responses of a Flexible Spinning Disk Misaligned with the Axis of Rotation," *Journal of Sound and Vibration*, 262, pp. 25-44.
- [71] Raman, A., and Mote, C.D., 2001, "Effects of Imperfection on the Non-Linear Oscillations of Circular Plates Spinning Near Critical Speed," *International Journal of Non-Linear Mechanics*, 36, pp. 261-289.
- [72] Manzione, P., and Nayfeh, A.H., 2001, "Instability Mechanisms of a Centrally Clamped Rotating Circular Disk Under a Space-Fixed Spring-Mass-Dashpot System," *Journal of Vibration and Control*, 7, pp. 1013-1034.
- [73] Jalali, M.A., and Angoshtari, A., 2006, "Phase Space Structure of Spinning Disks," *International Journal of Non-Linear Mechanics*, 41, pp. 726-35.

Chapter 2- On the Effects of Rigid Body Translational Mode*

2.1. Introduction

Elastically constrained rotating circular disks constitute components in many important engineering applications. In some of these applications the disks may be elastically constrained and have rigid body degrees of freedom. In these cases rigid body degrees of freedom need to be considered in the analysis of the vibration response. Hutton, Chonan, and Lehmann [1] studied the dynamic response characteristics of rotating circular disks when subjected to the effect of forces produced by stationary spring guides. Mote [2] studied the effect of a collar (which was allowed to move freely on the arbor) on the stability of a guided rotating disk. Price [3] studied the dynamics of plates with clamped-free boundary conditions and studied the effect of a rigid body translational mode on the dynamic response of rotating plates. Tian and Hutton [4] developed an analytical model for modeling wood cutting of circular saws in order to understand the mechanism of washboarding. Jia [5] studied the vibration characteristics of a disk which has initial non-flatness.

Jana and Raman [6] investigated the nonlinear dynamics of a flexible spinning disk coupled to a precompressed spring. They studied large amplitude wave motions and their stability using the averaging method. Nayfeh, Jilani and Manzione [7] used the method of multiple scales to investigate the transverse nonlinear vibrations of a centrally clamped rotating circular disk. Yang and Hutton [8] used a polynomial expansion for the approximation function in the Galerkin method to solve the nonlinear equations of motion for rotating thin disks.

* A version of this chapter has been accepted for publication. Khorasany, R.M.H., and Hutton, S.G., 2010, "An Analytical Study on the Effect of Rigid Body Translational Degree of Freedom on the Vibration Characteristics of Elastically Constrained Rotating Disks", *International Journal of Mechanical Sciences*.

Among all of the works that have been done so far in this subject, only a few of them have been concerned with the effect of rigid body degrees of freedom on the stability characteristics of spinning disks. Chen and Wong [9] used finite element analysis to study the effect of evenly fixed spaced springs on the divergence instability of rotating disks which have translation degrees of freedom. Yang [10] studied the transverse vibration of a disk with free-free boundary conditions and studied the effect of translational and tilting rigid body degrees of freedom. He used numerical techniques to study the effect of rigid body degrees of freedom on the vibrations of a spinning disk.

In this chapter, previous numerical work is generalized by the use of an analytical approach to investigate the stability characteristics of an elastically constrained spinning disk with one space fixed spring, around a critical speed. In order to do so, a three mode approximation is used around the critical speed and it is shown that the disk is neutrally stable at its critical speed. It is also confirmed that the critical speed does not change with changing the spring stiffness and it is the same as for the unguided disk

For a spinning disk, the rigid body translational mode may interact with a forward, a backward or a reflected wave. An analytical approach is taken to investigate the stability characteristics of the guided disk for each of the above three types of interaction.

2.2. Linear Equations of Motion

A flexible spinning disk having a rigid body translational degree of freedom is considered. The inner radius of the disk is “a”, its outer radius is “b” and its thickness is ‘h’. The disk is assumed to be elastically constrained with one space fixed spring. The disk is rotating with an angular speed Ω about the z axis and is free to have rigid body translation along the z axis. Figure 2. 1 presents a schematic diagram of the annular spinning disk.

In this chapter, we assume that the disk is capable of having rigid body translation. A flexible disk without having any rigid body degrees of freedom has three components of acceleration in the z direction: bending, Coriolis and centrifugal acceleration. When rigid body translation is added to the system, one more component of acceleration (rigid body translational acceleration, \ddot{Z}_0) should be taken into account. This component of acceleration is uniform in the disk domain. By simply adding this component of

acceleration to the left hand side of the equation of motion (Hutton et. al. [1]), one can find the governing equation for the bending of the spinning disk (Eq. (2.1)). It has to be noted that we assume that there is no lateral external force acting on the disk.

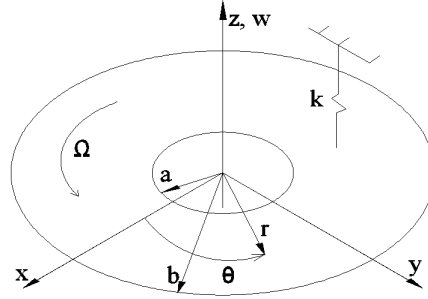


Figure 2. 1. A guided rotating disk with rigid body degrees of freedom

In addition to the governing equation for the disk bending, we need one more equation which governs the rigid body translational motion in the z direction. The same components of acceleration that have been stated above are potentially present in the governing equation for the rigid body motion and one has to find the net effect of them on the rigid body motion. It has to be emphasized that that the Coriolis and centrifugal accelerations only exist for the preferential modes. Therefore, the net effect of these two terms in the governing equation of rigid body motion in the z direction is zero. The only two remaining acceleration components are: rigid body acceleration and bending acceleration. One has to integrate the bending acceleration over the disk area to find the effect of this component of acceleration on the motion of the spinning disk in the z direction. Since the disk is elastically constrained, the spring exerts a force in the z direction that appears in both of the governing equations. Therefore, the non-dimensionalized equations of motion for an elastically constrained flexible spinning disk having rigid body translational degrees of freedom are obtained to be

$$\frac{\partial^2 w}{\partial t^2} + 2\Omega \frac{\partial^2 w}{\partial \theta \partial t} + \Omega^2 \frac{\partial^2 w}{\partial \theta^2} + \nabla^4 w - \frac{\Omega^2}{b^2} (C_{rr} w_{,rr} + C_r w_{,r} + C_{\theta\theta} w_{,\theta\theta}) + \ddot{Z}_0 = -(k/r) \delta(r - r^k) \delta(\theta - \theta^k) [w(r, \theta, t) + Z_0] \quad (2.1)$$

$$A_D \ddot{Z}_0 + \int_0^{2\pi} \int_a^b \frac{\partial^2 w}{\partial t^2} r dr d\theta + k [w(r^k, \theta^k, t) + Z_0] = 0, \quad (2.2)$$

where the relation between the actual parameters and normalized parameters (shown with prime) are

$$r' = \frac{r}{b}, \quad w' = \frac{bw}{h^2}, \quad Z'_0 = \frac{bZ_0}{h^2}, \quad t' = tT, \quad \Omega' = \frac{1}{T}\Omega, \quad k' = \frac{b^4}{D}k, \quad T = \frac{(D/\rho h)^{1/2}}{b^2}.$$

where w is the transverse deflection of the disk, Z_0 is the rigid body translational degree of freedom, ρ is disk density, E is Young's modulus, ν is Poisson's ratio, A_D is the area of the disk, D is the disk rigidity, Ω is the rotation speed, $\delta(\)$ is the Dirac delta function and k is the stiffness of the spring and (r^k, θ^k) is its space fixed polar location in the inertial coordinate system. In the current paper it is assumed that the disk is rigidly fixed in its inner boundary to a collar. The collar is capable of having rigid body translation in the z direction. C_{rr} , C_r and $C_{\theta\theta}$ are constants defining the in-plane stresses due to rotation found from the following equations

$$\begin{aligned} C_{rr} &= C_1 + \frac{C_2}{r^2 b^2} + C_3 r^2 b^2, \\ C_r &= b \left(\frac{C_1}{rb} - \frac{C_2}{r^3 b^3} + 3C_3 rb \right), \\ C_{\theta\theta} &= b^2 \left(\frac{C_1}{r^2 b^2} - \frac{C_2}{r^4 b^4} + C_4 \right), \end{aligned}$$

where

$$\begin{aligned} C_1 &= \frac{1+\nu}{8} \frac{(\nu-1)a^4 - (3+\nu)b^4}{(\nu-1)a^2 - (1+\nu)b^2}, \\ C_2 &= \frac{1-\nu}{8} a^2 b^2 \frac{(\nu+1)a^2 - (3+\nu)b^2}{(\nu-1)a^2 - (1+\nu)b^2}, \\ C_3 &= -(3+\nu)/8, \\ C_4 &= -(1+3\nu)/8. \end{aligned}$$

2.3. Interaction Between a Backward Traveling Wave and Its Complex Conjugate with Rigid Body Translational Mode

In order to investigate the stability of a guided disk at around its critical speed, a three mode approximation is used here. Let's consider the following approximation for the eigenfunction of the disk at around its critical speed

$$\tilde{w}(r, \theta, t) = \tilde{R}_{mn}^w(r) [c_1^w e^{+im\theta} + c_2^w e^{-im\theta}] + Z_0, \quad (2.3)$$

where i is the imaginary unit ($\sqrt{-1}$), $\tilde{R}_{mn}^w(r)$ is the mode shape in the radial direction of the disk at round its critical speed. $\tilde{R}_{mn}^w(r)e^{+im\theta}$ and $\tilde{R}_{mn}^w(r)e^{-im\theta}$ are the backward and forward traveling waves, respectively, and c_1^w and c_2^w are their associated expansion coefficients, respectively. It is assumed that m is positive. In order to simplify the equation of motion, we assume the natural frequency of the disk without rigid body degrees of freedom in the vicinity of the critical speed and in the inertial frame to be $\tilde{\omega}_{mn}$. Indeed at the critical speed one of the natural frequencies of the system is zero. Therefore using Eq. (2.1) and ignoring the rigid body translation mode we can see that

$$\left[\Omega^2 \frac{\partial^2}{\partial \theta^2} + \nabla^4 - \frac{\Omega^2}{b^2} \left(C_{rr} \frac{\partial^2}{\partial r^2} + C_r \frac{\partial}{\partial r} + C_{\theta\theta} \frac{\partial^2}{\partial \theta^2} \right) \right] \tilde{R}_{mn}^w(r) e^{\pm im\theta} = \tilde{\omega}_{mn} (\tilde{\omega}_{mn} \pm 2m\Omega) \tilde{R}_{mn}^w(r) e^{\pm im\theta}. \quad (2.4)$$

It is assumed that the spring acts at $r=1$ and $\theta=0$ and its stiffness is k . After substituting Eq. (2.3) into Eqs. (2.1) and (2.2) and using the general relation stated in Eq. (2.4) and then utilizing the Galerkin's projection the following coupled linear equations are obtained

$$\tilde{M} \ddot{\tilde{x}} + \tilde{G} \dot{\tilde{x}} + \tilde{K} \tilde{x} = 0, \quad (2.5)$$

$$\tilde{x} = \begin{Bmatrix} c_1^w \\ c_2^w \\ Z_0 \end{Bmatrix}, \quad \tilde{M} = \begin{bmatrix} 1 & 0 & 0 \\ 0 & 1 & 0 \\ 0 & 0 & A_D \end{bmatrix}, \quad \tilde{G} = \begin{bmatrix} 2m\Omega i & 0 & 0 \\ 0 & -2m\Omega i & 0 \\ 0 & 0 & 0 \end{bmatrix},$$

$$\tilde{K} = \begin{bmatrix} S_{mn} + kR^2 & kR^2 & kR \\ kR^2 & S_{mn} + kR^2 & kR \\ kR & kR & k \end{bmatrix},$$

where k is the stiffness of the spring and $R = \tilde{R}_{mn}^w(1)$. It should be mentioned that the natural frequencies of the two traveling waves interacting at the critical speed are the same but with opposite signs; therefore S_{mn} is the same for both of the interacting traveling waves and equals $\tilde{\omega}_{mn} (\tilde{\omega}_{mn} + 2m\Omega)$. In this equation $\tilde{\omega}_{mn}$ is assumed to be positive at the speed lower than the critical speed and negative for the speeds above the critical speed. If we substitute $e^{\lambda t}$ instead of $\tilde{x}(t)$ in Eq. (2.5), the characteristic equation is:

$$\alpha_1 \lambda^6 + \alpha_2 \lambda^4 + \alpha_3 \lambda^2 + \alpha_4 = 0, \quad (2.6)$$

where

$$\begin{aligned} \alpha_1 &= A_D, \\ \alpha_2 &= A_D(2kR^2 + 2S_{mn} + 4m^2\Omega^2) + k, \\ \alpha_3 &= A_D S_{mn}(2kR^2 + S_{mn}) + 2k(2m^2\Omega^2 + S_{mn}), \\ \alpha_4 &= k S_{mn}^2. \end{aligned}$$

Eq. (2.6) is a third order polynomial equation in terms of λ^2 . Therefore in order to have three distinct roots for λ^2 , the discriminant of Eq. (2.6) should be positive. The discriminant of the above equation is:

$$\Delta = -4\alpha_2^3\alpha_4 + \alpha_2^2\alpha_3^2 - 4\alpha_1\alpha_3^3 + 18\alpha_1\alpha_2\alpha_3\alpha_4 - 27\alpha_1^2\alpha_4^2. \quad (2.7)$$

After substituting $\alpha_1, \alpha_2, \alpha_3$ and α_4 into Eq. (2.7), the discriminant is found to have the following form

$$\Delta = \beta_5 S_{mn}^5 + \beta_4 S_{mn}^4 + \beta_3 S_{mn}^3 + \beta_2 S_{mn}^2 + \beta_1 S_{mn} + \beta_0, \quad (2.8)$$

where

$$\beta_0 = 16m^4\Omega^4k^2 \left[(4R^4A_D^2 + 1 + 4R^2A_D)k^2 + (16R^2A_D^2m^2\Omega^2 - 8m^2\Omega^2A_D)k + 16m^4\Omega^4A_D^2 \right] \quad (2.9a)$$

$$\beta_1 = 8m^2\Omega^2(2 + 8A_D^3R^6 + 16A_D^4R^4 + 10A_DR^2)k^4 + 64m^4\Omega^4(2A_D^2R^2 - 3A_D + 4A_D^3R^4)k^3 + 256m^6\Omega^6A_D^2(A_DR^2 + 2)k^2, \quad (2.9b)$$

$$\beta_2 = 4R^4A_D^2(1 + 4R^4A_D^2 + 4R^2A_D)k^4 + 8m^2\Omega^2A_D(-10R^2A_D + 8R^6A_D^3 - 8R^4A_D^2 - 8)k^3 + 32m^4\Omega^4A_D^2(4R^2A_D^3 + 11 + 8R^4A_D^2)k^2 - 128m^6\Omega^6A_D^3k, \quad (2.9c)$$

$$\beta_3 = 8R^4A_D^3(2R^2A_D - 1)k^3 + 16m^2\Omega^2A_D^2(6 + 8R^4A_D^2 - 5R^2A_D)k^2 + 64m^4\Omega^4A_D^3(-3 + R^2A_D), \quad (2.9d)$$

$$\beta_4 = 4R^4A_D^4k^2 + 8m^2\Omega^2A_D^3(10R^2A_D - 8)k + 16m^4\Omega^4A_D^4, \quad (2.9e)$$

$$\beta_5 = 16m^2\Omega^2A_D^4. \quad (2.9f)$$

In a very close vicinity of the critical speed, $\tilde{\omega}_{mn}$ is very close to zero. Therefore in the vicinity of critical speed we can conclude that $S_{mn} \ll 1$. As a result, it may be concluded from Eq. (2.8) that the only term which affects the sign of the discriminant in the vicinity of the critical speed is β_0 . From Eq. (2.9a) it can be seen that β_0 is a fourth order equation in terms of k . As shown in this equation, k^2 can be factored out and these

remains a second order polynomial equation in terms of k . So β_0 can be written as $16m^4\Omega^4k^2\beta'_0$ where

$$\beta'_0 = (4R^4A_D^2 + 1 + 4R^2A_D)k^2 + (16R^2A_D^2m^2\Omega^2 - 8m^2\Omega^2A_D)k + 16m^4\Omega^4A_D^2 \quad (2.10)$$

Therefore, the sign of the discriminant in the close vicinity of the critical speed depends upon the sign of β'_0 . β'_0 is a second order polynomial equation in terms of k . If we put $\beta'_0 = 0$, the two roots of the equation for the stiffness are obtained to be

$$k_{1,2} = -\frac{4(2A_DR^2 - 1 \pm 2R\sqrt{-2A_D})Am^2\Omega^2}{1 + 4R^4A_D^2 + 4R^2A_D}. \quad (2.11)$$

Since A_D is always positive, from Eq. (2.11) it can be seen that the numerator is imaginary. Therefore, there is no real root for k which can make β' to be zero, based on Eq. (2.10). The coefficient of the second order term (k^2) in Eq. (2.11) is positive. Therefore it can be concluded that β'_0 is always positive in the close vicinity of the critical speed for any value of k . As a result of that the discriminant of Eq. (2.6) is always positive. This implies that the characteristics equation has always three real roots for λ^2 in the vicinity of the critical speed. In a close vicinity of the critical speed $\alpha_1, \alpha_2, \alpha_3$ and α_4 are always positive for any value of k . This means that the three real roots for λ^2 must be negative which implies that all the eigenvalues at around the critical speed are imaginary. Indeed, the guided disk does not experience divergence type instability in the vicinity of the critical speed. If we substitute $\tilde{\omega}_{mn} = 0$ into Eq. (2.6) we can see that one of the roots for λ is zero which implies that by adding a spring to the system the critical speed does not change and remains the same as the one for an unguided disk. In order to investigate this issue numerically, a disk made of steel with clamped-free boundary conditions is considered. It is assumed that $E = 2e11 N/m^2, \nu = 0.3, \rho = 7800 kg/m^3, \eta = a/b = 0.3529, b = 0.2159 m, h = 1.27 mm$. In Figure 2. 2 comparisons between the normalized natural frequencies of the guided disk when $k = 0.057$ and $k = 2.85$ (broken lines) with the unguided disk (solid lines) are carried out. It should be emphasized that $k = 0.057$ and $k = 2.85$ are normalized stiffness and the actual corresponding stiffness are

10^3 N/m and $5 \times 10^4 \text{ N/m}$, respectively. In this figures (m,n)b means the backward traveling wave of the (m,n) mode and ‘RB’ stands for the rigid body translational mode. It can be seen that by adding a spring to the system, at a critical speed of the unguided disk, divergence instability is not induced. In fact, the guided disk has the same critical speeds as the unguided disk.

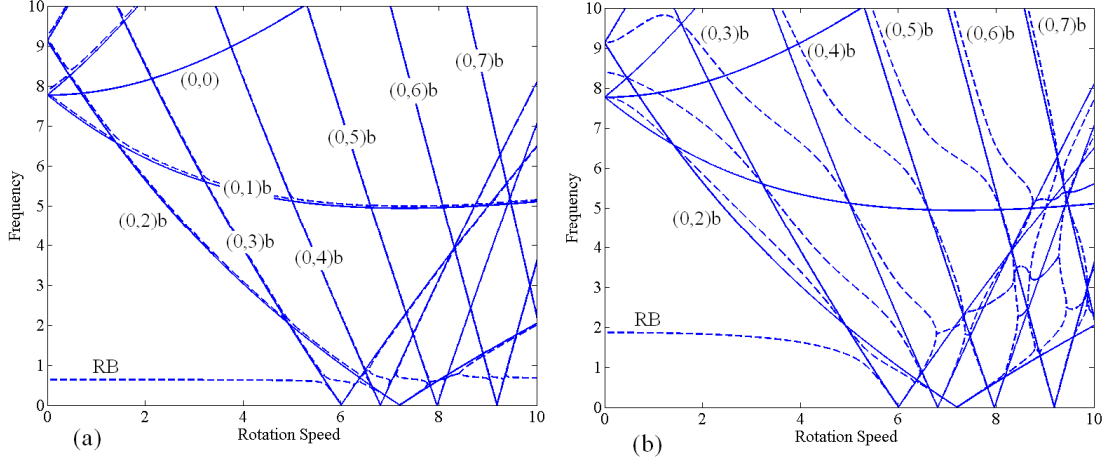


Figure 2. 2. Normalized natural frequencies of the guided disk (shown with the broken lines) versus normalized speed when (a) $k = 0.057$ and (b) $k = 2.85$. The solid lines show the normalized natural frequencies of the unguided disk

2.4. Interaction Between a Forward or Backward or Reflected Traveling Wave with Rigid Body Translational Mode

Another interesting issue that we can look at is the interaction of rigid body translational mode with another bending mode at speeds other than the critical speed. Generally we have three types of interactions and they happen when the rigid body translational mode interacts with a forward, backward or a reflected traveling wave mode. In order to investigate these three types of interactions, we can use the following approximation for the eigenfunction of the rotating disk:

$$\tilde{w}(r, \theta, t) = c_1^w \tilde{R}_m^w(r) e^{im\theta} + Z_0, \quad (2.12)$$

where $\tilde{R}_m^w(r) e^{im\theta}$ is the backward or forward traveling wave component (depending on the sign of m) and c_1^w is its associated expansion coefficient. When m is negative, the assumed mode is either a forward or reflected wave and when m is positive, the assumed

mode is a backward wave mode. After substituting Eq. (2.12) into Eqs. (2.1) and (2.2) and utilizing the Galerkin's projection the following coupled linear equations are obtained

$$\tilde{M} \ddot{\tilde{x}} + \tilde{G} \dot{\tilde{x}} + \tilde{K} \tilde{x} = 0, \quad (2.13)$$

where

$$\tilde{x} = \begin{Bmatrix} \tilde{c}_1^w \\ Z \end{Bmatrix}, \quad \tilde{M} = \begin{bmatrix} 1 & 0 \\ 0 & A_D \end{bmatrix}, \quad \tilde{G} = \begin{bmatrix} 2m\Omega i & 0 \\ 0 & 0 \end{bmatrix},$$

$$\tilde{K} = \begin{bmatrix} S_{mn} + kR^2 & kR \\ kR & k \end{bmatrix},$$

where S_{mn} equals $\tilde{\omega}_{mn}(\tilde{\omega}_{mn} + 2m\Omega)$. It is important to note that S_{mn} is less than zero when we deal with a reflected wave and greater than zero when we deal with a backward or forward traveling wave. After substitution of $\tilde{x} = Xe^{\lambda t}$ into Eq. (2.13), the following characteristic equation is obtained

$$A_D \lambda^4 + 2im\Omega A_D \lambda^3 + (A_D S_{mn} + A_D kR^2 + k) \lambda^2 + 2im\Omega k \lambda + S_{mn} k = 0. \quad (2.14)$$

We assume that $\lambda = i\omega$ where ω is a real number. After substitution of $\lambda = i\omega$ into Eq. (2.14), the following characteristics equation is obtained

$$f(\omega, k) = A_D \omega^4 + 2m\Omega A_D \omega^3 - (A_D S_{mn} + A_D kR^2 + k) \omega^2 - 2m\Omega k \omega + S_{mn} k = 0 \quad (2.15)$$

For a backward or forward wave it may be noted that $S_{mn} k$ is always positive. The general shape of $f(\omega, k)$ for any given values of k using the characteristics of a backward or forward traveling wave is shown in Figure 2. 3. As it can be seen from this figure, when $\omega = 0$, $f(\omega, k)$ is greater than zero. In order to show that when a backward or forward traveling wave interacts with the rigid body translational mode flutter type instability is not induced, we have to prove that Eq. (15) has always four real roots for a backward or forward wave.

At first consider a backward traveling wave. If we substitute $\omega_1 = -\tilde{\omega}_{mn} - 2m\Omega$ into Eq. (2.15), the following expression is found

$$f(-\tilde{\omega}_{mn} - 2m\Omega, k) = -kR^2 A_D (\tilde{\omega}_{mn} + 2m\Omega)^2. \quad (2.16)$$

Also if we substitute $\omega_2 = \tilde{\omega}_{mn}$ into Eq. (2.15), the following expression is found

$$f(\tilde{\omega}_{mn}, k) = -kR^2 A_D (\tilde{\omega}_{mn})^2. \quad (2.17)$$

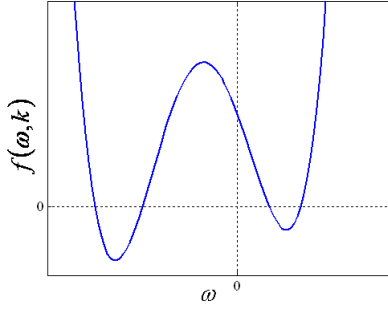


Figure 2. 3. A general shape for $f(\omega, k)$ using the characteristics of a backward or forward traveling wave

From Eqs. (2.16) and (2.17) it can be seen that at $\omega_1 = -\tilde{\omega}_{mn} - 2m\Omega$ and $\omega_2 = \tilde{\omega}_{mn}$, $f(\omega, k)$ is always negative for a backward traveling wave. For a backward or forward traveling wave, ω_2 is always positive. For a backward traveling wave ω_1 is always negative. For a forward traveling wave, ω_1 is negative for the speeds less than the critical speed and for the speeds above the critical speed it is positive. Therefore, for a forward traveling wave we use $\omega_3 = -\sqrt{k/A_D}$, instead of ω_1 , which is always a negative real value. If we substitute ω_3 into Eq. (2.15), the following expression is obtained

$$f\left(-\sqrt{k/A_D}, k\right) = -kR^2. \quad (2.18)$$

This equation implies that for a backward or forward traveling wave, there always exists a point in the left and right hand side of the vertical axis (Figure 2. 3) at which $f(\omega, k)$ is less than zero. Also in order to show that the plotted graph (Figure 2. 3) is a general shape of $f(\omega, k)$ for a backward or forward traveling wave, we also have to show that $f(\omega, k)$ has two inflection points. If we differentiate Eq. (2.15) with respect to ω , the following equation is obtained

$$\frac{\partial^2 f}{\partial \omega^2} = 12A_D\omega^2 + 12m\Omega A_D\omega - 2(A_D S_{mn} + A_D kR^2 + k) \quad (2.19)$$

Eq. (2.19) is a second order polynomial in terms of ω . Since the coefficients of the second and zero order terms have opposite signs, therefore the discriminant of the above equation is always greater than zero. As a result of that, Eq. (2.15) always has two inflection points. Having two inflection points for $f(\omega, k)$ implies that this function always has two local minima and one local maximum. Therefore based on the above

reasonings, Figure 2. 3 is a general shape of $f(\omega, k)$ for a backward or forward traveling wave.

Finally since $f(\omega, k)$ always has two local minima and one local maximum and also since this function is positive at $\omega = 0$ and negative at $\omega = \omega_1$ and $\omega = \omega_2$ for a backward wave (and negative at $\omega = \omega_1$ and $\omega = \omega_3$ for a forward traveling wave) ; it can be concluded that this function always has four real roots. Two of the real roots are positive and the other two are negative values. This implies that the interaction between the rigid body translational mode and a backward or forward traveling wave does not induce flutter type instability.

When the rigid body translational mode interacts with a reflected traveling wave mode, the situation is different and speed dependent. As was mentioned above, for a reflected traveling wave, S_{mn} is negative. Eq. (2.15) can be decomposed into two parts: the first part which does not depend upon the spring stiffness and the second part which depends upon the spring stiffness. Therefore we can write Eq. (2.15) in the following from

$$f(\omega, k) = f_1(\omega, k) + f_2(\omega, k), \quad (2.20)$$

where

$$\begin{aligned} f_1(\omega, k) &= A_D \omega^4 + 2m\Omega A_D \omega^3 - A_D S_{mn} \omega^2, \\ f_2(\omega, k) &= -(A_D k R^2 + k) \omega^2 - 2m\Omega k \omega + S_{mn} k. \end{aligned}$$

$f_2(\omega, k)$ is a second order polynomial equation in terms of ω . The discriminant of this equation ($f_2(\omega, k)$) is found to be

$$\Delta = 4k^2 [m^2 \Omega^2 + (A_D R^2 + 1) S_{mn}] \quad (2.21)$$

As can be seen from Eq. (2.21), the sign of the discriminant does not depend upon the stiffness of the spring. The sign only depends upon the speed, the mode itself and the disk characteristics such as area and also the radial position of the spring. Since S_{mn} is negative for a reflected wave, the two roots of $f_1(\omega, k)$ are positive real values and the other two roots are zero. There are two possibilities: either the discriminant of $f_2(\omega, k)$ is negative or positive. As a first step we assume that the discriminant of $f_2(\omega, k)$ is positive. In this case $f_2(\omega, k)$ has two real solutions for ω for any given value of spring

stiffness and both of them are negative real values. Figure 2. 4 shows a typical plot for $f_1(\omega, k)$ and $f_2(\omega, k)$ (using Eqs. (2.16) and (2.17) and the fact that ω_1 and ω_2 are the real roots of $f_1(\omega, k)$). By increasing the stiffness of the spring, the local maxima of $f_2(\omega, k)$ moves upward. This figure shows the plot of $f_2(\omega, k)$ for a relatively small and large value of spring stiffness (k). From this graph it can be seen that for a sufficiently small value of spring stiffness, $f(\omega, k)$ has four real roots of which three of them are positive and the fourth one is negative. If the stiffness is further increased to a certain level (e.g. stiffness is equal to k_1^-), a situation is reached at which $f(\omega, k)$ only intersects the horizontal axis at two points. This case can be qualitatively verified from Figure 2. 4 when the spring stiffness is relatively high. This point is the starting point of flutter type instability. It should be noted that k_1^- depends upon the mode, disk characteristics and rotation speed.

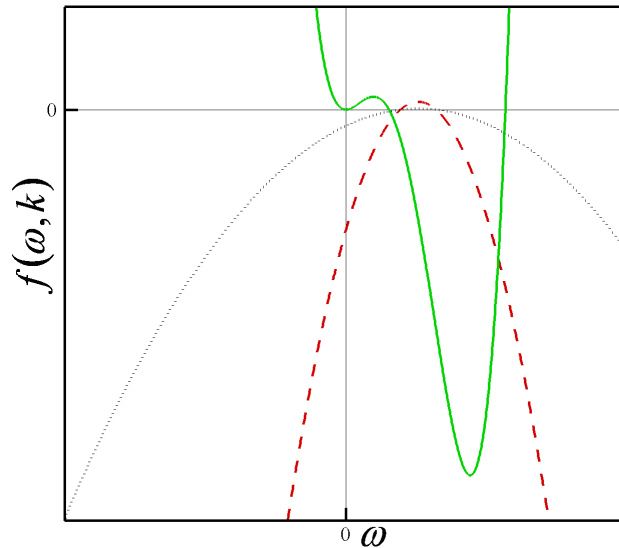


Figure 2. 4. A typical plot of $f_1(\omega, k)$ (solid line) and $f_2(\omega, k)$ for a relatively small (dotted line) and large (dashed line) value of k when the discriminant of $f_2(\omega, k)$ is positive

Since the discriminant of $f_2(\omega, k)$ is assumed to be positive, it can be concluded that the maximum value of $f_2(\omega, k)$ for any given value of spring stiffness is always positive. So if the stiffness is further increased (e.g. stiffness is equal to k_1^+) a situation is reached in which $f(\omega, k)$ starts to have four real roots again. In this case again, three of the real

roots are positive real values and the last one is negative. This stiffness (k_1^+) corresponds to the stiffness for which the flutter type instability disappears for a given rotation speed. Therefore at any speed that the discriminant of $f_2(\omega, k)$ is positive when $k_1^- < k < k_1^+$, the interaction of the backward wave and rigid body translational does not produce flutter type instability. Determination of the explicit values for k_1^+ and k_1^- is difficult.

Another possible situation is that the discriminant of $f_2(\omega, k)$ is less than zero. In this case $f_2(\omega, k)$ does not have any real roots. Also for any given value of the spring stiffness, $f_2(\omega, k)$ is always negative as shown in Figure 2. 5. One of the major differences between this situation and the previous situation is that $f_2(\omega, k)$ always lies below the horizontal axis for a nonzero given value of spring stiffness. In this case, when the spring stiffness is relatively small, $f(\omega, k)$ has four real roots of which three of them are positive and the fourth one is negative.

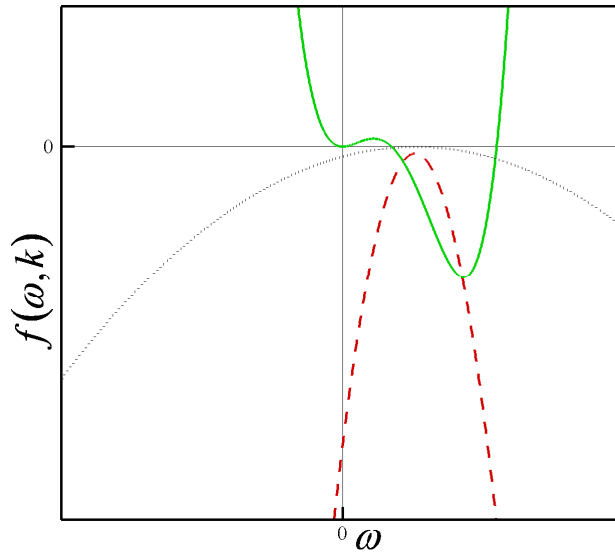


Figure 2. 5. A typical plot of $f_1(\omega, k)$ (solid line) and $f_2(\omega, k)$ for a relatively small (dotted line) and large (dashed line) value of k when the discriminant of $f_2(\omega, k)$ is negative

From Figure 2. 5 it can be seen that by increasing the stiffness of the spring to a certain level (k_2^-), a situation is reached at which $f(\omega, k)$ does not have four real roots any more. In this case, a flutter type instability is induced due to interaction between the rigid body mode and the reflected wave. From Figure 2. 5, it may be noted that by further

increasing the spring stiffness the flutter type instability does not disappear. Therefore, for any $k > k_2^-$, the disk loses its stability due to flutter type instability.

Figure 2. 6 shows non-dimensional natural frequencies (measured by a stationary observer) plotted against non-dimensional speed of the spinning disk with clamped-free boundary conditions for different levels of spring stiffness. The spring stiffnesses in this figure are normalized. It is assumed that the disk has a rigid body translational degree of freedom, as explained previously.

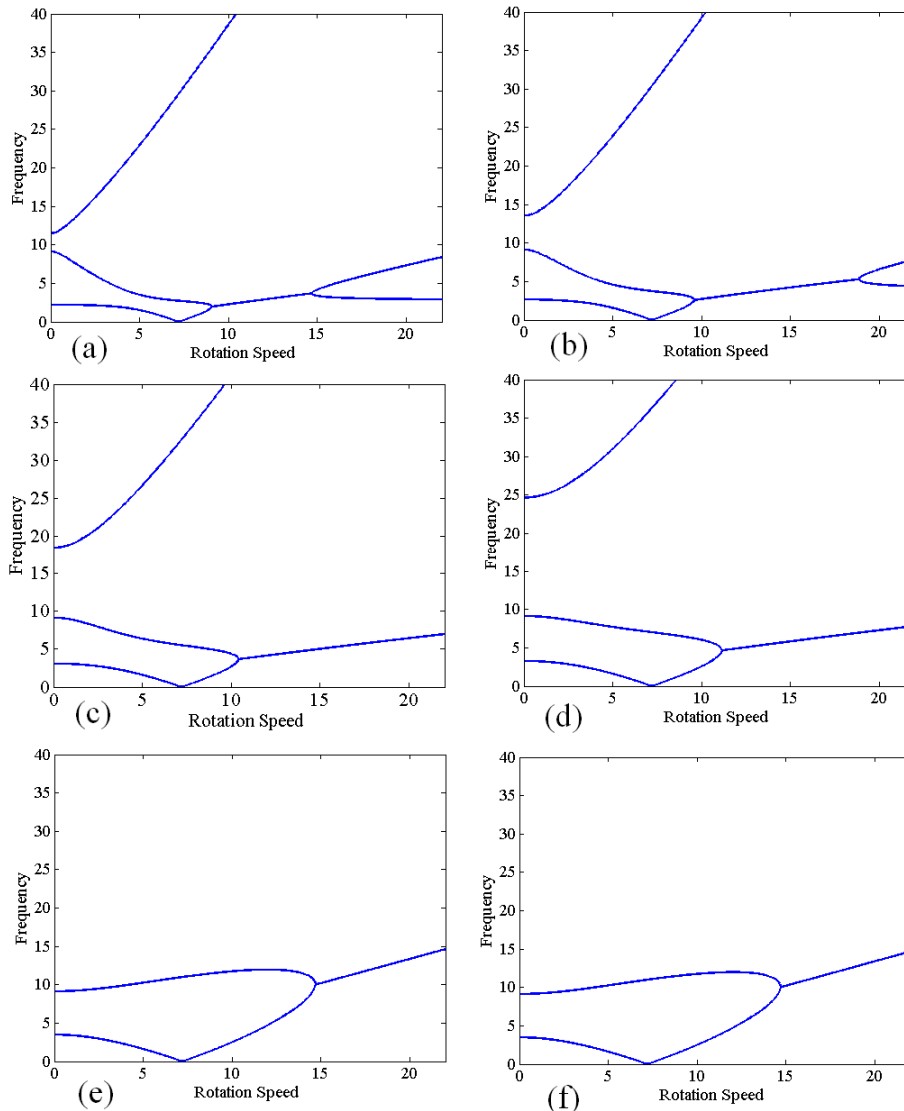


Figure 2. 6. The interaction between the (0,2) mode of the clamped disk with rigid body translational mode when (a) $k = 1$, (b) $k = 2$, (c) $k = 5$, (d) $k = 10$, (e) $k = 10^4$ and (f) $k = 10^6$

In Figure 2. 6, a two-mode approximation is used and the interaction between the (0,2) bending mode and the rigid body translation mode is investigated. The response depends upon the relationship between the magnitude of the spring stiffness and the bending stiffness of the (0,2) mode. For sufficiently high values of k the spring behaves as a rigid support. It can be seen that when the reflected wave of (0,2) mode interacts with the rigid body translational mode, flutter type instability is induced. It may be noted that as the stiffness increases up to $k = 10^4$, the region of flutter type instability moves toward higher speeds.

By a comparison between Figure 2. 6e and Figure 2. 6f it may be noted that although the spring stiffness is increased above 10^4 the response does not change and thus the spring acts as a rigid support and the starting point of flutter type instability is the same for both of these plots ($k = 10^4$ and $k = 10^6$) and occurs at $\Omega = 14.72$. This speed corresponds to the starting region of speeds at which the discriminant of $f_2(\omega, k)$ is negative. As can be seen from these figure, when the stiffness changes from $k = 10^4$ to $k = 10^6$, the starting point of flutter type instability regions does not change. Also for any speed greater than $\Omega = 14.72$, there is a threshold of the stiffness such that if the spring stiffness exceeds this threshold, the disk loses its stability due to flutter instability and never disappears. This flutter instability is induced due to interaction between the rigid body translational mode and the reflected wave of (0,2) mode. It is difficult to find an explicit value for the speed at which the gradient of $f_2(\omega, k)$ starts to be negative and also to find the stiffness threshold that was discussed above.

2.5. Conclusions

Using analytical calculations, the effect of rigid body translational motion on the stability characteristics of an elastically constrained disk with only one space fixed spring was studied. It was shown that because of the effect of the rigid body translational degree of freedom, divergence instability does not take place. In fact, it was shown that in this case the guided disk still has the same critical speeds as the unguided disk. This result corresponds to the fact that the bending wave speed in the disk is not altered by the presence of a point constraint.

Using analytical calculations, it was shown that the interaction of a forward or backward traveling wave with the rigid body translational mode does not induce flutter type instability. When the rigid body translational mode interacts with a reflected traveling wave, there are two possibilities: the discriminant of $f_2(\omega, k)$ is (i) positive or (ii) negative. It was shown that in the first case (discriminant is positive) there is a range of spring stiffness ($k_1^- < k < k_1^+$) for which flutter type instability will be induced. In the second case (discriminant is negative), if the spring stiffness exceeds a certain value ($k > k_2^-$), then flutter instability will be induced and never disappear as the spring stiffness is increased.

2.6. References

- [1] Hutton, S.G., Chonan, S., and Lehmann, B.F., 1987, "Dynamic Response of a Guided Circular Saw," *Journal of Sound and Vibration*, 112, pp. 527-539.
- [2] Mote, C.D., 1977, "Moving Load Stability of a Circular Plate on a Floating Central Collar," *Journal of Acoustical Society of America*, 61, pp. 439-447.
- [3] Price, K.B., 1987, "Analysis of the Dynamics of Guided Rotating Free Center Plates," Ph.D. Dissertation, University of California, Berkeley.
- [4] Tian, J.F., and Hutton, S.G., 2001, "Cutting-Induced Vibration in Circular Saws," *Journal of Sound and Vibration*, 242, pp. 907-922.
- [5] Jia, H. S., 2000, "Analysis of Transverse Runout in Rotating Flexible Disks by Using Galerkin's Method," *International Journal of Mechanical Sciences*, 42, pp. 237-248.
- [6] Jana, A., and Raman, A., 2005, "Nonlinear Dynamics of a Flexible Spinning Disc Coupled to a Precompressed Spring," *Nonlinear Dynamics*, 40, pp. 1-20.
- [7] Nayfeh, A. H., Jilani, A., and Manzione, P., 2001, "Transverse Vibrations of a Centrally Clamped Rotating Circular Disk," *Nonlinear Dynamics*, 26, pp. 163-178.
- [8] Yang, L., and Hutton, S.G., 1998, "Nonlinear Vibrations of Elastically-Constrained Rotating Discs," *Journal of Vibration and Acoustics*, 120, pp. 475-483.
- [9] Chen, J.S., and Wong, C.C., 1995, "Divergence Instability of a Spinning Disk with Axial Spindle Displacement in Contact With Evenly Spaced Stationary Springs," *Journal of Applied Mechanics*, 62, pp. 544-547.
- [10] Yang, S.M., 1993, "Vibration of a Spinning Annular Disk with Coupled Rigid-Body Motion," *Journal of Vibration and Acoustics*, 115, pp. 159-164.

Chapter 3- On the Effects of Initial Runout*

3.1. Introduction

Rotating disks have many industrial applications. However, no real disks are perfectly flat. Even if they are manufactured with the utmost care, imperfections will still exist. Although much research has been done on the subject of spinning disks [1-3], in most of these studies, the disk is assumed to be perfectly flat.

In some spinning disk applications, the lateral displacement of the disk is large compared to its thickness. For these, one must consider the effect of geometrical nonlinear terms in order to better predict the disk vibration behavior. Nowinski [4], one of the first researchers to study the nonlinear equations of motion of a spinning disk, presented a formulation for the nonlinear vibration of rotating disks. Later on, Yang and Hutton [5] used a polynomial approximation for the function in the Galerkin's method to solve the nonlinear equations developed by Nowinski. They studied the effect of geometrical nonlinear terms on the frequency behavior of a spinning disk.

All of the aforementioned researchers assumed that the disk was perfectly flat. There have been a few works in the literature concerned with the effect of initial runout on the dynamics of a spinning disk. Benson et al. [6] studied the effect of initial runout on the amplitude of oscillations, using both numerical and experimental techniques. At the same time, Carpino [7] investigated the effect of initial curvature of the dynamics of a disk rotating near a rigid surface. Later, Jia [8] used the linear equations of motion, which allow for initial non-flatness, to study the effect of initial runout on the amplitude of disk deflection. He also investigated its effect on in-plane stress distributions.

While the abovementioned studies employed linearized equations of motion, other literature has considered the effect of geometrical nonlinear terms on the response of a

* A version of this chapter has been accepted for publication. Khorasany, R.M.H., and Hutton, S.G., 2010, "The Effect of Axisymmetric Non-Flatness on the Oscillation Frequencies of a Rotating Disk," ASME Journal of Vibration and Acoustics.

non-flat spinning disk. Chen et al. [9] used the nonlinear governing equations of motion to investigate the impact of symmetrical initial runout on the amplitude of spinning disk deflection. He concluded that depending on the shape and level of initial non-flatness, the disk may snap from one side to another. To verify his results, he used a warped disk with an initial level of non-flatness almost eight times higher than the disk thickness. In another work, Chen et al. [10] used the nonlinear equations of motion to consider an unsymmetrical initial non-flatness for the disk. In this paper, he studied the effect of unsymmetrical terms on the snapping speed while the disk was spinning.

To the best of our knowledge, no research has been done to date on the effect of the initial runout on the frequency behavior of a spinning disk. In this paper, we use the previously developed nonlinear governing equations of motion for a disk with an initial runout to study the effect of an assumed initial runout on the frequency behavior. The initial runout is assumed to be of the axisymmetric type. The equations of motion are expressed in a fixed frame to allow future studies to more conveniently study the effect of space fixed constraints. It is assumed that the bending deflection of the disk is small compared to its thickness. Accordingly, we can neglect some nonlinear terms in the equation of motion. Using Galerkin's method, the equations of motion are discretized. The developed equations are then used to study the effect of initial axisymmetric runout on the frequency behavior of the disk. The mechanism by which the frequency is affected by the lack of flatness is discussed. Also, the effect of the lack of flatness on the critical speed behavior of the disk is studied. For verification purposes, the numerical results are compared with those predicted by a commercial software.

3.2. Formulation

The normalized form of the equations of motion of a spinning disk with initial runout in an inertial frame is [10]

$$\begin{aligned} \frac{\partial^2 w}{\partial t^2} + 2\Omega \frac{\partial^2 w}{\partial \theta \partial t} + \Omega^2 \frac{\partial^2 w}{\partial \theta^2} + \nabla^4 (w - w_0) = \varepsilon w_{,rr} (r^{-1} \phi_{,r} + r^{-2} \phi_{,\theta\theta}) \\ + \varepsilon \phi_{,rr} (r^{-1} w_{,r} + r^{-2} w_{,\theta\theta}) - 2\varepsilon (r^{-1} w_{,\theta})_{,r} (r^{-1} \phi_{,\theta})_{,r} - \Omega^2 \left(\frac{1}{2} r^2 \nabla^2 w + r \frac{\partial w}{\partial r} \right), \end{aligned} \quad (3.1)$$

$$\begin{aligned} \nabla^4 \phi = & \left[-w_{,rr} (r^{-1}w_{,r} + r^{-2}w_{,\theta\theta}) + (r^{-1}w_{,r\theta} - r^{-2}w_{,\theta})^2 + w_{0,rr}^R (r^{-1}w_{0,r}^R + r^{-2}w_{0,\theta\theta}^R) \right. \\ & \left. - (r^{-1}w_{0,r\theta}^R - r^{-2}w_{0,\theta}^R)^2 \right] + 2\rho h(1-\nu)\Omega^2/\varepsilon. \end{aligned} \quad (3.2)$$

The equations of motion are non-dimensionalized using the following non-dimensional variables (the actual parameters are denoted by primes)

$$\begin{aligned} r = \frac{r'}{b}, \quad w = \frac{bw'}{h^2}, \quad w_0^R = \frac{bw_0'^R}{h^2}, \quad t = t'T, \quad \Omega = \frac{1}{T}\Omega', \quad D = Eh^3/12(1-\nu^2) \\ \phi' = \frac{b^2}{Eh^5}\phi, \quad T = \frac{(D/\rho h)^{1/2}}{b^2}, \quad \varepsilon = 12(1-\nu^2)h^2/b^2, \end{aligned}$$

where w_0^R is the initial deformation (non-flatness) of the disk, w is the transverse displacement, E is Young's modulus, ν is Poisson's ratio, h is the disk thickness, D is the flexural rigidity of the disk, ρ is the density, outer radius is b , and ϕ is the stress function. Ω is the rotation speed of the disk, measured in a polar coordinate system designated by (r, θ) .

In order to make the equations of motion easier to manipulate, the displacement field is defined as

$$u = w - w_0^R. \quad (3.3)$$

Substitution of the newly defined displacement field (Eq. (3.3)) into Eqs. (3.1) and (3.2), results in the following non-dimensionalized equations of motion:

$$\begin{aligned} \frac{\partial^2 u}{\partial t^2} + 2\Omega \frac{\partial^2 u}{\partial \theta \partial t} + \Omega^2 \frac{\partial^2 u}{\partial \theta^2} + \nabla^4 u = & \varepsilon(u + w_0^R)_{,rr} (r^{-1}\phi_{,r} + r^{-2}\phi_{,\theta\theta}) \\ & + \varepsilon\phi_{,rr} [r^{-1}(u + w_0^R)_{,r} + r^{-2}(u + w_0^R)_{,\theta\theta}] - 2\varepsilon(r^{-1}\phi_{,\theta})_{,r} [r^{-1}(u + w_0^R)_{,\theta}]_r \\ & - \Omega^2 \left(\frac{1}{2}r^2 \nabla^2 (u + w_0^R) + r(u + w_0^R)_{,r} \right), \end{aligned} \quad (3.4)$$

$$\begin{aligned} \nabla^4 \phi = & \left[-u_{,rr} (r^{-1}u_{,r} + r^{-2}u_{,\theta\theta}) + (r^{-1}u_{,r\theta} - r^{-2}u_{,\theta})^2 + 2(r^{-1}u_{,r\theta} - r^{-2}u_{,\theta}) \times \right. \\ & \left. (r^{-1}w_{0,r\theta}^R - r^{-2}w_{0,\theta}^R) - w_{0,rr}^R (r^{-1}u_{,r} + r^{-2}u_{,\theta\theta}) - u_{,rr} (r^{-1}w_{0,r}^R + r^{-2}w_{0,\theta\theta}^R) \right] \\ & + 2(1-\nu)\Omega^2/\varepsilon, \end{aligned} \quad (3.5)$$

In many industrial applications of spinning disks, the runout is nearly axisymmetric. Therefore, in this paper we study the effect of axisymmetric runout on the frequency behavior. Assuming that the initial runout is axisymmetric, the equations of motion can be simplified as follows:

$$\begin{aligned} \frac{\partial^2 u}{\partial t^2} + 2\Omega \frac{\partial^2 u}{\partial \theta \partial t} + \Omega^2 \frac{\partial^2 u}{\partial \theta^2} + \nabla^4 u = \varepsilon (u + w_0^R)_{,rr} (r^{-1} \phi_{,r} + r^{-2} \phi_{,\theta\theta}) \\ + \varepsilon \phi_{,rr} [r^{-1} (u + w_0^R)_{,r} + r^{-2} u_{,\theta\theta}] - 2\varepsilon (r^{-1} \phi_{,\theta})_{,r} (r^{-1} u_{,\theta})_{,r} \\ - \Omega^2 \left(\frac{1}{2} r^2 \nabla^2 (u + w_0^R) + r (u + w_0^R)_{,r} \right), \end{aligned} \quad (3.6)$$

$$\begin{aligned} \nabla^4 \phi = [-u_{,rr} (r^{-1} u_{,r} + r^{-2} u_{,\theta\theta}) + (r^{-1} u_{,r\theta} - r^{-2} u_{,\theta})^2 \\ - w_{0,rr}^R (r^{-1} u_{,r} + r^{-2} u_{,\theta\theta}) - r^{-1} u_{,rr} w_{0,r}^R] \\ + 2(1-\nu)\Omega^2/\varepsilon. \end{aligned} \quad (3.7)$$

Chen et al. [9] assumed that in the snapping phenomenon of a spinning disk with initial axisymmetric non-flatness, the deformations may be considered axisymmetric. They then simplified the equations of motion accordingly. Here, we do not make this assumption and it will be seen that the initial axisymmetric non-flatness can change the frequency behavior of all the modes. Eqs. (3.6-7) are the simplified nonlinear equations of motion. To discretize the equations of motion, we approximate the stress function and transverse displacement as the summation of known spatial functions with unknown time-dependent coefficients. Then, using Galerkin's method, we discretize the equations of motion.

The disk is assumed to have an inner radius 'a'. It is also assumed that it has clamped-free boundary conditions. Therefore, at the inner rim ($\eta = a/b$), the transverse displacement and its slope vanish as follows:

$$u = 0 \quad \text{at} \quad r = \eta, \quad (3.8)$$

$$u_{,r} = 0 \quad \text{at} \quad r = \eta. \quad (3.9)$$

At the outer rim, the bending moment and Kirchoff edge reaction are zero. In non-dimensional form, they can be expressed as follows:

$$\frac{\partial}{\partial r} \nabla^2 u + \frac{1-\nu}{r^2} \frac{\partial^2}{\partial \theta^2} \left(\frac{\partial u}{\partial r} - \frac{u}{r} \right) = 0 \quad \text{at} \quad r = 1, \quad (3.10)$$

$$\frac{\partial^2 u}{\partial r^2} + \nu \left(\frac{1}{r} \frac{\partial u}{\partial r} + \frac{1}{r^2} \frac{\partial^2 u}{\partial \theta^2} \right) = 0 \quad \text{at} \quad r = 1. \quad (3.11)$$

Moreover, at the inner rim, radial and hoop displacement must vanish, as is expressed in the following forms: ([11])

$$\frac{\partial^2 \phi}{\partial r^2} - \nu \left(\frac{1}{r} \frac{\partial \phi}{\partial r} + \frac{1}{r^2} \frac{\partial^2 \phi}{\partial \theta^2} \right) - \frac{1-\nu}{2\varepsilon} \Omega^2 r^2 = 0 \quad \text{at} \quad r = \eta, \quad (3.12)$$

$$\frac{\partial^3 \phi}{\partial r^3} + \frac{1}{r} \frac{\partial^2 \phi}{\partial r^2} - \frac{1}{r^2} \frac{\partial \phi}{\partial r} + \frac{2+\nu}{r^2} \frac{\partial^3 \phi}{\partial r \partial \theta^2} - \frac{3+\nu}{r^3} \frac{\partial^2 \phi}{\partial \theta^2} - \frac{1-\nu}{\varepsilon} \Omega^2 r = 0 \quad \text{at } r = \eta. \quad (3.13)$$

Also, at the outer rim, in-plane stresses σ_{rr} and $\sigma_{r\theta}$ are zero. In terms of the non-dimensional variables, these boundary conditions can be written ([11])

$$\frac{1}{r} \frac{\partial \phi}{\partial r} + \frac{1}{r^2} \frac{\partial^2 \phi}{\partial \theta^2} - \frac{1}{2\varepsilon} \Omega^2 r^2 = 0 \quad \text{at } r = 1, \quad (3.14)$$

$$-\frac{1}{r} \frac{\partial^2 \phi}{\partial r \partial \theta} + \frac{1}{r^2} \frac{\partial \phi}{\partial \theta} = 0 \quad \text{at } r = 1. \quad (3.15)$$

The stress function can be separated into two parts: homogenous (ϕ^h) and particular (ϕ^p). The homogenous part is a function of speed and satisfies the speed-dependent part of Eq. (3.7). The particular part is a function of lateral displacement and satisfies the nonlinear part of Eq. (3.7). Therefore, one can write the stress function in the following form:

$$\phi = \phi^h + \phi^p. \quad (3.16)$$

From Eq. (3.7), the governing equation for ϕ^h is obtained as follows:

$$\nabla^4 \phi^h = 2(1-\nu)\Omega^2/\varepsilon. \quad (3.17)$$

The general solution for ϕ^h , using Eq. (3.17) is obtained as

$$\phi^h = \frac{c_1 r^2 + c_2 \ln r + (1-\nu)\Omega^2 r^4/32}{\varepsilon}. \quad (3.18)$$

c_1 and c_2 are constants that can be found using the boundary conditions. Since ϕ^h is not a function of θ , the boundary condition stated in Eq. (3.15) is automatically satisfied. Also, if we substitute ϕ^h into Eq. (3.13), we see that this boundary condition is also automatically met. Using Eq. (3.18) and the boundary conditions stated in Eqs. (3.12) and (3.14), c_1 and c_2 are found to be

$$c_1 = \frac{(1+\nu)[3+\nu+(1-\nu)\eta^4]}{16[1+\nu+(1-\nu)\eta^2]} \Omega^2,$$

$$c_2 = \frac{(1-\nu)\eta^2[3+\nu-(1+\nu)\eta^2]}{8[1+\nu+(1-\nu)\eta^2]} \Omega^2.$$

3.3. Solution Method

In this part, the equations of motion are discretized using Galerkin's method. The eigenfunctions of the following two eigenvalue problems are used as the approximation functions in Galerkin's method:

$$\nabla^4 u = (\lambda_{mn}^u)^4 u, \quad (3.19)$$

$$\nabla^4 \phi = (\lambda_{mn}^\phi)^4 \phi. \quad (3.20)$$

The eigenfunctions of Eq. (3.19) are $U_{mn} = R_{mn}^u(\lambda_{mn}^u r) \sin m\theta$ and $R_{mn}^u(\lambda_{mn}^u r) \cos m\theta$ and the eigenfunctions of Eq. (3.20) are assumed to be $\phi_{mn} = R_{mn}^\phi(\lambda_{mn}^\phi r) \sin m\theta$ and $R_{mn}^\phi(\lambda_{mn}^\phi r) \cos m\theta$. Here, m is the number of nodal diameters and n is the number of nodal circles. In this paper, a mode with m number of nodal diameters and n number of nodal circles is shown as the (n, m) mode. The associated boundary conditions for the eigenvalue problem stated in Eq. (3.19) are those stated in Eqs. (3.8-15), assuming that the speed is zero. The eigenfunctions of the eigenvalue problem stated in Eq. (3.19) form an orthonormal basis. Therefore, any initial axisymmetric runout can be approximated in terms of the eigenfunctions of Eq. (3.19) as follows:

$$w_0^R(r) = \sum_{i=0}^{N_R} W_{i0}^R R_{0i}^u(\lambda_{0i}^u r), \quad (3.21)$$

where W_{i0}^R is the amplitude of runout corresponding to an axisymmetric mode with i nodal circles (and zero nodal diameter) and N_R is the number of axisymmetric modes with which the runout of the disk can be approximated. The transverse displacement can be described by a modal expansion as:

$$u(r, \theta, t) = \sum_{m,n=0}^{M,N} [S_{mn}^u(t) \sin m\theta + C_{mn}^u(t) \cos m\theta] R_{mn}^u(\lambda_{mn}^u r). \quad (3.22)$$

In Eq. (3.22), M and N are, respectively, the number of nodal diameters and nodal circles that have been used in the approximation. Based on Eq. (3.7), the governing equation for the particular part is

$$\begin{aligned} \nabla^4 \phi^p = & \left[-u_{,rr} (r^{-1} u_{,r} + r^{-2} u_{,\theta\theta}) + (r^{-1} u_{,r\theta} - r^{-2} u_{,\theta})^2 \right. \\ & \left. - w_{0,rr} (r^{-1} u_{,r} + r^{-2} u_{,\theta\theta}) - r^{-1} u_{,rr} w_{0,r} \right] \end{aligned} \quad (3.23)$$

If we substitute $u(r, \theta, t)$ from Eq. (3.22) into Eq. (3.23), some second-order expressions will appear in the right-hand side in terms of the coefficients of the expansion functions (S_{mn}^u and C_{mn}^u). Of course, to better predict the frequency behavior of the disk, one must consider all of the terms. In this paper, as an approximation, we assume that the bending deflection of the disk is small compared to disk thickness. In other words, we suppose that the ratio of u/h is small enough that we can neglect the effect of the nonlinear terms that appear in the equations of motion. Therefore, those terms that are second order regarding S_{mn}^u and C_{mn}^u can be neglected. After dismissing these terms in Eq. (3.23), the following governing equation is obtained for the particular part of the stress function:

$$\nabla^4 \phi^p = \left[-w_{0,rr} (r^{-1}u_{,r} + r^{-2}u_{,\theta\theta}) - r^{-1}u_{,rr}w_{0,r} \right] \quad (3.24)$$

To solve the above equation, the particular part of the stress function is approximated as follows:

$$\phi^p(r, \theta, t) = \sum_{m,n=0}^{M,N} \left[S_{mn}^\phi(t) \sin m\theta + C_{mn}^\phi(t) \cos m\theta \right] R_{mn}^\phi(\lambda_{mn}^\phi r) \quad (3.25)$$

The eigenfunctions of the eigenvalue problems stated in Eqs. (3.19) and (3.20) are normalized using the following relations:

$$\int_S U_{mn} U_{ij} dS = \delta_{mi} \delta_{nj},$$

$$\int_S \phi_{mn} \phi_{ij} dS = \delta_{mi} \delta_{nj}.$$

In the above two relations, δ_{ij} is the Kronecker delta and S is the disk domain. After substituting Eqs. (3.25) and (3.22) into Eq. (3.24) and multiplying both sides by $R_{pq}^\phi(\lambda_{pq}^\phi r) \sin p\theta$ and another time by $R_{pq}^\phi(\lambda_{pq}^\phi r) \cos p\theta$, and integrating the resultant over the area of the plate, using the orthogonal property of the eigenfunctions, the following equations are obtained for the coefficients of the expansion functions of the particular part of the stress function:

$$S_{mn}^\phi = \frac{-\pi}{(\lambda_{mn}^\phi)^4} \sum_{i=0}^{N_R} \sum_{q=0}^N Lwup_{1(0i)(mq)(mn)} S_{mq}^u, \quad (3.26a)$$

$$C_{mn}^\phi = \frac{-\pi}{(\lambda_{mn}^\phi)^4} \sum_{i=0}^{N_R} \sum_{q=0}^N Lwup_{1(0i)(mq)(mn)} C_{mq}^u, \quad (3.26b)$$

where

$$Lwup_{1(0i)(pq)(mn)} = W_{i0}^R \int_{\eta}^1 \left[\left(\frac{d^2 R_{0i}^u(\lambda_{0i}^u r)}{dr^2} \right) \left(\frac{dR_{pq}^u(\lambda_{pq}^u r)}{rdr} - \frac{p^2}{r^2} R_{pq}^u(\lambda_{pq}^u r) \right) + \frac{dR_{0i}^u(\lambda_{0i}^u r)}{rdr} \frac{d^2 R_{pq}^u(\lambda_{pq}^u r)}{dr^2} \right] R_{mn}^{\phi}(\lambda_{mn}^{\phi} r) r dr,$$

From Eqs. (3.26), it may be noted that the coefficient of the sinusoidal term in the stress function depends solely upon the coefficient of the sin waves of the lateral displacement. In other words, the amplitude of the sinusoidal terms in the stress function do not depend upon the amplitude of the cos waves of the lateral deflection. Also, the coefficients of the approximating functions with m nodal diameters only depend upon the coefficients of the expansion function of transverse displacement with the same number of nodal diameters. Indeed, this means that in this case the transverse displacement of a mode with m nodal diameters can only affect the in-plane stress (due to bending) of a mode with the same number of nodal diameters. Therefore, Eqs. (3.26) can be rewritten in the following form:

$$S_{mn}^{\phi} = \sum_{q=0}^N a_{mnq}^{\phi} S_{mq}^u, \quad (3.27a)$$

$$C_{mn}^{\phi} = \sum_{q=0}^N a_{mnq}^{\phi} C_{mq}^u, \quad (3.27b)$$

where

$$a_{mnq}^{\phi} = \frac{-\pi}{(\lambda_{mn}^{\phi})^4} \sum_{i=0}^{N_R} Lwup_{1(0i)(mq)(mn)}$$

If we substitute ϕ^p (from Eqs. (3.26)) into Eq. (3.6), second-order expressions will appear in terms of the coefficients of the expansion functions of the transverse displacement. As mentioned earlier, we assume that the transverse displacement of the disk is small enough that we can ignore these terms. After dismissing the second-order terms, the following governing equation of motion is obtained:

$$\begin{aligned}
 \frac{\partial^2 u}{\partial t^2} + 2\Omega \frac{\partial^2 u}{\partial \theta \partial t} + \Omega^2 \frac{\partial^2 u}{\partial \theta^2} + \nabla^4 u &= \varepsilon r^{-1} u_{,rr} \phi_{,r}^h \\
 + \varepsilon w_{0,rr} (r^{-1} \phi_{,r} + r^{-2} \phi_{,\theta\theta}) + \varepsilon \phi_{,rr}^h [r^{-1} u_{,r} + r^{-2} u_{,\theta\theta}] &+ \varepsilon r^{-1} \phi_{,rr} w_{0,r} \\
 - \Omega^2 \left(\frac{1}{2} r^2 \nabla^2 u + \frac{1}{2} r^2 \left(\frac{\partial^2}{\partial r^2} + \frac{1}{r} \frac{\partial}{\partial r} \right) w_0 + r(u + w_0)_{,r} \right) &.
 \end{aligned} \tag{3.28}$$

If we substitute Eqs. (3.22) and (3.27) into Eq. (3.28) and multiply both sides once by $R_{pq}^u(\lambda_{pq}^u r) \sin p\theta$ and another time by $R_{pq}^u(\lambda_{pq}^u) \cos p\theta$, then integrate the resultant over the area of the plate, using the orthogonal property of the eigenfunctions, we will obtain the following equations:

$$\begin{aligned}
 \ddot{S}_{mn}^u - 2\Omega m \dot{C}_{mn}^u + \left((\lambda_{mn}^u)^4 - m^2 \Omega^2 \right) S_{mn}^u &= \pi (1 - \delta_{0m}) \sum_{q=0}^N (L u u p_{1(pq)(mn)} \delta_{mp} S_{mq}^u) \\
 + \pi (1 - \delta_{0m}) \sum_{i=0}^{N_R} \sum_{q=0}^N \sum_{s=0}^N (L w u p_{2(0i)(pq)(mn)} \delta_{mp} a_{pqs}^\phi S_{ps}^u) &.
 \end{aligned} \tag{3.29a}$$

$$\begin{aligned}
 \ddot{C}_{mn}^u + 2\Omega m \dot{S}_{mn}^u + \left((\lambda_{mn}^u)^4 - m^2 \Omega^2 \right) C_{mn}^u &= \pi \sum_{q=0}^N (L u u p_{1(pq)(mn)} \delta_{mp} C_{mq}^u) \\
 + \pi \sum_{i=0}^{N_R} \sum_{q=0}^N \sum_{s=0}^N (L w u p_{2(0i)(pq)(mn)} \delta_{mp} a_{pqs}^\phi C_{ps}^u) + F_{mn}^{C0}, &.
 \end{aligned} \tag{3.29b}$$

where

$$\begin{aligned}
 L u u p_{1(pq)(mn)} &= \varepsilon \int_{\eta}^1 \left[\frac{d^2 R_{pq}^u(\lambda_{pq}^u r)}{dr^2} \frac{d\phi^h}{r dr} + \frac{d^2 \phi^h}{dr^2} \left(\frac{dR_{pq}^u(\lambda_{pq}^u r)}{r dr} - \frac{p^2}{r^2} R_{pq}^u(\lambda_{pq}^u r) \right) \right. \\
 &\quad \left. - \frac{r^2 \Omega^2}{2} \left(\frac{d^2 R_{pq}^u(\lambda_{pq}^u r)}{dr^2} + \frac{dR_{pq}^u(\lambda_{pq}^u r)}{r dr} - \frac{p^2}{r^2} R_{pq}^u(\lambda_{pq}^u r) \right) \right. \\
 &\quad \left. - r \Omega^2 \frac{dR_{pq}^u(\lambda_{pq}^u r)}{dr} \right] R_{mn}^u(\lambda_{mn}^u r) r dr
 \end{aligned}$$

$$\begin{aligned}
 L w u p_{2(0i)(pq)(mn)} &= \varepsilon W_{i0}^R \int_{\eta}^1 \left[\left(\frac{d^2 R_{0i}^u(\lambda_{0i}^u r)}{dr^2} \right) \left(\frac{dR_{pq}^\phi(\lambda_{pq}^\phi r)}{r dr} - \frac{p^2}{r^2} R_{pq}^\phi(\lambda_{pq}^\phi r) \right) \right. \\
 &\quad \left. + \frac{dR_{0i}^u(\lambda_{0i}^u r)}{r dr} \frac{d^2 R_{pq}^\phi(\lambda_{pq}^\phi r)}{dr^2} \right] R_{mn}^u(\lambda_{mn}^u r) r dr
 \end{aligned}$$

$$F_{mn}^{C0} = 2\pi\delta_{0m} \int_{\eta}^1 \left[\varepsilon \frac{d^2 R_{0i}^u(\lambda_{0i}^u r)}{dr^2} \frac{d\phi^h}{rdr} + \varepsilon \frac{dR_{0i}^u(\lambda_{0i}^u r)}{dr} \frac{d^2\phi^h}{rdr^2} - r^2\Omega^2 \frac{dR_{0i}^u(\lambda_{0i}^u r)}{dr} \right] R_{mn}^u(\lambda_{mn}^u r) r dr.$$

As the disk rotates at a certain speed, an equilibrium solution for Eqs. (3.29) can be found by neglecting time-dependent terms. These equilibrium solutions are called S_{mn}^{ue} and C_{mn}^{ue} , corresponding to the amplitude of ‘sin’ and ‘cos’ waves. Here, we consider some perturbations for the amplitude of sin and cos waves, shown by $\hat{S}_{mn}^u(t)$ and $\hat{C}_{mn}^u(t)$, respectively. Therefore, we can write

$$S_{mn}^u(t) = \hat{S}_{mn}^u(t) + S_{mn}^{ue}, \quad (3.30a)$$

$$C_{mn}^u(t) = \hat{C}_{mn}^u(t) + C_{mn}^{ue}. \quad (3.30b)$$

After substituting Eqs. (3.30) into Eqs. (3.29), the equations of motion in terms of considered perturbations, $\hat{S}_{mn}^u(t)$ and $\hat{C}_{mn}^u(t)$, are obtained. These are similar to Eqs. (3.29), with the forcing term (F_{mn}^{C0}) being neglected and the coefficients of the expansion functions, $S_{mn}^u(t)$ and $C_{mn}^u(t)$, being replaced by $\hat{S}_{mn}^u(t)$ and $\hat{C}_{mn}^u(t)$, respectively. These equations can be used to investigate the effect of axisymmetric runout on the frequency behavior of a spinning disk.

3.4. Numerical Simulations

In this section, the previously developed governing equations of motion are used to investigate the effect of disk runout on the oscillation frequencies of a non-flat spinning disk. For this purpose, an in-house code is written, based on the developed equations. The disk in this analysis is assumed to have clamped-free boundary conditions. It is also assumed that $E = 2e11 N/m^2$, $\nu = 0.3$, $\rho = 7800 kg/m^3$, $\eta = 0.3529$, $b = 0.2159 m$, $h = 1.27 mm$. Table 3. 1 summarizes the ratio of initial disk deflection due to runout at the outer rim to its thickness when $W_{i0}^R = 100$ ($i = 0, 1, \dots, 4$).

Table 3. 1. Ratio of disk deflection to its thickness at the outer rim when $W_{i0}^R = 100$

Runout	W_{00}^R	W_{10}^R	W_{20}^R	W_{30}^R	W_{40}^R
$w'_0(1)/h$	0.5972	0.5926	0.5868	0.5855	0.5849

To verify the accuracy of the results obtained by the proposed method, the abovementioned disk with an initial non-flatness is modeled in the widely used commercial software, ANSYS. The non-flatness is assumed to be in the form of the (0,0) mode. A shell element (Shell63) is used for meshing the disk. The frequencies of the first four modes of the stationary disk are calculated using the proposed formulation and the ANSYS software. The results are displayed in Table 3. 2. There is a close agreement between the results predicted by the current analysis and those predicted by ANSYS.

Table 3. 2. Comparison between the results of the proposed analysis and those predicted by ANSYS

Mode	$W_{00}^R = 100$		$W_{00}^R = 200$		$W_{00}^R = 300$	
	Current	ANSYS	Current	ANSYS	Current	ANSYS
(0,0)	8.358	8.309	9.915	9.852	12.042	11.963
(0,1)	7.971	7.928	8.539	8.489	9.387	9.331
(0,2)	9.164	9.111	9.270	9.215	9.438	9.381
(0,3)	13.999	13.911	14.006	13.916	14.016	13.927

In Figure 3. 1, the calculated oscillation frequencies of the spinning disk when the runout is zero are compared with those where the runout is assumed to be in the form of the (0,0) mode. In the current analysis it is assumed that $M = 7$. Also, after doing a convergence test it is found that if we select $N = 4$, the change in the calculated frequencies are negligible and the convergence is achieved. The dotted lines show the frequency results when the runout is assumed to be $W_{00}^R = 100$; the solid lines show the results when the disk is assumed to be perfectly flat. Among all the modes shown in this figure, the frequencies of the (0,0) and (0,1) modes are more affected by assuming that the disk has an initial runout. The frequencies of the oscillations of the other modes also change by a very small amount, which cannot be distinguished in this figure. As the rotation speed increases, the difference between the calculated frequencies of the warped and unwarped disk decreases. This is because increasing the rotation speed makes the disk flatten and the effect of runout decrease.

The above example shows that the modal stiffness of some of the modes change as the initial runout is considered in the analysis. The effect of the initial runout on the stiffness of the mode shapes can be inferred from Eqs. (3.28). As may be observed from

these equations, the modal stiffness due to the lack of flatness is influenced by the term $\sum_{i=0}^{N_R} \sum_{q=0}^N (Lwup_{2(0i)(mq)(mn)} a_{mqn}^\phi)$. In fact, the sign of this term indicates whether the initial runout increases or decreases the modal stiffness of each mode. It is difficult to determine the sign of this term analytically, and hence numerical investigations are employed here. These revealed that for any mode (n,m), this term is always negative. Indeed, the initial axisymmetric runout increases modal stiffness. On the other hand, since the modal mass of each mode is unchanged, an axisymmetric initial runout increases the frequencies of the oscillations of each mode, as can be verified in Figure 3. 1.

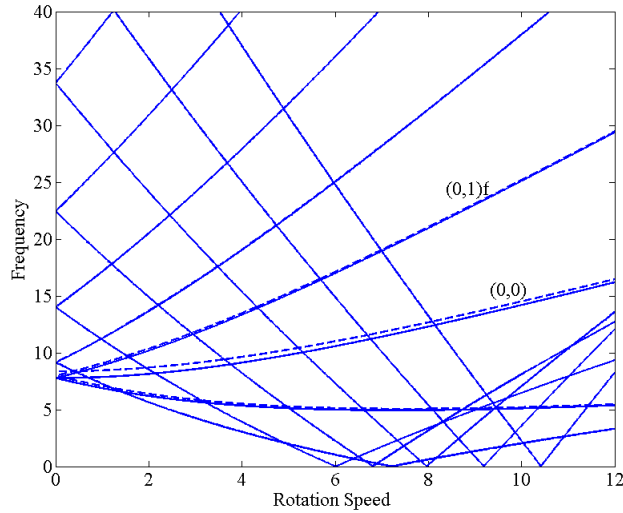


Figure 3. 1. Non-dimensionalized oscillation frequencies versus non-dimensionalized rotation speed when the runout is zero (solid lines) and when $W_{00}^R = 100$ (broken lines)

Figure 3. 2 shows the frequencies of the oscillations of the spinning disk versus the rotation speed when the initial runout is assumed to be in the shape of the (1, 0) mode. In this plot, it is supposed that $W_{10}^R = 100$. In this case also, the oscillation frequencies of all the modes are changed by assuming that the disk is not perfectly flat. Unlike the previous results shown in Figure 3. 1, in this case the change in the frequencies of the oscillations of the (0,1) mode is not significant when compared to the other modes, and it cannot be distinguished in this figure. When the disk is not perfectly flat and has small oscillations, an in-plane stress is induced in the disk due disk non-flatness (in addition to the in-plane stress induced due to the effect of rotation). The effect of this in-plane stress on the (0,1)

mode is smaller than that on the other modes when the non-flatness is in the shape of (1,0) mode.

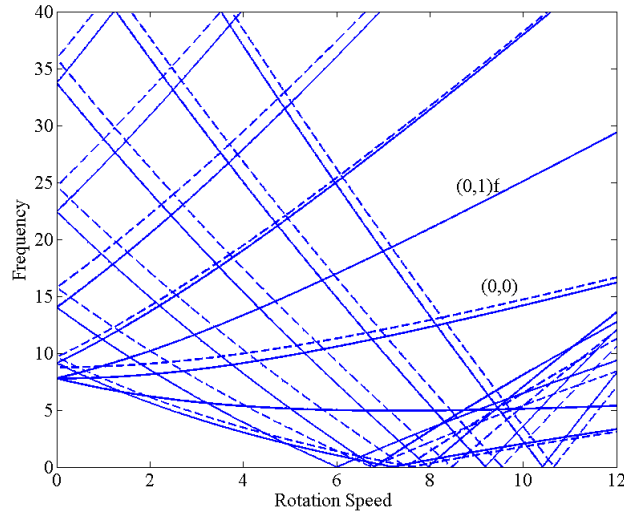


Figure 3. 2. Non-dimensionalized oscillation frequencies versus non-dimensionalized rotation speed when the runout is zero (solid lines) and when $W_{10}^R = 100$ (broken lines)

It is noted that the initial runout changes the critical speeds of the disk. The critical speed is a speed at which one of the frequencies of the oscillations of the spinning disk is zero. (The effect of the initial runout on the critical speed of the spinning disk will be discussed later.) Moreover, by comparing Figure 3. 1 with Figure 3. 2, it is evident that different forms of the initial runout may result in different oscillation frequencies for a given mode. Therefore, it may be concluded that the level of increase in the modal stiffness of each mode for a given shape of the initial runout is different from one mode to another.

To further study the effect of disk runout on the oscillation frequency of the modes, the disk is here assumed to be stationary. Different levels of runout with different axisymmetric shapes are assumed and the results are obtained numerically. In Figure 3. 3, the frequencies of the first four modes of the stationary disk when the runout is assumed to be in the form of the (0,0) mode are plotted against the level of non-flatness. It may be noted that, in general, the frequencies of all the modes shown in this graph increase as the level of non-flatness increases. It also may be observed that the frequencies of the oscillations of the (0,0), (0,1), (0,2) and (0,3) modes increase by 86.12, 35.56, 6.08 and 0.22 percent, respectively, as W_{00}^R increases from zero to 400. In this example, the non-

flatness in the shape of the (0,0) mode has the most substantial effect on the oscillation frequency of the (0,0) mode and the least effect on that of the (0,3) mode. It should be emphasized that the imperfection of the disk which is due to the lack of flatness is assumed to be axisymmetric. Therefore, for a non-flat stationary disk, the oscillation frequencies of the backward and forward traveling waves of each mode are the same. It is also interesting that in this case, the rate of change of the oscillation frequency of the (0,0) mode with respect to change in W_{00}^R is high enough that the frequency of its oscillations exceeds those of (0,2) and (0,3) modes when W_{00}^R changes from zero to 400.

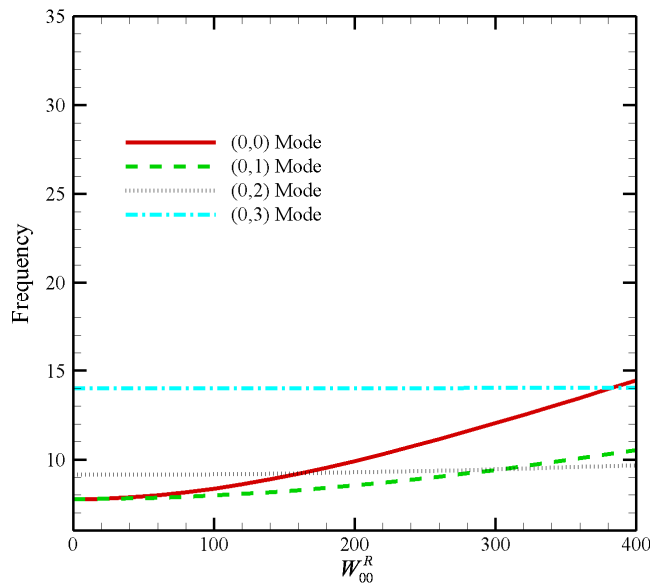


Figure 3. 3. Non-dimensionalized oscillation frequencies of the stationary disk when the non-flatness is assumed to be in the shape of the (0,0) mode

In Figure 3. 4, the frequency behavior of the stationary disk when the runout is assumed to be in the shape of the (1,0) mode is plotted against the level of non-flatness. As can be seen in this figure, unlike the previous case, the frequency of oscillations of the (0,3) mode is highly affected by the disk's non-flatness. Based on the current numerical analysis, it is found that the frequencies of the oscillations of the (0,0), (0,1), (0,2) and (0,3) modes increase by 107.19, 55.33, 30.02 and 44.23 percent, respectively, as W_{10}^R increases from zero to 400. Unlike the previous instance, the frequency of the oscillations of the (0,0) mode does not exceed that of the (0,3) mode when W_{01}^R increases from zero to 400.

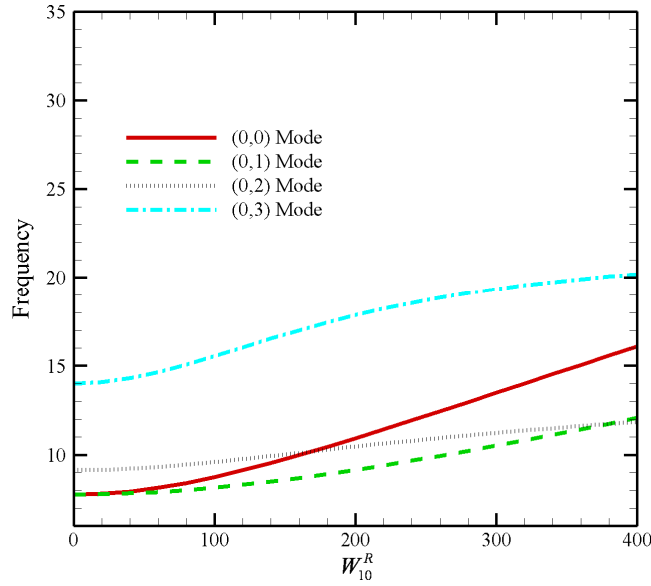


Figure 3. 4. Non-dimensionalized oscillation frequencies of the stationary disk when the non-flatness is assumed to be in the shape of the (1,0) mode

Figure 3. 5 and Figure 3. 6 show the oscillation frequencies of the stationary disk when the disk non-flatness is assumed to be in the form of the (2,0) and (3,0) modes. The frequency of the oscillations of the (0,0), (0,1), (0,2) and (0,3) modes increases by 153.01, 80.30, 67.22 and 132.47 percent, respectively, when W_{20}^R increases from zero to 400. Also, the oscillation frequencies of these modes increase by 167.08, 87.23, 54.44 and 146.93 percent, respectively, as W_{30}^R increases from zero to 400.

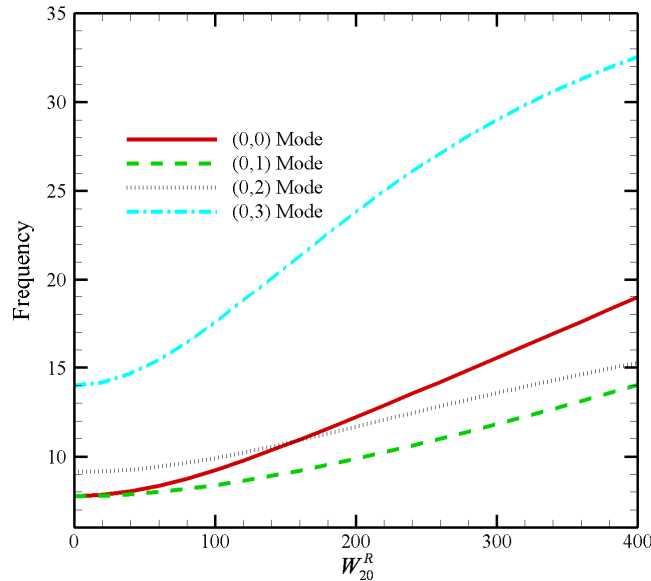


Figure 3. 5. Non-dimensionalized oscillation frequencies of the stationary disk when the non-flatness is assumed to be in the shape of the (2,0) mode

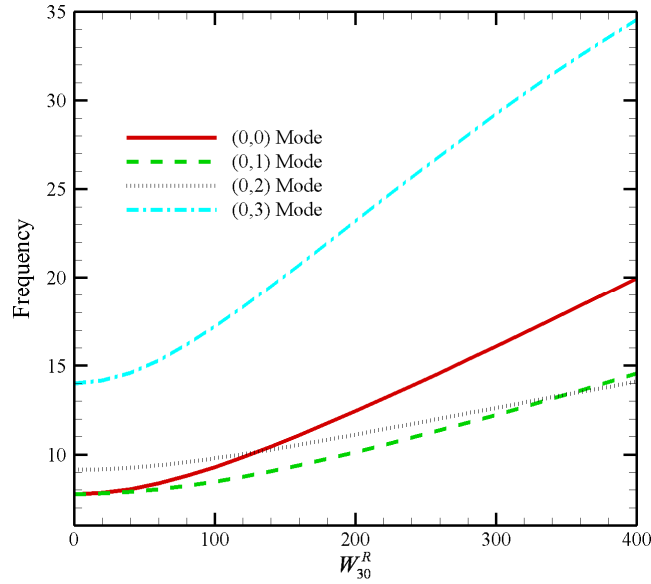


Figure 3. 6. Non-dimensionalized oscillation frequencies of the stationary disk when the non-flatness is assumed to be in the shape of the (3,0) mode

In the first case, corresponding to the initial runout in the shape of the (0,0) modes (shown in Figure 3. 3), there are two modes for which the increase in oscillation frequencies is less than ten percent as the level of non-flatness changes from zero to four hundred. It is interesting to note that in the cases corresponding to the initial runout in the form of the (1,0), (2,0) and (3,0) modes (shown in Figure 3. 4, Figure 3. 5 and Figure 3. 6), the increase in the oscillation frequencies of all the modes is almost always above thirty percent. Therefore, it may be concluded that the frequencies of oscillations are substantially affected by the initial runout in the shape of axisymmetric modes with a higher number of nodal circles. It may also be observed that as the number of nodal circles for the initial shape increases, the oscillation frequency increases, too.

As indicated earlier in some of the cases, the frequency of the oscillations of the (0,0) mode exceeds that of the (0,2) and (0,3) modes. Table 3. 3 summarizes the level of the initial runouts for which the frequency of the (0,0) mode exceeds that of the (0,2) and (0,3) modes for the range of non-flatness studied in this paper. The bar ('-') indicates that for the specified shape of the initial runout, the frequency of the (0,0) mode does not exceed that of the (0,3) mode. When the initial non-flatness is in the shape of the (2,0) mode, the frequency of oscillations of the (0,0) mode exceeds that of the (0,2) mode for relatively low levels of non-flatness.

Table 3. 3. Level of runout by which the frequencies of the oscillations of the (0,0) mode exceed those of the (0,2) and (0,3) modes

	(0,2)	(0,3)
W_{00}^R	160.97	382.66
W_{10}^R	168.97	-
W_{20}^R	157.01	-
W_{30}^R	129.97	-

It was observed that different shapes of the initial non-flatness may have different effects on the oscillation frequencies of the mode shapes. To explain the effect of each form of the disk non-flatness on the oscillation frequency of a given mode, one should determine the mechanism by which the runout may affect the frequency behavior.

As previously noted, the particular part of the stress function is approximated by the summation of the eigenfunctions of an eigenvalue problem. The coefficients of these approximations are found in Eq. (3.27). According to this equation, when the disk has an initial runout and its transverse deflection is not zero (i.e. S_{mq}^u or C_{mq}^u is not zero), the particular part of the stress function is not zero. An in-plane stress is induced, due to the interaction between the disk runout and its transverse deflection. This in-plane stress is in addition to that caused by the effect of disk rotation. The distribution of this in-plane stress is different from one shape of disk non-flatness to another.

To see how the level and shape of the runout may change the frequency behavior of the disk, we will now consider the (n,m) mode. The general form of the particular part of the stress function is given in Eq. (3.25). As previously discussed, only the terms in the particular part of the stress function that have m nodal diameters affect the modal stiffness of the (n,m) mode.

It is clear that the expansion functions used to approximate the particular part of the stress function are orthonormal. Therefore, for this mode, among all the approximating functions with m number of nodal diameters, the one that also has n number of nodal circles may be considered more effective in determining the modal stiffness of that mode. Thus, for this mode one may be able to look at S_{mn}^ϕ and C_{mn}^ϕ and explain the effect of initial runout on the frequency behavior of some of the modes.

From Eq. (3.27) it is observed that S_{mn}^ϕ and C_{mn}^ϕ are proportional to a_{mnq}^ϕ . If we substitute the particular part of the stress function into the equation of motion, among all the values of a_{mnq}^ϕ (for different values of q), the one that may directly change the modal stiffness of mode (n,m) is a_{mnn}^ϕ . In other words, the effect of a_{mnn}^ϕ on the modal stiffness of the assumed mode may be considered more substantial than that of other values of a_{mnq}^ϕ ($q \neq n$). It should be emphasized that other values of a_{mnq}^ϕ ($q \neq n$) may affect the modal stiffness of the (n,m) mode as well.

As shown in the foregoing analysis, one may be able to look at a_{mnn}^ϕ for the (n,m) mode to explain the effect of different shapes of the initial non-flatness on the frequency behavior of the disk. Table 3. 4 summarizes the values of a_{mnn}^ϕ for different mode shapes, assuming two different forms of the initial runout. In this table it is assumed that the level of initial runout for all of the forms is $W_{i0}^R = 100$.

Table 3. 4. a_{mnn}^ϕ for different modes and different forms of initial runout when $W_{i0}^R = 100$

	W_{00}^R	W_{10}^R
(0,0)	4.43×10^{-3}	2.76×10^{-3}
(0,1)	1.62×10^{-3}	6.94×10^{-4}
(0,2)	2.24×10^{-4}	1.86×10^{-3}
(0,3)	4.74×10^{-5}	2.99×10^{-3}
(0,4)	6.08×10^{-6}	3.02×10^{-3}

In Figure 3. 3 it was observed that when the initial runout was assumed to have the shape of the (0,0) mode, the frequency behavior of the (0,0) mode is highly affected and that of the (0,3) mode is unaffected to some extent. Table 3. 4 shows that the value of a_{mnn}^ϕ for the (0,0) and (0,3) modes—when the non-flatness is assumed to be in the form of the (0,0) mode—are 4.43×10^{-3} and 4.74×10^{-5} , respectively. These values of a_{mnn}^ϕ indicate that the effect of induced in-plane stresses due to the initial runout and bending deflection on the oscillation frequency of the (0,3) mode is less significant than that for the (0,0) mode. Therefore, it may be concluded that the modal stiffness of the (0,3) mode is

changed less compared to that of the (0,0) mode when considering the initial non-flatness of the disk.

It must be emphasized that one may use the above approach to compare the effect of an assumed initial runout on the frequency behaviors of two different modes only if their values for a_{mnn}^ϕ are different by at least one to two orders of magnitude.

When the initial runout is in the form of the (1,0) mode, the values of a_{mnn}^ϕ have almost the same order of magnitude and some of them are close together. Therefore, in this case this approach cannot be employed to explore the effect of an assumed initial runout on the frequency behavior of the disk. In such cases, complex analytical methods should be used. Indeed, from Table 3. 4, it may generally be concluded that when the initial runout is in the form of the (1,0) mode, all of the oscillation frequencies are affected for the range of the initial runout considered here. To see why some modes are more affected by the initial runout in this form, some other mathematical tools should be employed.

It was seen that not only does the frequency behavior of the disk change with the shape and level of the disk's non-flatness, its critical speeds change as well. Using the developed solution method, the effect of different forms of the initial runout on the critical speed behaviour of the disk is studied. In Figure 3. 7, the non-dimensionalized critical speed of the (0,2) mode is plotted against the level of initial non-flatness for different shapes of the initial runout. It can be seen that the critical speed of the (0,2) mode is less affected by the initial runout in the shape of (0,0) mode compared to the other forms of the initial runout. This is because when the initial runout is in this form, the contribution of the induced in-plane stress due to the lack of flatness on the modal stiffness of this mode is small compared to that of the other forms of the initial runout. This can be verified in Table 3. 4.

Figure 3. 8 shows the effect of non-flatness on the non-dimensionalized critical speed behavior of the (0,3) mode. As may be seen, for this mode among all of the shapes of the initial runout considered here, the ones in the form of the (0,0) mode and the (3,0) mode have the lowest and highest influence on its critical speed, respectively. Also, in Figure 3. 9, the non-dimensionalized critical speed of the (0,4) mode is plotted against the

level of non-flatness, assuming different shapes for the initial runout. Again, based on these results, among all of the forms of the initial runout considered, those that are in the shape of (0,0) and (3,0) modes have the lowest and highest effect on the critical speed of this mode, respectively.

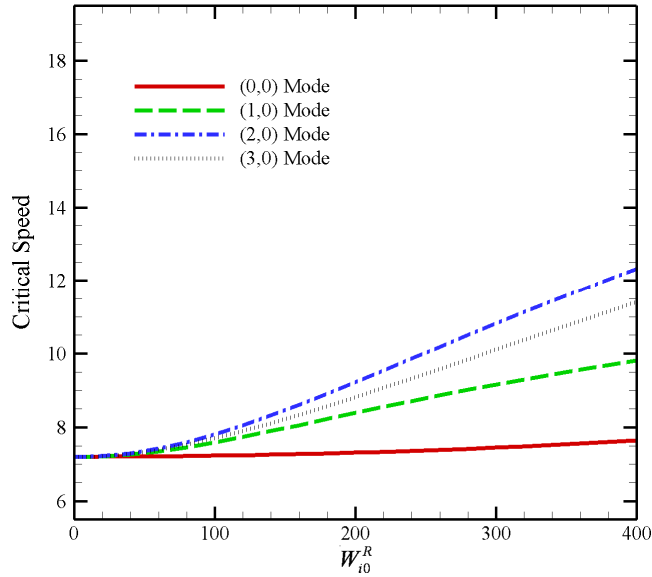


Figure 3. 7. Change in the critical speed of the (0,2) Mode, assuming different shapes of runout (the legends show the shape of initial non-flatness)

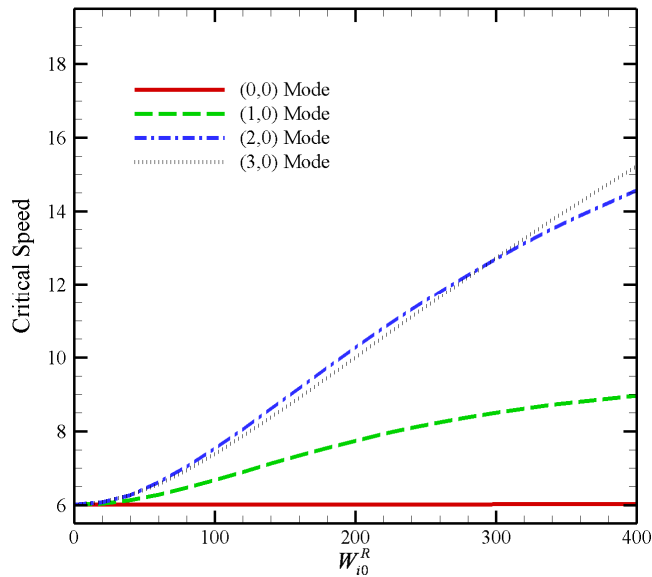


Figure 3. 8. Change in the critical speed of the (0,3) Mode, assuming different shapes of runout (the legends show the shape of initial non-flatness)

As it may be seen in Table 3. 4, the effect of induced in-plane stress, due to the disk non-flatness in the form of (0,0) mode, on the modal stiffness of the (0,3) and (0,4) modes is lower than those of the other forms of initial non-flatness. Therefore, the critical speeds of these two modes is less effect by the initial non-flatness in the form of the (0,0) mode compared to other modes. Numerical investigations show that when the disk non-flatness is in the form of the (3,0) mode, the induced in-plane stress due to lack of flatness contributes more toward the modal stiffness of the (0,3) and (0,4) modes compared to other forms of initial non-flatness. Therefore, the critical speeds of these two modes are more affected by the initial non-flatness in the (3,0) mode compared to the other forms of non-flatness.

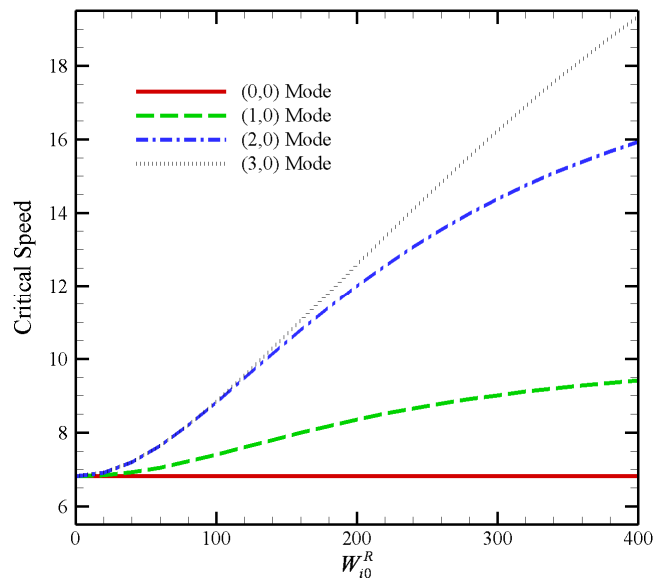


Figure 3. 9. Change in the critical speed of the (0,4) Mode, assuming different shapes of runout (the legends show the shape of initial non-flatness)

3.5. Conclusions

This chapter presents the results of an investigation into the effect of initial axisymmetric runout on the frequency behavior and critical speed behavior of a spinning disk. The nonlinear equations of motion based on Von Karman's plate model were used. As an approximation, it was assumed that the bending deflection of the disk was small compared to its thickness. Using this assumption and Galerkin's method, the equations of

motion were discretized. The proposed method for finding the oscillation frequencies of the static disk was verified by comparing the results with those obtained using ANSYS.

In general, it was found that the initial runout increased the modal stiffness of the modes. For a given shape of runout, the level of increase in the modal stiffness was different from one mode to another. Since the initial runout was assumed to be axisymmetric, there was no separation between the oscillation frequencies of the backward and forward travelling waves of a given mode at zero speed. It was also found that the oscillation frequencies of the disk oscillations were more affected by the initial runout in the shape of axisymmetric modes with a higher number of nodal circles.

The mechanism by which the initial axisymmetric runout affected the modal stiffness of the modes was discussed. It was found that an in-plane stress due to lack of flatness and bending deflection was induced in the disk domain. This in-plane stress distribution had different effects for different mode shapes. It was observed that when the initial runout was in the form of the (0,0) mode, the modal stiffness of some of the modes were not affected extensively by the disk non-flatness.

Also, the effect of an assumed initial runout on the critical speed behavior of some of the modes was considered. It was found that the initial axisymmetric runout increased the critical speed of the spinning disk. Generally speaking, the more complicated the shape of the initial runout, the greater its effect on the critical speeds of the disk.

3.6. References

- [1] Mote, C.D., 1965, "Free Vibration of Initially Stressed Circular Plates," *Journal of Engineering for Industry*, 87, pp. 258-264.
- [2] Hutton, S.G., Chonan, S., and Lehmann, B.F., 1987, "Dynamic Response of a Guided Circular Saw," *Journal of Sound and vibration*, 112 (3), pp. 527-539.
- [3] Vogel, S. M. and Skinner, D. W., 1965, "Natural Frequencies of Transversely Vibrating Uniform Annular Plates," *ASME Journal of Applied Mechanics*, 32, pp. 926-931.
- [4] Nowinski, J.L., 1964, "Nonlinear Transverse Vibrations of a Spinning Disk," *Journal of Applied Mechanics*, 31, pp. 72-78.
- [5] Yang, L. and Hutton, S.G., 1998, "Non Linear Vibrations of Elastically-Constrained Rotating Discs," *ASME Journal of Vibration and Acoustics*, 120(2), pp. 475-483.
- [6] Benson, R.C. and Cole, K. A., 1991, "Transverse Runout Of A Nonflat Spinning Disk," *Tribology Transactions*, 34, pp. 545-552.
- [7] Carpino, M., 1991, "The Effect of Initial Curvature in a Flexible Disk Rotating Near a Flat Plate," *ASME Journal of Tribology*, 113, pp. 355-360.
- [8] Jia, H. S., 2000, "Analysis of Transverse Runout in Rotating Flexible Disks by Using Galerkin's Method," *International Journal of Mechanical Sciences*, 42(2), pp. 237-248.
- [9] Chen, J.S. and Lin, C., 2005, "Axisymmetrical Snapping of a Spinning Nonflat Disk," *Journal of Applied Mechanics*, 72(6), pp. 879-886.
- [10] Chen, J.S. and Chang, Y., 2007, "On the Unsymmetrical Deformation and Reverse Snapping of a Spinning Non-Flat Disk," *International Journal of Non-Linear Mechanics*, 42(8), pp. 1000-1009.
- [11] Nayfeh, A. H., Jilani, A. and Manzione, P., 2001, "Transverse Vibrations of a Centrally Clamped Rotating Circular Disk," *Nonlinear Dynamics*, 26(2), pp. 163-178.

Chapter 4- Experimental Investigations on the Nonlinear Frequency Behavior *

4.1. Introduction

Rotating disks constitute key elements in many industrial applications ranging from hard disk drives to aircrafts rotors. In some engineering applications such as the wood cutting industry, the disk may be subjected to the application of space-fixed lateral forces. These lateral forces produce lateral displacements that may not be small compared to the disk thickness. In such circumstances, the effect of geometrical nonlinear terms cannot be ignored. As such, the linear equations of motion cannot accurately predict the response of the disks.

Tobias and Arnold [1] investigated the effect of disk imperfections on the dynamic behavior of spinning disks. In their studies, they conducted experiments on the amplitude response of a spinning disk in the region of its critical speeds while subjected to a space fixed external force. They observed that a stationary wave develops in the region of a critical speed and collapses sometime after the critical speed. They did not consider the effect of large deformation on the frequency response characteristics of the disks tested. Chen et al. [2] used the nonlinear governing equations of motion to investigate the impact of symmetrical initial runout on the amplitude of spinning disk deflection. They concluded that, depending on the shape and level of initial non-flatness, the disk may exhibit snap through buckling. They verified experimentally their theoretical results using a warped disk with an initial level of non-flatness almost eight times higher than that of the disk thickness. In another work, Chen et al. [3] used the nonlinear equations of motion to consider an unsymmetrical initial non-flatness for the disk. In this work, he studied the

* A version of this chapter has been submitted for publication. Khorasany, R.M.H., and Hutton, S.G., 2010, "Vibration Characteristics of Rotating Thin Discs, Part I: Experimental Results".

effect of unsymmetrical terms on the snapping speed while the disk was spinning. Again, they verified their results using an experimental set up.

Thomas et. al. [4] measured the amplitude response of an imperfect stationary disk. Due to the presence of imperfection, there are two different configurations associated with each mode. He was able to measure the amplitude response of each configuration and compare them with analytical predictions. Raman and Mote [5] conducted experiments to study the behavior of an imperfect spinning disk at around its critical speeds. In their experiments, they were able to record the existence of a critical speed for very small disk deflections. D'Angelo and Mote [6] conducted an experimental study on the frequency and amplitude behavior of a disk which was spinning in a fluid. They studied the effect of fluid density on the frequency response. They found a lock-in phenomena for the frequency behavior at supercritical speeds.

Raman et. al. [7] investigated experimentally the post-flutter frequency response of spinning disks. They recorded sudden jump and drops in the frequency response of the disks tested. Also, they noticed that the frequency response of the backward traveling wave of one of the modes was nearly constant over a specific speed region. Namchelo and Raman [8] studied the vibrations of a spinning disk in a gas filled enclosure. More recently, Jana et. al. [9] conducted experiments to investigate aeroelastic phenomena of a disk rotating in air. They measured the amplitude and frequency responses of a spinning disk and noticed jumps and drops in the frequency response. They also reported that, in some supercritical speed ranges, a frequency lock-in phenomenon occurred.

The primary objective of the present work is to study the frequency response of spinning disk under the application of a space fixed external force. Of particular interest is to determine how the frequencies of a spinning disk change when the applied force gives rise to deflections that are not small compared to the disk thickness.

4.2. Experimental Setup

A schematic of the experimental setup is shown in Figure 4. 1. Four space fixed inductance probes, with a linear range of 0.25in, were used to measure the displacement of four different points located around the rim of the spinning disk. In order to find the dc

level of the disk displacement, the deflection for each probe was averaged over a period of two seconds.

Different levels of disk deflection were induced by the application of an air jet whose pressure could be varied to provide different levels of displacement (and nonlinearity). The air jet was located on the opposite side of the blade to probe 3. In order to optimize modal excitation an electromagnet was also used to provide white noise excitation over the frequency range 0-100Hz.

Results were obtained by measuring the vibration profile of the disk at the four probes as the speed was run up from 0 RPM to 4,000 RPM and run down from 4,000 RPM to 0 RPM at a constant rate over a time interval of 500sec. Three different levels of air jet excitation were applied to each rotating disk providing different levels of disk deflection.

Using National Instrumentation software “Signal Express” the data was analyzed to produce waterfall and frequency colour maps that illustrated the variation of disk frequencies with rotational speed. Three disks with different thicknesses were used in the tests. All of them were made from steel. The inner diameter was clamped to the arbor by a 6 in. collar and the outer diameter was free. This clamping arrangement was not stiff enough to produce a perfectly clamped boundary condition. The disks used in these tests were typical of those used as wood cutting saw blades. As such they were not perfectly flat. The disk dimensions and flatness indicators are given in Table 4. 1. “Mean dish” refers to average displacement measured at the rim perpendicular to a plane passing through the disk in the clamp, and runout refers to the maximum difference between the mean value and the value at any other point on the disk rim. As can be seen the 0.030in disk had a significant amount of dishing, and when clamped suffered snap through buckling causing the dishing to change signs.

Table 4. 1. Disk Dimensions and Flatness Indicators (inches)

Disk	Inner Dia.	Outer Dia.	Thickness	Mean Dish	Runout
#1	6	17	0.050	0.006	0.005
#2	6	17	0.040	0.005	0.003
#3	6	17	0.030	0.011	0.005

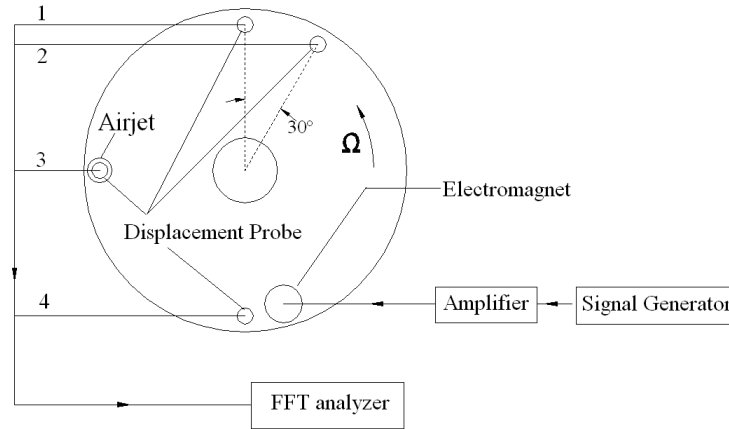


Figure 4. 1. The Experimental Setup

4.3. Experimental Results

4.3.1. Disk #1 – 0.050” Thickness

Figure 4. 2 shows the measured frequency response of the 0.050” disk for different levels of applied force for both run up and run down over the speed range dc to 4000RPM. In this figure w_0 is the maximum deflection of the stationary disk at the outer rim caused by the application of air jet. In Figure 4. 3 the dc amplitude response of the spinning disk versus speed is plotted. The amplitude is measured at the location of probe 3. The dc amplitude is calculated using the mean value of two seconds of displacement data. The disk deflection is measured from the position of the disk after the application of air-jet excitation when the disk is stationary. Mode (n,m) refers to a mode with n and m nodal circles and diameters, respectively.

From Figure 4. 2a-b it may be noted that when only white noise excitation is used, the frequency response shows behavior which is characteristic of a linear system. The frequencies of backward traveling waves decrease smoothly and reach a speed where the measured frequency is zero or close to zero. This speed is the critical speed of that mode. However, the response at these low frequencies is noisy and it is difficult to make definitive statements about the frequency paths in this region. Although air jet excitation is not used for Figure 4. 2a-b, it seems that the frequencies of the backward traveling waves of the (0,2) and (0,3) modes maintain a constant level for a small speed range

between 2800 RPM and 3200 RPM. The waterfall plot given in Figure 4. 4 more clearly defines the paths of the measured frequencies of the (0,2) and (0,3) modes.

In Figure 4. 3a, (no applied air jet force) it may be noticed that several stationary waves develop and then collapse in the critical speed region between 2800 RPM and 3200 RPM (in the run-up case). Although the disk deflection is small at sub-critical speeds, at supercritical speeds the ratio of dc deflection to thickness reaches almost 0.37. At such levels, nonlinear effects are important. However the level of the applied force is insufficient to sustain the developed stationary waves over a significant speed range.

Figure 4. 2c and Figure 4. 2d show the response when $w_0/h = 0.1$. In these two cases the measured frequencies, at sub-critical speeds, are essentially the same as those measured in the case with only white noise excitation. A major difference occurs when the speed approaches the first critical speed around 2800RPM. At this speed, the measured frequencies of the backward traveling waves of the (0,2) and (0,3) modes level off and have a nearly constant frequency. From Figure 4. 3b it can be seen that in the run-up case, 2800 RPM represents the onset of development of a stationary wave. The primary instability [7] that occurs at this speed causes the amplitude of the disk response to grow.

From Figure 4. 3b it may be noted that the amplitude of the dc displacement fluctuates at speeds above 2800RP. This is due to the fact that the level of nonlinearity is relatively small and the stationary wave cannot be sustained over a large speed range and thus collapses shortly after development. From Figure 4. 2b, it can be seen that the critical speeds of the (0,2), (0,3) and (0,4) modes lies between 3000 to 4000 RPM. Therefore, when the stationary wave associated with one of these modes collapses the stationary wave for the next mode starts to develop after a short increase in speed.

From the dc amplitude response plotted in Figure 4. 3b, it can be seen that in the run up case when the speed approaches 3800 RPM, the last stationary wave collapses which is an indication of a secondary instability [7]. As shown Figure 4. 2c , the run up case, in the speed range of 2800 and 3200 RPM there is the initiation of a lock-in phenomena in the measured frequency of the (0,0) mode. After this speed range, when the last

stationary nodal diameter wave collapses, a jump in the measured frequency of the (0,0) mode is evident.

From Figure 4. 3b, it can be seen that in the run down case, the stationary wave starts to develop at a speed close to 3600 RPM. A drop at this same speed, in the frequency of the (0,0) mode, is also evident in the run down case shown in Figure 4. 2d,. The frequency of this mode then remains almost constant until the speed reaches 2800 RPM.

Raman et al. [7] has identified two types of instabilities that arise in the study of spinning disks. The first type of instability is called “primary instability”. In this set of experiments, primary instability happens when the spinning disk is subjected to a constant space fixed force and is rotating at a speed close to one of its critical speeds. In this situation the dc amplitude response of the spinning disk starts to increase and a stationary wave starts to develop. Another type of instability called “secondary instability” gives rise to the collapse of the stationary wave. At the speed corresponding to this type of instability, a sudden change in the amplitude and the frequency of the wave occurs. At the speed corresponding to the secondary instability a bifurcation occurs which is an indication of the existence of multiple solution branches. The results in Figure 4. 2c,d and also Figure 4. 3b indicate that the secondary instabilities occur at 3800 and 3600 RPM on run up and rundown, respectively.

In Figure 4. 2e and Figure 4. 2f, the measured frequencies are plotted for the case where $w_0/h = 0.4$. In this case the measured frequencies of the forward and backward traveling of the (0,2) mode at zero speed are found (by extrapolating the curves to zero speed) to be more separated than the cases with no air jet excitation or when $w_0/h = 0.1$. The separation of these frequencies for the (0,1) mode is not so significant.

Application of the air jet destroys the axial symmetry of the disk resulting in separation of the zero speed frequencies. Hutton et. al. [11] showed that, in the linear case, adding space fixed springs to a rotating disk system, destroys disk symmetry and results in separate backward and forward traveling waves frequencies of the same mode at zero speed. Another source of separation in the measured frequencies is the presence of non symmetric internal residual stresses.

Table 4. 2 presents estimates of the frequencies of the (0,2)f and (0,2)b modes of the stationary wave as a function of initial disk displacement produced by the air jet ('f' and 'b' stand for forward and backward traveling waves, respectively). The frequency values presented in this table correspond to the run-up case. From this table it may be noted that the difference between the measured frequencies of the backward and forward traveling waves of the (0,2) mode increases as the initial displacement due to the air jet excitation increases.

Figure 4. 2e and Figure 4. 2f show the measured frequencies when $w_0/h = 0.4$. As may be noted from these two figures, at sub-critical speed, the measured frequency is close to the linear frequency response (Figure 4. 2a). It may also be noted that backward traveling waves of the (0,2) and (0,3) modes decreases smoothly when the speed increases until it reaches 2800 RPM. At around 2800 RPM, a stationary wave starts to develop. It is observed that the developed stationary wave is in the form of the (0,3) mode as shown in Figure 4. 5. After this speed, the measured frequencies of the backward traveling waves of the (0,2) and (0,3) modes maintain a constant level up to 4000 RPM. It also can be seen that the frequencies of the backward and forward traveling waves of the (0,2) and (0,3) modes do not approach zero.

Since there is no sign of a sudden drop or change in the frequency and amplitude responses, it can be concluded that in this case, for the range of speed used, there is no secondary instability. It also can be seen that not only the frequencies of these two modes maintain a constant level, the frequency curves for other modes also diverge from their linear paths. For example, the curve for the frequency response of the (0,6) mode bends and tends to level off and maintain a constant level. This behaviour can be attributed to the fact that the dc configuration of the rotating disk now has strain energy characteristics different from those possessed by the disk in its zero speed configuration.

When the speed decreases from 4000 RPM in the run down case, the dc amplitude and measured frequencies, follow almost the same path as measured in the run up case. This is because the developed stationary wave is stable at all speeds below 4000 RPM.

Figure 4. 2g and Figure 4. 2h shows the measured frequency response of the disk for the case of $w_0/h = 0.6$. Once again, the measured frequencies of the (0,2) and (0,3) modes

are almost constant in the speed range that the stationary wave is developed. There is not a significant difference between this case and the previous one with $w_0/h = 0.4$.

Figure 4. 2e-h clearly indicate that no backward travelling waves (for these levels of nonlinearity) approach a zero frequency level. Instead, as they approach their critical speeds they veer off to adopt constant levels independent of speed. Thus no critical speeds exist for these cases. Figure 4. 5 plots the mode shape of the DC response of Disk 1 for $w_0/h = 0.6$ at 3600RPM estimated from the data obtained from the four displacement probes and show the response is primarily in the (0,3) mode

Table 4. 2. Estimated Frequencies at Zero Speed (Hz); (0,2) Mode

	(0,2)b	(0,2)f	Difference (Hz)
$w_0/h = 0.0$	65.5	66.2	0.7
$w_0/h = 0.1$	66.4	68.1	1.7
$w_0/h = 0.4$	67.3	70.2	2.9
$w_0/h = 0.6$	67.7	70.9	3.2

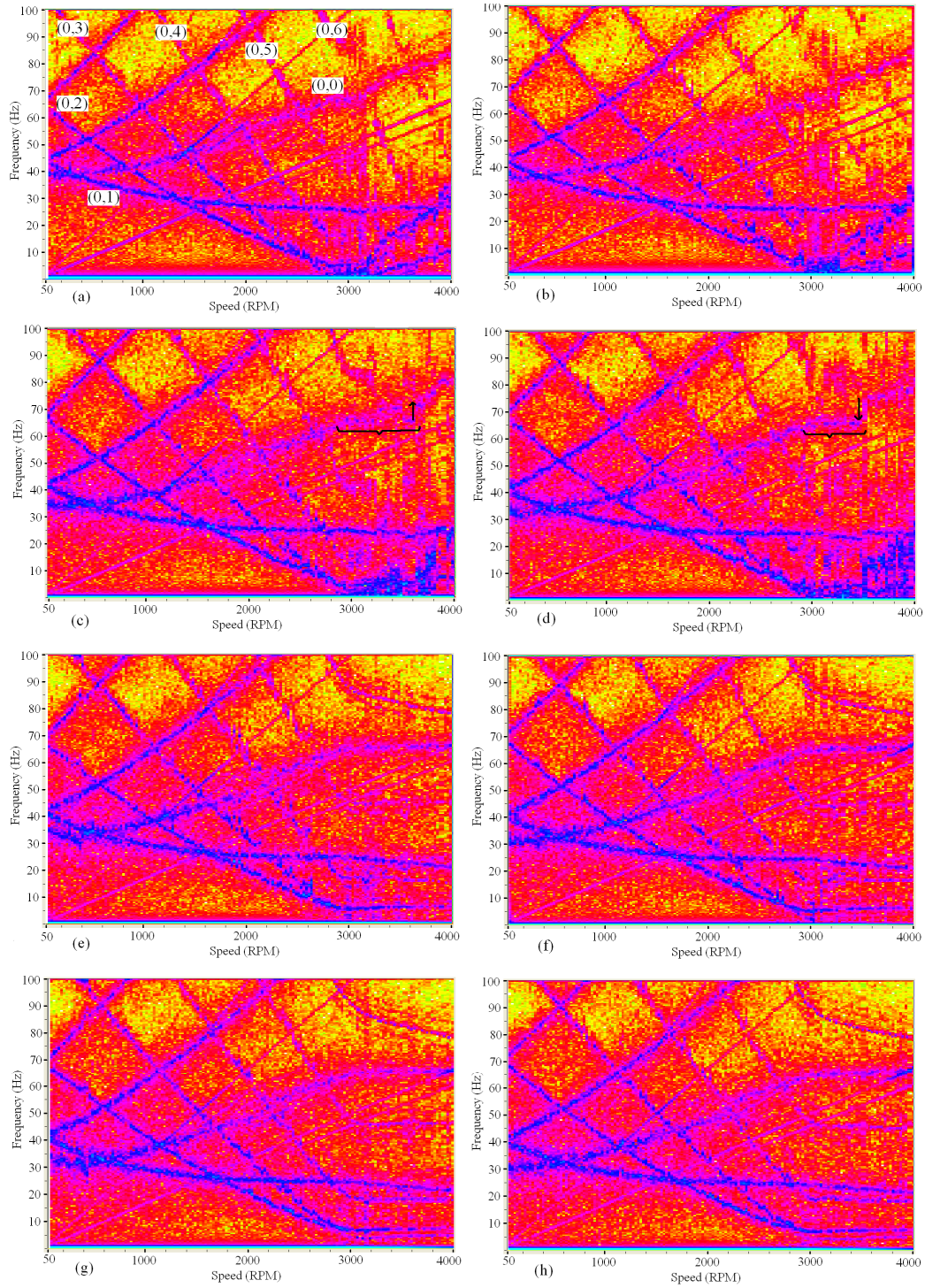


Figure 4. 2. Frequency Response of Disk #1 for Different Force Levels
 Run-Up: (a) $w_0/h = 0.0$, (c) $w_0/h = 0.1$, (e) $w_0/h = 0.4$, (g) $w_0/h = 0.6$
 Run-Down: (b) $w_0/h = 0.0$, (d) $w_0/h = 0.1$, (f) $w_0/h = 0.4$, (h) $w_0/h = 0.6$

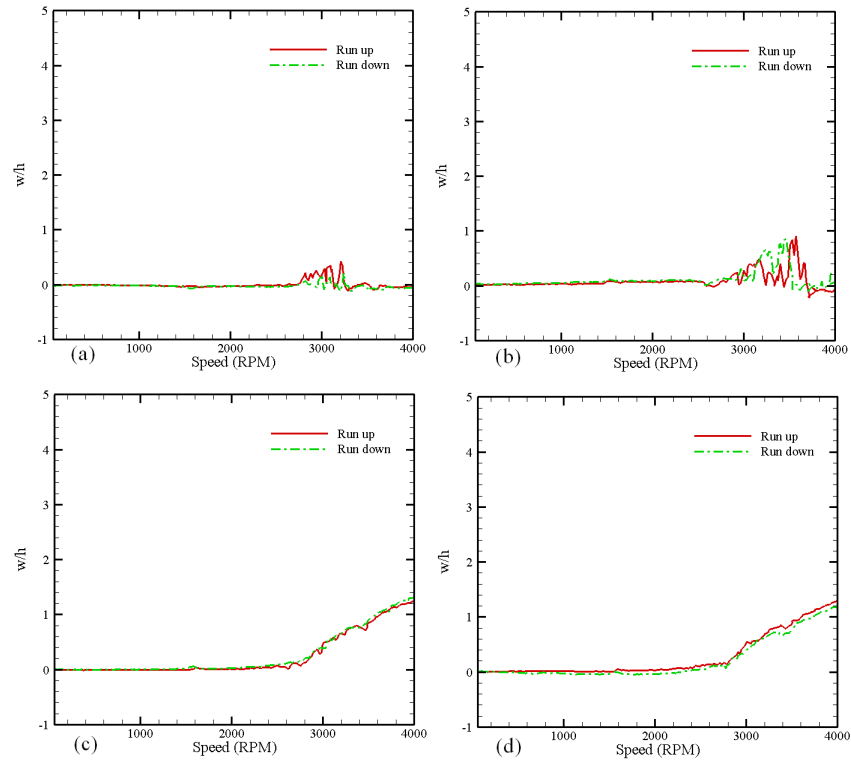


Figure 4.3. Disk 1- DC Displacement versus Speed (probe 3)
 (a) $w_0/h = 0.0$, (b) $w_0/h = 0.1$, (c) $w_0/h = 0.4$ (d) $w_0/h = 0.6$

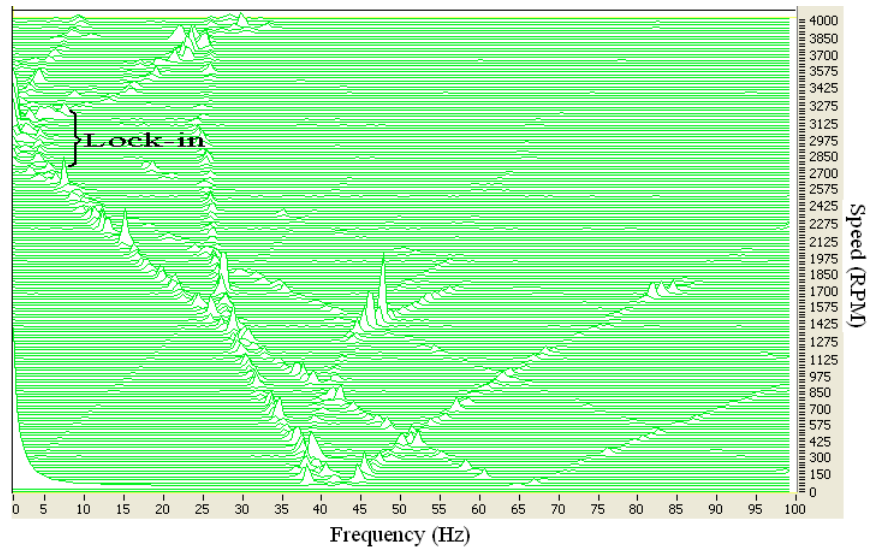


Figure 4.4. Disk 1- Waterfall plot with white noise magnetic excitation ($w_0/h = 0.0$) in the run-up case

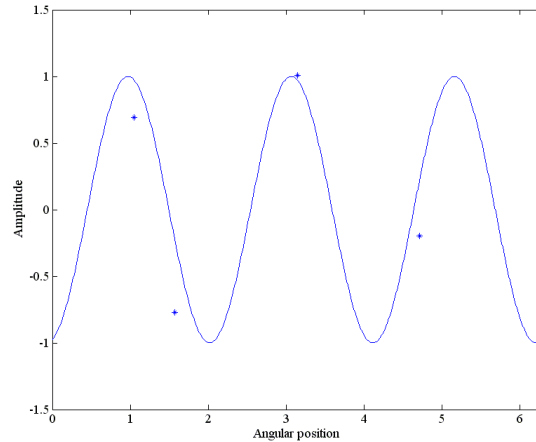


Figure 4. 5. Disk 1- DC amplitude at 3600 RPM at the location of four probes (shown with stars) and the (0,3) mode curve fitting (solid lines) when $w_0/h = 0.6$

4.3.2. Disk #2 – 0.040” Thickness

The maximum displacement that the air jet could produce in the 0.050” disk was $w_0/h = 0.6$. To examine the effect of higher levels of nonlinearity, a thinner disk was used which, when subjected to the same maximum air jet force, produced higher levels of displacement. Figure 4. 6 shows the measured frequency response of this disk, as a function of speed, for different values of w_0/h for a 0.040” disk. Figure 4. 7 show the associated measured DC deflections versus speed.

When the air-jet excitation is not used ($w_0/h = 0$), and for the speeds below the first critical speed (2600 RPM), the measured frequency response shows linear characteristics. From Figure 4. 7a it may be noted that in the run-up case, at around the first critical speed (2600RPM), a stationary wave starts to develop. Also, from Figure 4. 6a it may be seen that the measured frequencies of the backward traveling waves of the (0,2) and (0,3) modes maintain a constant level for a small speed range (1000 RPM) starting at 2600 RPM. In the speed range between 2600 and 3600 RPM several stationary waves develop and collapse (Figure 4. 7a) as the disk speed increases. The last stationary wave collapses suddenly at 3600 RPM and as a result a sudden jump in the frequency response of the (0,0) mode is evident in Figure 4. 6a.

In the run-down case in Figure 4. 7a, the first stationary wave starts to develop around 3200 RPM. From 4000 to 3200RPM the DC response is small and thus linear

behaviour would be expected in this region. From Figure 4. 6b it may be seen that from 4000 to 3200 RPM the measured frequency response is somewhat noisy and definitive statements are difficult to make regarding the character of the measured response.

In the run down case, with no air jet excitation, a secondary instability occurs close to 3200RPM (Figure 4. 7a). As a result of this instability, a sudden drop in the measured frequency of the (0,0) mode is notable in Figure 4. 6b.

In all cases in Figure 4. 6, with non zero force excitation, the development of a stationary wave coincides with a speed regime in which the low frequency modes are essentially invariant with blade speed. This behaviour appears to be consistent with the “lock-in” phenomenon described by Jana et. al [9]. It may be noted that this behaviour occurs with the (0,0) mode as well as the nodal diameter modes.

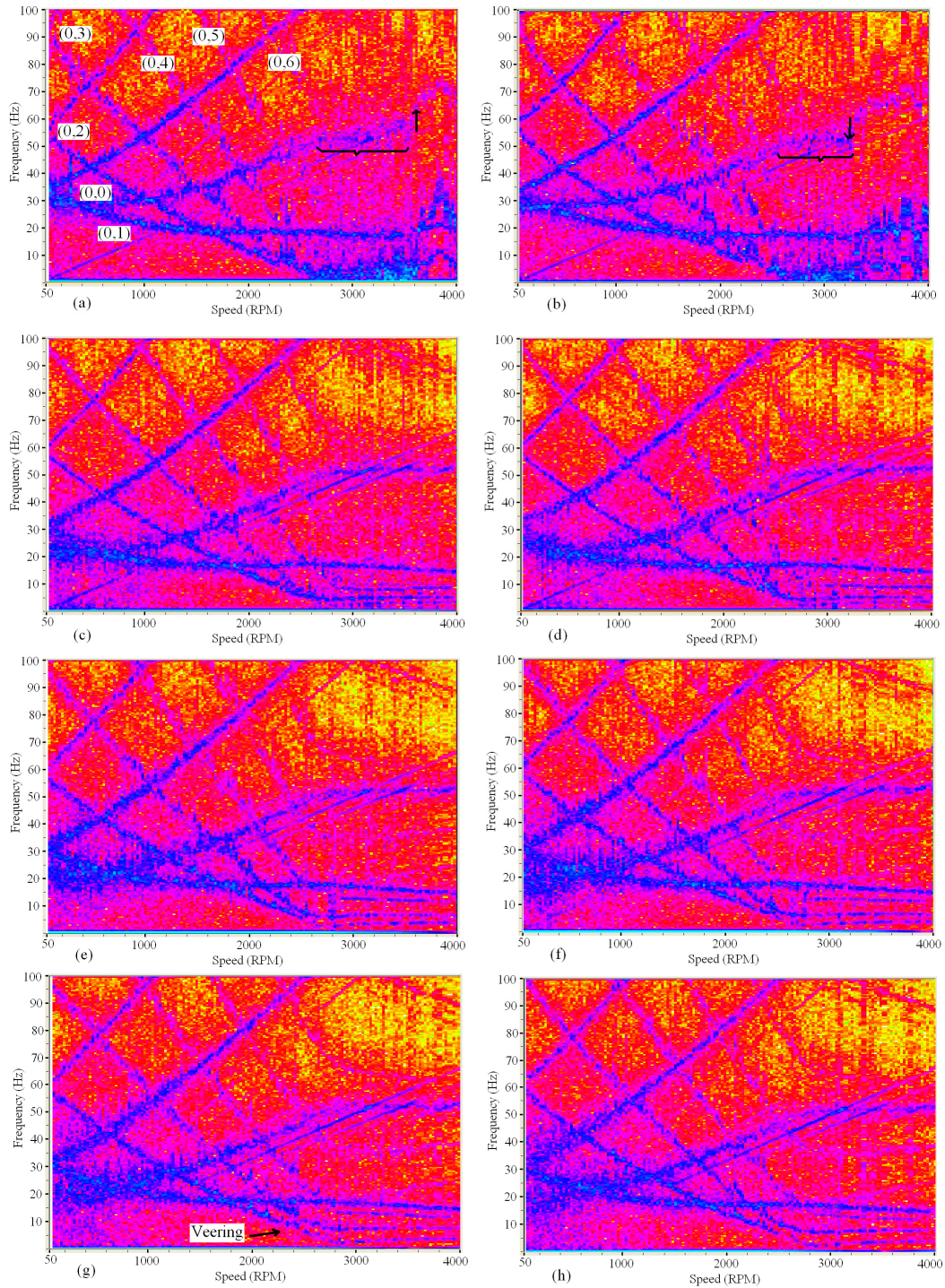


Figure 4. 6. Frequency Response of Disk #2 for Different Force Levels
 Run-Up: (a) $w_0/h = 0.0$, (c) $w_0/h = 0.5$, (e) $w_0/h = 1.0$, (g) $w_0/h = 2.0$
 Run-Down: (b) $w_0/h = 0.0$, (d) $w_0/h = 0.5$, (f) $w_0/h = 1.0$, (h) $w_0/h = 2.0$

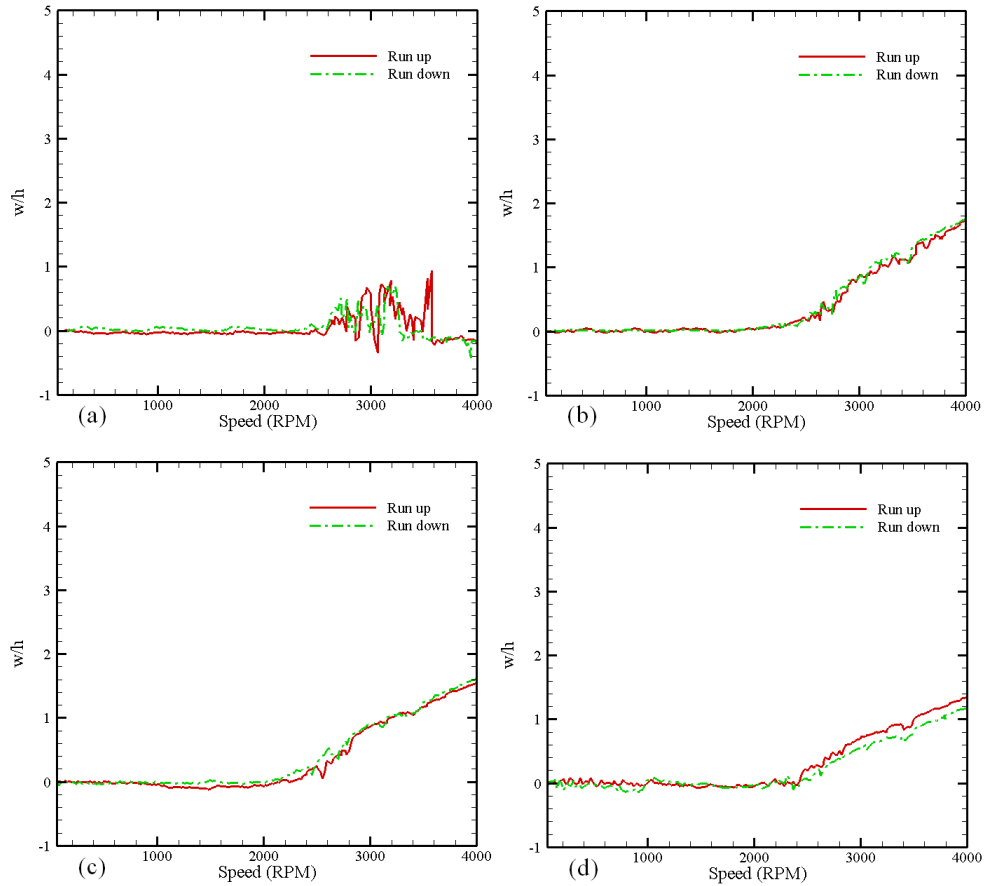


Figure 4. 7. Disk 2- DC Displacement versus Speed (probe 3)
 (a) $w_0/h = 0.0$, (b) $w_0/h = 0.5$, (c) $w_0/h = 1.0$ (d) $w_0/h = 2.0$

4.3.3. Disk #3 – 0.030” Thickness

This disk is very thin; it is approximately 5 times more flexible than the 0.050” disk and displays different characteristics to the previous two blades. For the previous two disks the initial runout was small. In the case of Disk #3 this was not the case and the non clamped disk was dished (see Table 4. 1). In the process of clamping the disk to the arbor, snap through buckling occurred. This resulted in a deformation of the disk into approximately the shape of the (0,0) mode with a displacement at the rim of 0.055”. Thus significant internal stresses would have been induced by the clamping process.

The mean amplitude of the disk, at the location of all four probes, is presented in Figure 4. 8 for the case where $w_0/h = 0.5$. The amplitude is measured from its zero speed deformed position. Up to approximately 2300 RPM all of the points move in the same

direction. This indicates that the disk deflection is in the form of the (0,0) mode as it tends to straighten out due to centrifugal effects. Although the air pressure is applied to the disk at one specific point (location of probe #3), the disk deflections have almost the same amplitudes at all probe locations up to approximately 2000 RPM. Above 2000 RPM the disk is no longer dished and for speeds higher than 2300 RPM the probes move in different directions. From the mean amplitudes measured at the location of probes, it may be concluded that a stationary wave is developed for the speeds higher than 2300 RPM.

In Figure 4. 9 the measured frequencies of the spinning disk, using different levels of nonlinearity, are plotted against the speed. From Figure 4. 9a, the lowest critical speed appears to be in the region of 2600RPM. The plots with non zero force are very noisy for frequencies below 40Hz but there appears to be evidence, at frequencies above this, of the backward travelling waves displaying the same behaviour as previous disks with the frequency tending toward a constant value above speeds of 2600RPM. There does not appear to be any evidence that the (0,0) mode is excited for speeds below 2000 RPM.

In Figure 4. 10c a snap through buckling is indicated at 1300RPM. This is also reflected in Figure 4. 9e,f where there appears to be a discontinuous frequency response at 1300RPM for all modes resulting from the changed modal configuration at this speed.

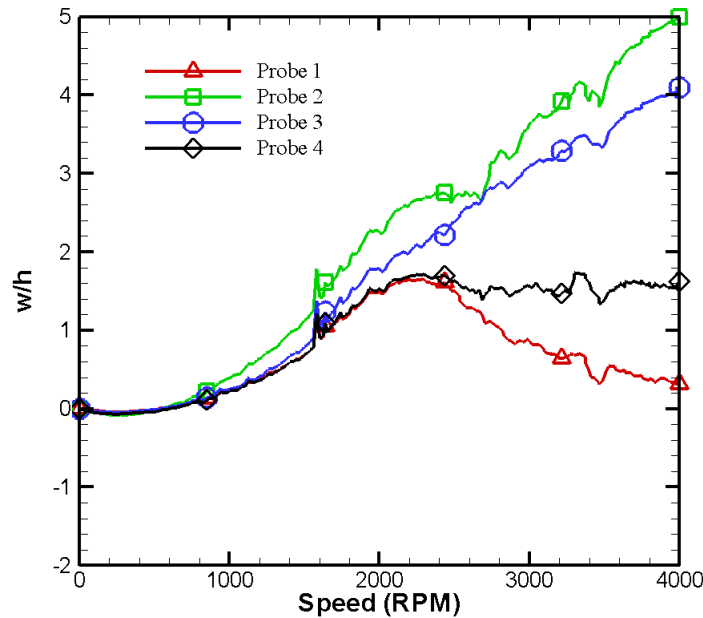


Figure 4. 8. DC displacement of disk #3, when $w_0/h = 0.5$ at all probes

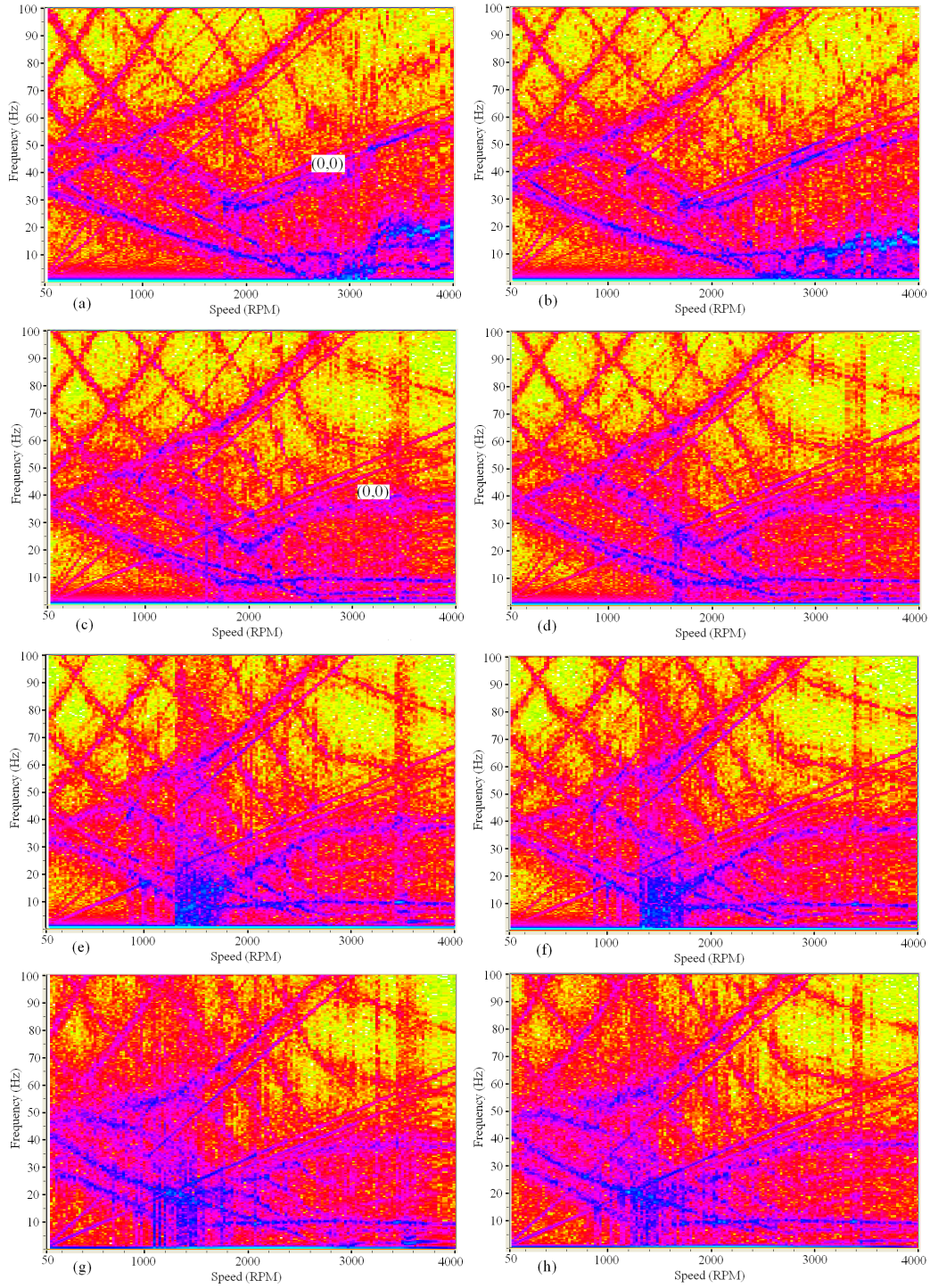


Figure 4. 9. Frequency Response of Disk #3 for Different Force Levels
 Run-Up: (a) $w_0/h = 0.0$, (c) $w_0/h = 0.5$, (e) $w_0/h = 1.0$, (g) $w_0/h = 2.0$
 Run-Down: (b) $w_0/h = 0.0$, (d) $w_0/h = 0.5$, (f) $w_0/h = 1.0$, (h) $w_0/h = 2.0$

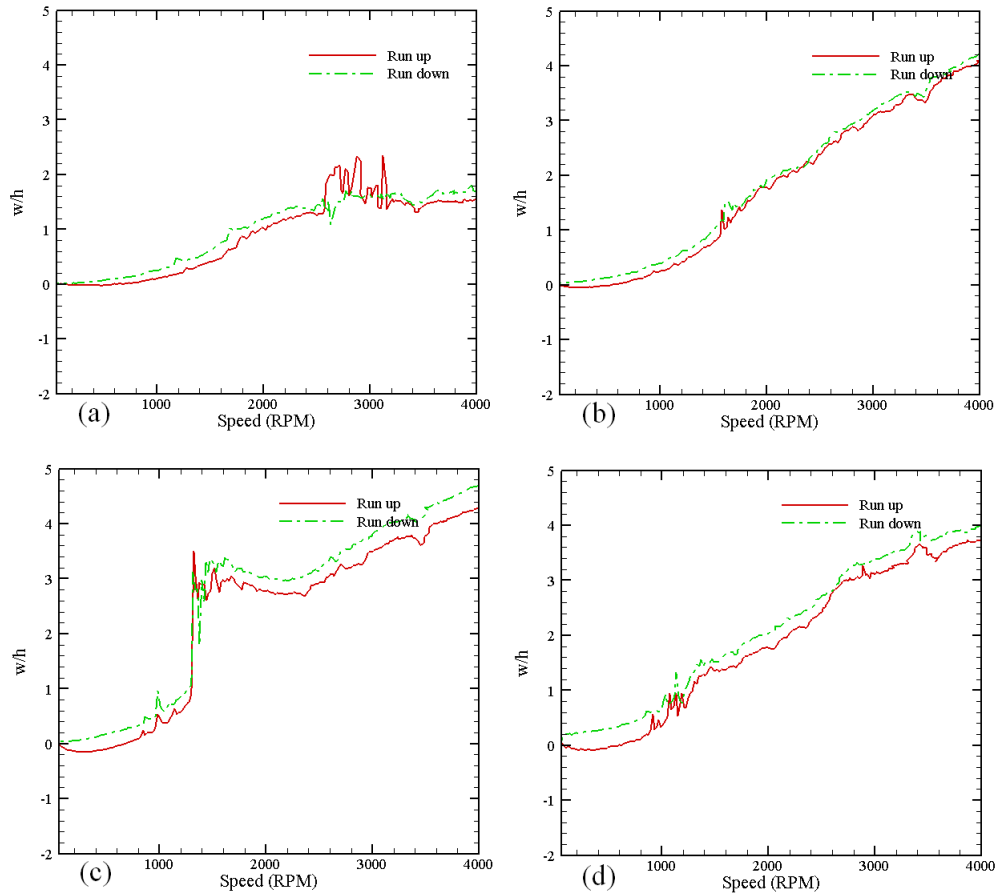


Figure 4. 10. Disk 3- DC Displacement versus Speed (probe 3)
 (a) $w_0/h = 0.0$, (b) $w_0/h = 0.5$, (c) $w_0/h = 1.0$ (d) $w_0/h = 2.0$

4.4. Conclusions

Experimental results have been presented that illustrate the vibration behavior of three uniform, thin, spinning disks of different thicknesses (0.050”, 0.040” and 0.030”) subjected to a constant lateral force of different magnitudes. In particular frequency and amplitude characteristics are measured as a function of speed and applied force. Using different levels of air-jet excitation, different levels of nonlinearity are induced and the resulting responses recorded and compared to linear behaviour.

The 0.050” and the 0.040” disks had behaviour characteristic that were similar. The thinnest disk 0.030” behaved in a different manner. This difference in behaviour was in part due to the large dished runout of this disk which caused it to undergo snap through buckling when clamped to the arbor. It also may be that this disk is so thin that its

characteristics were more dictated by membrane behaviour than the other two disks. Further conclusions will be restricted to the behavior of the 0.050” and 0.040” disks.

DC displacement results obtained for speeds below the lowest critical speed were not sensitive to the level of nonlinearity for the tests conducted in this study. At and above the critical speed the results obtained illustrated the important effects of nonlinearity. At very low levels of nonlinearity the dc response in the critical speed region was characterized by the formation and collapse of stationary waves over a short speed interval. Above a certain level of nonlinearity stationary waves developed and were stable up the maximum speeds tested. It should be noted that these stationary waves were measured using a two second averaging algorithm and in practice would consist of both a dc component (as recorded) plus a superimposed frequency component (not recorded).

The formation of these stationary waves coincided with a change in the path of the frequencies of the backward travelling waves of all the modes recorded. At the speed corresponding to the formation of the stationary waves the backward travelling waves veered from their linear path to one where the frequency remained constant with speed. Thus the effect of the nonlinearity was to modify the lowest backward traveling waves such that they do not experience a zero natural frequency. As a result a pure standing wave does not exist in the presence of nonlinearity. This in turn indicates that the theoretical critical speed, based upon linear analysis, does not exist in the presence of nonlinearity. A consequence of the backward travelling waves adopting a constant value is that there are no reflected waves and thus no supercritical speed conditions for flutter instability arise.

The experimental results verified that the introduction of a space fixed external force causes separation of the backward and forward traveling waves of a given mode at zero speed. This would be expected due to the lack of symmetry of the internal stresses distribution. Further, it would be expected that the resulting nodal patterns would be such as to provide minimum and maximum frequencies for the existing imperfection distribution. Of course it is likely that the disks tested had other imperfections that contributed to the lack of symmetry which would add to and affect this issue.

4.5. References

- [1] Tobias, S.A., and Arnold, R.N., 1957, "The Influence of Dynamical Imperfections on the Vibration of Rotating Disks," Institution of Mechanical Engineers, Proceedings 171, pp. 669-690.
- [2] Chen, J.S., and Lin, C., 2005, "Axisymmetrical Snapping of a Spinning Nonflat Disk," Journal Of Applied Mechanics, 72(6), pp. 879-886.
- [3] Chen, J.S., and Chang, Y., 2007, "On the Unsymmetrical Deformation and Reverse Snapping of a Spinning Non-Flat Disk," International Journal of Non-Linear Mechanics, 42(8), pp. 1000-1009.
- [4] Thomas, O., Touze, C., and Chaigne, A., 2003, "Asymmetric Non-Linear Forced Vibrations of Free-Edge Circular Plates. Part II: Experiments," Journal of Sound and Vibration, 265(5), pp. 1075-1101.
- [5] Raman, A., and Mote, C.D. , 2001, "Experimental Studies on the Non-Linear Oscillations of Imperfect Circular Disks Spinning Near Critical Speed," International Journal of Non-Linear Mechanics, 36(2), 2001, pp. 291-305.
- [6] D'Angelo, C., Mote, C.D., 1993, "Aerodynamically Excited Vibration and Flutter of a Thin Disk Rotating at Supercritical Speed," Journal of Sound and Vibration, 168, pp. 15-30.
- [7] Raman, A., Hansen, M. H., and Mote, C.D., 2002, "A Note on the Post-Flutter Dynamics of a Rotating Disk," Journal of Applied Mechanics, 69(6), pp. 864-866.
- [8] Kang, N., and Raman, A., 2006, "Vibrations and Stability of a Flexible Disk Rotating in a Gas-Filled Enclosure-Part 2: Experimental Study," Journal of Sound and Vibration, 296(4-5), pp. 676-68.
- [9] Jana, A., and Raman, A., 2005, "Nonlinear aeroelastic flutter phenomena of a flexible disk rotating in an unbounded fluid," Journal of Fluids and Structures, 20(7), pp. 993-1006.
- [10] Khorasany, R.M.H., and Hutton, S.G., 2010, "Vibration Characteristics of Rotating Thin Disks, Part II: Analytical Predictions", submitted to ASME Journal of Applied Mechanics.

- [11] Hutton, S.G., Chonan, S., and Lehmann, B.F., 1987, "Dynamic Response of a Guided Circular Saw," *Journal of Sound and Vibration*, 112, pp. 527-539.

Chapter 5- Analytical Investigations on the Nonlinear Frequency Behavior *

5.1. Introduction

Spinning disks have many industrial applications. In some the disk deflection exceeds the limit at which the linear theory is valid. In these circumstances, the frequency predictions based upon the linear theory are not accurate and geometric nonlinear effects must be considered.

Theoretical studies of this problem using linear analysis started with the work of Lamb and Southwell [1]. They investigated the transverse linear vibration of a flat, isotropic circular disk of uniform thickness rotating about its axis with constant angular velocity. Mote [2] analyzed the free vibration characteristics of centrally clamped, variable thickness disks by the Rayleigh-Ritz technique. Natural frequencies of transverse vibration were computed taking into consideration rotational and thermal in-plane stress as well as purposely induced initial stresses. Hutton et. al. [3] studied the dynamic response characteristics of rotating circular disks when subjected to the effect of forces produced by stationary spring guides. Chen and Bogy [4] used the orthogonality properties that govern the modes, to develop a method for finding the derivative of mode shapes with respect to a certain parameter. Using this method, they found the derivative of the natural frequencies of the system with respect to constraint parameters such as mass, damper and stiffness. Tian and Hutton [5] developed an analytical model of a wood-cutting circular saw blade for the purpose of understanding the mechanics of a lateral vibration instability known as washboarding. The governing equation developed contains inertial, gyroscopic and stiffness terms with the cutting forces being represented

* A version of this chapter has been submitted for publication. Khorasany, R.M.H., and Hutton, S.G., 2010, "Vibration Characteristics of Rotating Thin Discs, Part II: Analytical Predictions".

by the product of a time-dependent periodic function and the lateral displacement of the saw teeth.

There is also an extensive body of research work that considers the effect of geometrical nonlinear terms on the response of spinning disks. Nowinski [6] presented a formulation for the nonlinear vibration of rotating disks due to large displacements. Tobias [7] studied the nonlinear vibrations of imperfect rotating discs and Jana and Raman [8] investigated the nonlinear dynamics of a flexible spinning disk coupled to a pre-compressed spring. They studied large amplitude wave motions and their stability using the averaging method. Nayfeh, Jilani and Manzione [9] used the method of multiple scales to investigate the transverse nonlinear vibrations of a centrally clamped rotating circular disk. Chen [10] used the multiple scales method to investigate the internal resonance between a pair of forward and backward modes of a spinning disk under spaced fixed pulsating edge loads. Touze et. al. [11] studied the nonlinear oscillations of a stationary disk with imperfections. They studied the coupling between preferential configurations and investigated its effect on the traveling wave components in the response.

Yang and Hutton [12] used polynomial expansion functions as the approximation function in the Galerkin's method to solve the nonlinear equations of motion for rotating thin disks. Luo and Mote [13] used a new plate theory to study the effect of large amplitude displacements on the frequency behavior of spinning disks. Based on energy principles they calculated the frequencies of a spinning disk considering the effect of nonlinear terms.

The specific aim of this chapter is to investigate the effects of large deformation on the frequency behavior of spinning disks. The response of a thin, idealized rotating disc subjected to a space fixed external force (and the resulting nonlinear deformations) is analyzed. In particular the frequency behaviour of travelling waves at supercritical speeds is investigated.

To validate the accuracy of the numerical predictions, comparisons are made with experimental results presented in a companion paper [14] which is chapter 4 of this thesis, (hereafter referred to as Part I).

5.2. Formulation

A thin annular disk of thickness h , inner radius a and outer radius b (with $b \gg h$) is considered. It is assumed that the disk is perfectly flat and made of an isotropic homogenous material with Young's modulus E , Poisson's ratio ν and density ρ . It is also assumed that the disk is free of any initial stress and that the effect of in-plane vibrations and rotary inertia are negligible. Based on these assumptions, Nowinski [6] developed the nonlinear equations of motion of a spinning disk with speed Ω in the space-fixed polar coordinate system $((r, \theta))$ as:

$$\begin{aligned} \frac{\partial^2 w}{\partial t^2} + 2\Omega \frac{\partial^2 w}{\partial \theta \partial t} + \Omega^2 \frac{\partial^2 w}{\partial \theta^2} + \nabla^4 w = \varepsilon L(w, \phi) - \frac{1}{2} \Omega^2 r^2 \nabla^2 w \\ - \Omega^2 r \frac{\partial w}{\partial r} + (F/r) \delta(r - r_F) \delta(\theta - \theta_F), \end{aligned} \quad (5.1)$$

$$\nabla^4 \phi = -\frac{1}{2} L(w, w) + \frac{2(1-\nu)\Omega^2}{\varepsilon}, \quad (5.2)$$

$$\begin{aligned} L(f, g) = \frac{\partial^2 f}{\partial r^2} \left(\frac{1}{r} \frac{\partial g}{\partial r} + \frac{1}{r^2} \frac{\partial^2 g}{\partial \theta^2} \right) + \frac{\partial^2 g}{\partial r^2} \left(\frac{1}{r} \frac{\partial f}{\partial r} + \frac{1}{r^2} \frac{\partial^2 f}{\partial \theta^2} \right) \\ - 2 \left(\frac{1}{r} \frac{\partial^2 g}{\partial r \partial \theta} - \frac{1}{r^2} \frac{\partial g}{\partial \theta} \right) \left(\frac{1}{r} \frac{\partial^2 f}{\partial r \partial \theta} - \frac{1}{r^2} \frac{\partial f}{\partial \theta} \right), \end{aligned}$$

where w is the transverse deflection of the disk, ϕ is the stress function, F is a space-fixed applied external force acting at (r_F, θ_F) . The above equations are in normalized form. The relations between the actual (denoted by prime) and normalized parameters are

$$\begin{aligned} r = \frac{r'}{b}, \quad w = \frac{bw'}{h^2}, \quad t = t'T, \quad \Omega = \frac{1}{T} \Omega', \quad F = \frac{b^5}{Dh^2} F', \\ \phi' = \frac{b^2}{Eh^5} \phi, \quad T = \frac{(D/\rho h)^{1/2}}{b^2}, \quad \varepsilon = 12(1-\nu^2)h^2/b^2 \end{aligned}$$

$D = Eh^3/12(1-\nu^2)$ is the disk flexural rigidity. The effect of in-plane stresses are taken into account via the stress function. The solution of Eq.(5.2) consists of two components ϕ^h (homogeneous solution) and ϕ^p (particular solution) where ϕ^h is speed dependant and ϕ^p is displacement dependant.

In this chapter, it is assumed that the spinning disk is clamped at the inner rim and free at the outer rim. Therefore, at the inner rim ($\eta = \frac{a}{b}$) the boundary conditions have the following form

$$\begin{aligned} w &= 0 & \text{at} & \quad r = \eta, \\ \frac{\partial w}{\partial r} &= 0 & \text{at} & \quad r = \eta. \end{aligned} \quad (5.3)$$

At the outer rim the bending moment and Kirchhoff edge reaction are zero which in the nondimensional form can be expressed as [12]:

$$\begin{aligned} \frac{\partial}{\partial r} \nabla^2 w + \frac{1-\nu}{r^2} \frac{\partial^2}{\partial \theta^2} \left(\frac{\partial w}{\partial r} - \frac{w}{r} \right) &= 0 & \text{at} & \quad r = 1, \\ \frac{\partial^2 w}{\partial r^2} + \nu \left(\frac{1}{r} \frac{\partial w}{\partial r} + \frac{1}{r^2} \frac{\partial^2 w}{\partial \theta^2} \right) &= 0 & \text{at} & \quad r = 1. \end{aligned} \quad (5.4)$$

Moreover at the inner rim, radial and hoop displacements must vanish. These constraints can be expressed in the following forms [8]

$$\frac{\partial^2 \phi}{\partial r^2} - \nu \left(\frac{1}{r} \frac{\partial \phi}{\partial r} + \frac{1}{r^2} \frac{\partial^2 \phi}{\partial \theta^2} \right) - \frac{1-\nu}{2\varepsilon} \Omega^2 r^2 = 0 \quad \text{at} \quad r = \eta, \quad (5.5a)$$

$$\frac{\partial^3 \phi}{\partial r^3} + \frac{1}{r} \frac{\partial^2 \phi}{\partial r^2} - \frac{1}{r^2} \frac{\partial \phi}{\partial r} + \frac{2+\nu}{r^2} \frac{\partial^3 \phi}{\partial r \partial \theta^2} - \frac{3+\nu}{r^3} \frac{\partial^2 \phi}{\partial \theta^2} - \frac{1-\nu}{\varepsilon} \Omega^2 r = 0 \quad \text{at} \quad r = \eta. \quad (5.5b)$$

Also, at the outer rim, in-plane stresses σ_{rr} and $\sigma_{r\theta}$ are zero. In terms of the non dimensional variables, these boundary conditions can be written as:

$$\frac{1}{r} \frac{\partial \phi}{\partial r} + \frac{1}{r^2} \frac{\partial^2 \phi}{\partial \theta^2} - \frac{1}{2\varepsilon} \Omega^2 r^2 = 0 \quad \text{at} \quad r = 1, \quad (5.6a)$$

$$-\frac{1}{r} \frac{\partial^2 \phi}{\partial r \partial \theta} + \frac{1}{r^2} \frac{\partial \phi}{\partial \theta} = 0 \quad \text{at} \quad r = 1. \quad (5.6b)$$

As was discussed above, the stress function can be decomposed into two different parts as follows

$$\phi = \phi^h + \phi^p. \quad (5.7)$$

The associated boundary conditions for the homogenous part of the stress function are those stated in (5.5a) and (5.6a). After finding the homogenous part of the stress function and substituting into the boundary conditions stated in Eqs (5.5-6), the speed dependent part of these equations will be satisfied. Therefore, the associated boundary conditions for the particular part of the stress function are the ones that are stated in Eqs.

(5.5) and (5.6) neglecting the speed dependent parts. After finding the homogenous part of the stress function through Eq. (5.2), the following expression is obtained:

$$\phi^h = \frac{c_1 r^2 + c_2 \ln r + (1-\nu)\Omega^2 r^4 / 32}{\varepsilon}. \quad (5.8)$$

The homogenous part of the stress function is only a function of 'r'. c_1 and c_2 are constants that can be found using the appropriate boundary conditions for the homogenous part of the stress function. Since ϕ^h is not a function of θ , the boundary condition stated in Eq. (5.6b) is automatically satisfied. Also if we substitute ϕ^h from Eq. (5.8) into Eq. (5.5b) we find that this boundary condition is also automatically satisfied. Using Eq. (5.8) and the boundary conditions stated in Eqs. (5a) and (6a), c_1 and c_2 are found to be

$$c_1 = \frac{(1+\nu)[3+\nu+(1-\nu)\eta^4]}{16[1+\nu+(1-\nu)\eta^2]} \Omega^2,$$

$$c_2 = \frac{(1-\nu)\eta^2[3+\nu-(1+\nu)\eta^2]}{8[1+\nu+(1-\nu)\eta^2]} \Omega^2.$$

Numerous techniques can be used to develop a solution method for the governing equations. In the present paper, the Galerkin's method is used with approximating functions derived from the solution of the eigenfunctions of the following two eigenvalue problems:

$$\nabla^4 w = (\lambda_{mn}^w)^4 w,$$

$$\nabla^4 \phi = (\lambda_{mn}^\phi)^4 \phi.$$

The first eigenvalue problem stated in the above is associated with the transverse deflection and the second one is associated with the stress function. The eigenfunctions of the transverse displacement eigenvalue problem stated in the above are assumed to be: $W_{mn} = R_{mn}^w(\lambda_{mn}^w r) \sin m\theta$ and $R_{mn}^w(\lambda_{mn}^w r) \cos m\theta$ and those of the stress function are assumed to be $\phi_{mn} = R_{mn}^\phi(\lambda_{mn}^\phi r) \sin m\theta$ and $R_{mn}^\phi(\lambda_{mn}^\phi r) \cos m\theta$. The boundary conditions of the above eigenvalue problems are given in Eqs. (5.3) and (5.4) for the transverse displacement eigenvalue problem and in Eqs. (5.5) and (5.6) with the assumption that the speed is zero for the stress function eigenvalue problem. Therefore, the transverse displacement and stress function can be approximated by modal expansions:

$$w(r, \theta, t) = \sum_{m,n=0}^{M,N} [S_{mn}^w(t) \sin m\theta + C_{mn}^w(t) \cos m\theta] R_{mn}^w(\lambda_{mn}^w r), \quad (5.9)$$

$$\phi(r, \theta, t) = \phi^h + \sum_{m,n=0}^{M,N} [S_{mn}^\phi(t) \sin m\theta + C_{mn}^\phi(t) \cos m\theta] R_{mn}^\phi(\lambda_{mn}^\phi r). \quad (5.10)$$

M and N are the number of nodal diameters and nodal circles which have been used in the approximation, respectively. It should be noted that the eigenfunctions are normalized using the following relations

$$\int_S W_{mn} W_{ij} dS = \delta_{mi} \delta_{nj}, \quad \int_S \phi_{mn} \phi_{ij} dS = \delta_{mi} \delta_{nj},$$

where δ_{ij} is the Kronecker delta and S is the disk domain. After substitution of Eq. (5.9) into Eq. (5.1) and then multiplying both sides one time by $R_p^w(\lambda_{pq}^w r) \sin p\theta$ and another time by $R_p^w(\lambda_{pq}^w r) \cos p\theta$, and then integrating the resultant over the area of the plate, using the orthogonal property of the eigenfunctions, the following equations are obtained

$$\ddot{S}_{mn}^w - 2\Omega m \dot{C}_{mn}^w + \left((\lambda_{mn}^w)^4 - m^2 \Omega^2 \right) S_{mn}^w = \int_0^{2\pi} \int_\eta^1 \left[\varepsilon L(w, \phi) - \frac{1}{2} \Omega^2 r^2 \nabla^2 w - \Omega^2 r \frac{\partial w}{\partial r} + \left(\left(\frac{F}{r} \right) \delta(r - r_F) \delta(\theta - \theta_F) \right) \right] R_{mn}^w(\lambda_{mn}^w r) \sin m\theta r dr d\theta \quad (5.11a)$$

$$\ddot{C}_{mn}^w + 2\Omega m \dot{S}_{mn}^w + \left((\lambda_{mn}^w)^4 - m^2 \Omega^2 \right) C_{mn}^w = \int_0^{2\pi} \int_\eta^1 \left[\varepsilon L(w, \phi) - \frac{1}{2} \Omega^2 r^2 \nabla^2 w - \Omega^2 r \frac{\partial w}{\partial r} + \left(\left(\frac{F}{r} \right) \delta(r - r_F) \delta(\theta - \theta_F) \right) \right] R_{mn}^w(\lambda_{mn}^w r) \cos m\theta r dr d\theta \quad (5.11b)$$

It should be noted that the above equations are nonlinear ordinary differential equations in terms of the coefficients of the expansion functions and those of the stress function. The source of nonlinearity comes from the term $L(w, \phi)$. The coefficients of the approximation functions for the stress function can be found as a function of those of the transverse displacement. In order to do so, we substitute Eq. (5.9) into nonlinear part of Eq. (5.2) and then multiply both sides one time by $R_{pq}^\phi(\lambda_{pq}^\phi r) \sin p\theta$ and another time by $R_{pq}^\phi(\lambda_{pq}^\phi r) \cos p\theta$. After integrating the resultant over the area of the plate, using the orthogonal property of the eigenfunctions, the following equation will be obtained

$$S_{mn}^{\phi} = \frac{-1}{2(\lambda_{mn}^{\phi})^4} \int_0^{2\pi} \int_{\eta} L(w, w) R_{mn}^{\phi}(\lambda_{mn}^{\phi} r) \sin m\theta r dr d\theta, \quad (5.12a)$$

$$C_{mn}^{\phi} = \frac{-1}{2(\lambda_{mn}^{\phi})^4} \int_0^{2\pi} \int_{\eta} L(w, w) R_{mn}^{\phi}(\lambda_{mn}^{\phi} r) \cos m\theta r dr d\theta. \quad (5.12b)$$

5.3. Linearization

In Chapter (Experimental Results), it was seen that when the amplitude of oscillations is significant compared to the disk thickness, the measured frequency response was both a function of speed and a function of the magnitude of the disk displacement. For low levels of nonlinearity, the measured frequencies show the characteristics of a linear system.

To analyze the effect of large deformations on the frequency behavior of the disk, at any given speed we conduct a linear perturbation analysis. In this analysis we find the equilibrium solution of the spinning disk under the application of a space fixed external force and conduct a small displacement linear vibration analysis about this equilibrium condition. The equilibrium solution found corresponds to the dc amplitude of oscillations recorded in the experimental tests. After linearizing about the numerically found equilibrium solution, a set of coupled linear equations in terms of the coefficients of the expansion functions for the transverse displacement are obtained. Using the linearized form of the equations, we can study the effect of large deformation on the small displacement frequency behavior of the spinning disks.

Substituting Eqs. (9) and (10) into Eqs. (11) and (12), the following nonlinear ordinary differential equations are obtained

$$\begin{aligned} \ddot{S}_{mn}^w - 2\Omega m \dot{C}_{mn}^w + \left((\lambda_{mn}^w)^4 - m^2 \Omega^2 \right) S_{mn}^w = \varepsilon \sum_{i,j=0}^{M,N} \sum_{k,l=0}^{M,N} [Lwp_{1(ij)(kl)(mn)} (I_{1ikm} S_{ij}^w S_{kl}^{\phi} + I_{2ikm} S_{ij}^w C_{kl}^{\phi} \\ + I_{3ikm} C_{ij}^w S_{kl}^{\phi} + I_{4ikm} C_{ij}^w C_{kl}^{\phi}) + Lwp_{2(ij)(kl)(mn)} (I_{4ikm} S_{ij}^w S_{kl}^{\phi} - I_{3ikm} S_{ij}^w C_{kl}^{\phi} - I_{2ikm} C_{ij}^w S_{kl}^{\phi} \\ + I_{1ikm} C_{ij}^w C_{kl}^{\phi})] + \varepsilon \sum_{j=0}^N [(Lwh_{(mj)(mn)} + \varepsilon^{-1} Lwd_{(mj)(mn)}) S_{mj}^w] + F \sin(m\theta_F) R_{mn}^w(\lambda_{mn}^w r_F), \end{aligned} \quad (5.13a)$$

$$\begin{aligned}
 \ddot{C}_{mn}^w + 2\Omega m \dot{S}_{mn}^w + \left((\lambda_{mn}^w)^4 - m^2 \Omega^2 \right) C_{mn}^w = \varepsilon \sum_{i,j=0}^{M,N} \sum_{k,l=0}^{M,N} & \left[LWP_{1(ij)(kl)(mn)} \left(I_{5ikm} S_{ij}^w S_{kl}^\phi + I_{6ikm} S_{ij}^w C_{kl}^\phi \right. \right. \\
 + I_{7ikm} C_{ij}^w S_{kl}^\phi + I_{8ikm} C_{ij}^w C_{kl}^\phi \left. \right) + LWP_{2(ij)(kl)(mn)} & \left(I_{8ikm} S_{ij}^w S_{kl}^\phi - I_{7ikm} S_{ij}^w C_{kl}^\phi - I_{6ikm} C_{ij}^w S_{kl}^\phi \right. \\
 + I_{5ikm} C_{ij}^w C_{kl}^\phi \left. \right) \left. \right] + \varepsilon \sum_{j=0}^N & \left[(Lwh_{(mj)(mn)} + \varepsilon^{-1} Lwd_{(mj)(mn)}) C_{mj}^w \right] + F \cos(m\theta_F) R_{mn}^w \left(\lambda_{mn}^w r_F \right). \tag{5.13b}
 \end{aligned}$$

Equations (5.13) are nonlinear equations in terms of the generalized coordinates of the transverse displacement and stress function defined in Eqs. (5.9) and (5.10). In order to solve these equations, we have to find S_{mn}^ϕ and C_{mn}^ϕ in terms of S_{mn}^w and C_{mn}^w . In order to do so, we substitute the transverse displacement from Eq. (5.9) into Eq. (5.12). After doing so, the following expressions are found for the coefficients of the stress function:

$$\begin{aligned}
 S_{mn}^\phi = \frac{-1}{2(\lambda_{mn}^\phi)^4} \sum_{i,j=0}^{M,N} \sum_{k,l=0}^{M,N} & \left[LWW_{1(ij)(kl)(mn)} \left(I_{1ikm} S_{ij}^w S_{kl}^w + I_{2ikm} S_{ij}^w C_{kl}^w + I_{3ikm} C_{ij}^w S_{kl}^w \right. \right. \\
 + I_{4ikm} C_{ij}^w C_{kl}^w \left. \right) + LWW_{2(ij)(kl)(mn)} & \left(I_{4ikm} S_{ij}^w S_{kl}^w - I_{3ikm} S_{ij}^w C_{kl}^w - I_{2ikm} C_{ij}^w S_{kl}^w + I_{1ikm} C_{ij}^w C_{kl}^w \right) \left. \right] \tag{5.14a}
 \end{aligned}$$

$$\begin{aligned}
 C_{mn}^\phi = \frac{-1}{2(\lambda_{mn}^\phi)^4} \sum_{i,j=0}^{M,N} \sum_{k,l=0}^{M,N} & \left[LWW_{1(ij)(kl)(mn)} \left(I_{5ikm} S_{ij}^w S_{kl}^w + I_{6ikm} S_{ij}^w C_{kl}^w + I_{7ikm} C_{ij}^w S_{kl}^w \right. \right. \\
 + I_{8ikm} C_{ij}^w C_{kl}^w \left. \right) + LWW_{2(ij)(kl)(mn)} & \left(I_{8ikm} S_{ij}^w S_{kl}^w - I_{7ikm} S_{ij}^w C_{kl}^w - I_{6ikm} C_{ij}^w S_{kl}^w + I_{5ikm} C_{ij}^w C_{kl}^w \right) \left. \right] \tag{5.14b}
 \end{aligned}$$

where $I_{1mpu}, \dots, I_{8mpu}$ and also $LWP_{1(mn)(pq)(uv)}, LWP_{2(mn)(pq)(uv)}, LWW_{1(mn)(pq)(uv)}$ and $LWW_{2(mn)(pq)(uv)}$ are defined in the Appendix A. As can be seen from Eqs. (5.14), S_{mn}^ϕ and C_{mn}^ϕ are second order functions of S_{mn}^w and C_{mn}^w . If we substitute S_{mn}^ϕ and C_{mn}^ϕ from Eqs. (5.14) into Eqs. (5.13), it can be seen that \ddot{S}_{mn}^w and \ddot{C}_{mn}^w are third-order functions of S_{mn}^w and C_{mn}^w .

Using the Newton-Raphson method, the equilibrium solutions can be found. At any given speed, by investigating the stability characteristics of the possible equilibrium solutions, the dc displacement of a spinning disk is found. This dc displacement corresponds to a set of equilibrium solution for the coefficients of the expansion functions. This set of equilibrium solution is assumed to be $\{\dots S_{mn}^{ew} \dots C_{mn}^{ew} \dots\}$. Therefore, around the equilibrium position we can write:

$$\{\dots S_{mn}^w(t) \dots C_{mn}^w(t) \dots\} = \{\dots S_{mn}^{ew} \dots C_{mn}^{ew} \dots\} + \{\dots \hat{S}_{mn}^w(t) \dots \hat{C}_{mn}^w(t) \dots\} \quad (5.15)$$

After substituting Eq. (5.15) into Eqs. (5.13) and dropping the hats, the following linearized equations of motion are obtained

$$\begin{aligned} \ddot{S}_{mn}^w - 2\Omega m \dot{C}_{mn}^w + \left((\lambda_{mn}^w)^4 - m^2 \Omega^2 \right) S_{mn}^w = & \varepsilon \sum_{i,j=0}^{M,N} \sum_{k,l=0}^{M,N} \left\{ S_{ij}^w \left[Lwp_{1(ij)(kl)(mn)} \left[I_{1ikm} \left(S_{kl}^{e\phi} + S_{ij}^{ew} \frac{\partial S_{kl}^{e\phi}}{\partial S_{ij}^w} \right) + \right. \right. \right. \\ & I_{2ikm} \left(C_{kl}^{e\phi} + S_{ij}^{ew} \frac{\partial C_{kl}^{e\phi}}{\partial S_{ij}^w} \right) + I_{3ikm} C_{ij}^{ew} \frac{\partial S_{kl}^{e\phi}}{\partial S_{ij}^w} + I_{4ikm} C_{ij}^{ew} \frac{\partial C_{kl}^{e\phi}}{\partial S_{ij}^w} \left. \right] + Lwp_{2(ij)(kl)(mn)} \left[I_{4ikm} \left(S_{kl}^{e\phi} + S_{ij}^{ew} \frac{\partial S_{kl}^{e\phi}}{\partial S_{ij}^w} \right) \right. \\ & \left. \left. - I_{3ikm} \left(C_{kl}^{e\phi} + S_{ij}^{ew} \frac{\partial C_{kl}^{e\phi}}{\partial S_{ij}^w} \right) - I_{2ikm} C_{ij}^{ew} \frac{\partial S_{kl}^{e\phi}}{\partial S_{ij}^w} + I_{1ikm} C_{ij}^{ew} \frac{\partial C_{kl}^{e\phi}}{\partial S_{ij}^w} \right] \right] + C_{ij}^w \left[Lwp_{1(ij)(kl)(mn)} \left[I_{1ikm} S_{ij}^{ew} \frac{\partial S_{kl}^{e\phi}}{\partial C_{ij}^w} \right. \right. \\ & \left. \left. + I_{2ikm} S_{ij}^{ew} \frac{\partial C_{kl}^{e\phi}}{\partial C_{ij}^w} + I_{3ikm} \left(S_{kl}^{e\phi} + C_{ij}^{ew} \frac{\partial S_{kl}^{e\phi}}{\partial C_{ij}^w} \right) + I_{4ikm} \left(C_{kl}^{e\phi} + C_{ij}^{ew} \frac{\partial C_{kl}^{e\phi}}{\partial C_{ij}^w} \right) \right] + Lwp_{2(ij)(kl)(mn)} \left[I_{4ikm} S_{ij}^{ew} \frac{\partial S_{kl}^{e\phi}}{\partial C_{ij}^w} \right. \right. \\ & \left. \left. - I_{3ikm} S_{ij}^{ew} \frac{\partial C_{kl}^{e\phi}}{\partial C_{ij}^w} - I_{2ikm} \left(S_{kl}^{e\phi} + C_{ij}^{ew} \frac{\partial S_{kl}^{e\phi}}{\partial C_{ij}^w} \right) + I_{1ikm} \left(C_{kl}^{e\phi} + C_{ij}^{ew} \frac{\partial C_{kl}^{e\phi}}{\partial C_{ij}^w} \right) \right] \right\} + \\ & \varepsilon \sum_{j=0}^N \left[\left(Lwh_{(mj)(mn)} + \frac{1}{\varepsilon} Lwd_{(mj)(mn)} \right) S_{mj}^w \right], \end{aligned} \quad (5.16a)$$

$$\begin{aligned} \ddot{C}_{mn}^w + 2\Omega m \dot{S}_{mn}^w + \left((\lambda_{mn}^w)^4 - m^2 \Omega^2 \right) C_{mn}^w = & \varepsilon \sum_{i,j=0}^{M,N} \sum_{k,l=0}^{M,N} \left\{ S_{ij}^w \left[Lwp_{1(ij)(kl)(mn)} \left[I_{5ikm} \left(S_{kl}^{e\phi} + S_{ij}^{ew} \frac{\partial S_{kl}^{e\phi}}{\partial S_{ij}^w} \right) + \right. \right. \right. \\ & I_{6ikm} \left(C_{kl}^{e\phi} + S_{ij}^{ew} \frac{\partial C_{kl}^{e\phi}}{\partial S_{ij}^w} \right) + I_{7ikm} C_{ij}^{ew} \frac{\partial S_{kl}^{e\phi}}{\partial S_{ij}^w} + I_{8ikm} C_{ij}^{ew} \frac{\partial C_{kl}^{e\phi}}{\partial S_{ij}^w} \left. \right] + Lwp_{2(ij)(kl)(mn)} \left[I_{8ikm} \left(S_{kl}^{e\phi} + S_{ij}^{ew} \frac{\partial S_{kl}^{e\phi}}{\partial S_{ij}^w} \right) \right. \\ & \left. \left. - I_{7ikm} \left(C_{kl}^{e\phi} + S_{ij}^{ew} \frac{\partial C_{kl}^{e\phi}}{\partial S_{ij}^w} \right) - I_{6ikm} C_{ij}^{ew} \frac{\partial S_{kl}^{e\phi}}{\partial S_{ij}^w} + I_{5ikm} C_{ij}^{ew} \frac{\partial C_{kl}^{e\phi}}{\partial S_{ij}^w} \right] \right] + C_{ij}^w \left[Lwp_{1(ij)(kl)(mn)} \left[I_{5ikm} S_{ij}^{ew} \frac{\partial S_{kl}^{e\phi}}{\partial C_{ij}^w} \right. \right. \\ & \left. \left. + I_{6ikm} S_{ij}^{ew} \frac{\partial C_{kl}^{e\phi}}{\partial C_{ij}^w} + I_{7ikm} \left(S_{kl}^{e\phi} + C_{ij}^{ew} \frac{\partial S_{kl}^{e\phi}}{\partial C_{ij}^w} \right) + I_{8ikm} \left(C_{kl}^{e\phi} + C_{ij}^{ew} \frac{\partial C_{kl}^{e\phi}}{\partial C_{ij}^w} \right) \right] + Lwp_{2(ij)(kl)(mn)} \left[I_{8ikm} S_{ij}^{ew} \frac{\partial S_{kl}^{e\phi}}{\partial C_{ij}^w} \right. \right. \\ & \left. \left. - I_{7ikm} S_{ij}^{ew} \frac{\partial C_{kl}^{e\phi}}{\partial C_{ij}^w} - I_{6ikm} \left(S_{kl}^{e\phi} + C_{ij}^{ew} \frac{\partial S_{kl}^{e\phi}}{\partial C_{ij}^w} \right) + I_{5ikm} \left(C_{kl}^{e\phi} + C_{ij}^{ew} \frac{\partial C_{kl}^{e\phi}}{\partial C_{ij}^w} \right) \right] \right\} + \\ & \varepsilon \sum_{j=0}^N \left[\left(Lwh_{(mj)(mn)} + \frac{1}{\varepsilon} Lwd_{(mj)(mn)} \right) C_{mj}^w \right] \end{aligned} \quad (5.16b)$$

$S_{mn}^{e\phi}$ and $C_{mn}^{e\phi}$ can be obtained by substituting S_{mn}^{ew} and C_{mn}^{ew} into Eqs. (5.14). Also

$\frac{\partial S_{mn}^{e\phi}}{\partial S_{ij}^w}$, $\frac{\partial S_{mn}^{e\phi}}{\partial C_{ij}^w}$, $\frac{\partial C_{mn}^{e\phi}}{\partial S_{ij}^w}$ and $\frac{\partial C_{mn}^{e\phi}}{\partial C_{ij}^w}$ are obtained to be as follow

$$\frac{\partial S_{mn}^{e\phi}}{\partial S_{kl}^w} = \frac{-1}{2(\lambda_{mn}^\phi)^4} \sum_{i,j=0}^{M,N} \left[(LwW_{1(ij)(kl)(mn)} + LwW_{1(kl)(ij)(mn)}) I_{1ikm} S_{kl}^{ew} + (LwW_{1(kl)(ij)(mn)} I_{2kim} + LwW_{1(ij)(kl)(mn)} I_{3ikm}) C_{ij}^{ew} + LwW_{2(ij)(kl)(mn)} (2I_{4ikm} S_{ij}^{ew} - (I_{3ikm} + I_{2kim}) C_{kl}^{ew}) \right] \quad (5.17a)$$

$$\frac{\partial S_{mn}^{e\phi}}{\partial C_{kl}^w} = \frac{-1}{2(\lambda_{mn}^\phi)^4} \sum_{i,j=0}^{M,N} \left[(LwW_{1(ij)(kl)(mn)} I_{2ikm} + LwW_{1(kl)(ij)(mn)} I_{3ikm}) S_{ij}^{ew} + (LwW_{1(ij)(kl)(mn)} I_{4ikm} + LwW_{1(kl)(ij)(mn)} I_{4kim}) C_{ij}^{ew} + LwW_{2(ij)(kl)(mn)} (-(I_{3ikm} + I_{2kim}) S_{ij}^{ew} + 2I_{1ikm} C_{ij}^{ew}) \right] \quad (5.17b)$$

$$\frac{\partial C_{mn}^{e\phi}}{\partial S_{kl}^w} = \frac{-1}{2(\lambda_{mn}^\phi)^4} \sum_{i,j=0}^{M,N} \left[(LwW_{1(ij)(kl)(mn)} + LwW_{1(kl)(ij)(mn)}) I_{5ikm} S_{ij}^{ew} + (LwW_{1(kl)(ij)(mn)} I_{6kim} + LwW_{1(ij)(kl)(mn)} I_{7ikm}) C_{ij}^{ew} + LwW_{2(ij)(kl)(mn)} (2I_{8ikm} S_{ij}^{ew} - (I_{7kim} + I_{6ikm}) S_{ij}^{ew}) \right] \quad (5.17c)$$

$$\frac{\partial C_{mn}^{e\phi}}{\partial C_{kl}^w} = \frac{-1}{2(\lambda_{mn}^\phi)^4} \sum_{i,j=0}^{M,N} \left[(LwW_{1(ij)(kl)(mn)} I_{6ikm} + LwW_{1(kl)(ij)(mn)} I_{6kim}) S_{ij}^{ew} + (LwW_{1(ij)(kl)(mn)} + LwW_{1(kl)(ij)(mn)}) I_{8ikm} C_{ij}^{ew} + LwW_{2(ij)(kl)(mn)} (-(I_{7ikm} + I_{6kim}) S_{ij}^{ew} + 2I_{5ikm} C_{ij}^{ew}) \right] \quad (5.17d)$$

By introducing $\mathbf{x} = \{\dots S_{mn}^w \dots C_{mn}^w \dots\}$ and after substitution of Eqs. (5.17) into Eqs. (5.16), the linearized equations of motion in the following form is obtained

$$\mathbf{M}\ddot{\mathbf{x}} + \mathbf{C}\dot{\mathbf{x}} + \mathbf{K}\mathbf{x} = 0. \quad (5.18)$$

By inspecting Eq (5.16), it may be noted that some of the time independent parts are a function of the equilibrium position. These terms come from the in-plane stress distribution due to the middle plane stretching. In fact, these are the terms that come from the geometrical nonlinear effects and we call them to be \mathbf{K}^{NL} . Therefore, the nonlinear stiffness matrix is a function of disk dc displacement. There are some other terms in the stiffness part of Eq. (5.16) that are not affected by the equilibrium position of a spinning disk. These terms have the coefficients such as $\left((\lambda_{mn}^w)^4 - m^2 \Omega^2 \right)$ or $\left(Lwh_{(mj)(mn)} + \varepsilon^{-1} Lwd_{(mj)(mn)} \right)$. These are the terms that contribute towards the linear part of the stiffness matrix. Using Eq. (5.18), we can find the eigenvalues of the linearized system.

5.4. Numerical Analysis

In this section the linearization method that was developed in the previous section is used to study the effect of large deformations on the frequency characteristics of a rotating disk with clamped-free boundary conditions. Attention is confined to the analysis of the disk with outer diameter 17.0", inner diameter 6.0" and plate thickness 0.050". It is assumed that $E = 29 \times 10^6 \text{ psi}$, $\nu = 0.3$, $\rho = 487 \text{ lb/ft}^3$. In the numerical results presented in this paper, it is assumed that the external force is applied at outer rim and $\theta_F = 0$.

Figure 5. 1 shows the natural frequencies (measured by a stationary observer) versus the speed for the spinning disk, using linear form of the equations of motion. The associated mode shape for each frequency path is indicated in the graph. Mode (n,m) indicates a mode with n nodal circles and m nodal diameters respectively. As can be seen from this figure; 2890, 2410 and 2740 RPM are the first three critical speeds associated with the (0,2), (0,3) and (0,4) modes, respectively. It may be noted that the lowest critical speed is associated with the (0,3) mode.

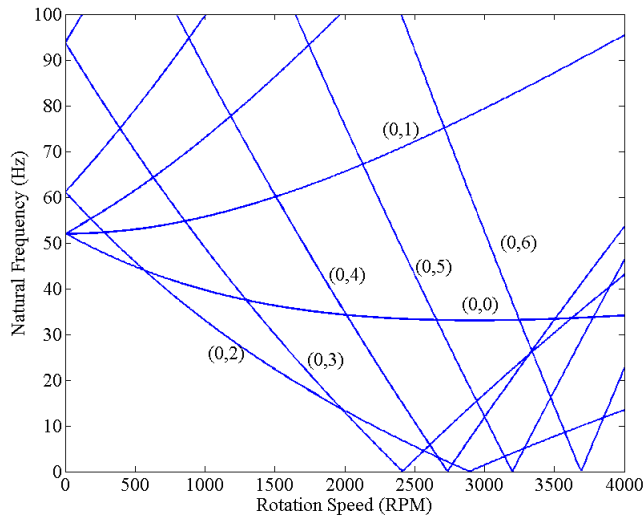


Figure 5. 1. Linear natural frequencies of the disk versus rotation speed

A multi-mode approximation is used to calculate the frequencies of the spinning and stationary the disk. It is assumed that the spinning disk is under the application of a space fixed external force. In the nonlinear analysis it is assumed that $M=6$ and $N=4$. Here, for

the purpose of clarity, the frequencies calculated using the above mentioned procedure are called “nonlinear frequencies”.

5.4.1. Stationary Disk

In the experimental part (Part I, Chapter 4) it was seen that the application of a sufficiently large space fixed external force resulted in splitting of the measured frequencies of the backward and forward traveling waves for a stationary disk. In Figure 5. 2, the nonlinear frequencies of the backward and forward traveling waves of three modes are calculated for different levels of nonlinearity. w_0 is the maximum deflection of the stationary disk at the outer rim measured at the point of application of the space fixed external force. As expected, the nonlinear frequencies of all the modes increase as the level of nonlinearity increases. The nonlinear frequencies of forward traveling waves are more affected than those of the backward traveling waves. As w_0/h increases from zero to four, the nonlinear frequencies of the forward traveling waves of the (0,2), (0,3) and (0,4) modes increase by approximately 14, 21 and 11 percent, respectively.

These increases are caused by the increased internal stresses induced in the disk due to the application of the lateral force. It may be noted that this force induced internal stress distribution is space-fixed and therefore in the case of disc rotation, does not display the same characteristics as in the case where stresses or imperfections are fixed in the disk as was the case in the work of Tobias [15].

The case $w_0/h = 0$, represents the case where there is no applied force and the stress distribution in the disk is symmetric. In this case the natural frequencies of each mode at zero speed consist of repeated pairs. When w_0/h is sufficiently large, the resulting non-symmetrical stress distribution will result in two separate frequencies at zero speed. These two frequencies are associated with nodal configurations that correspond to the maximum and minimum frequencies of the disc under the given stress distribution.

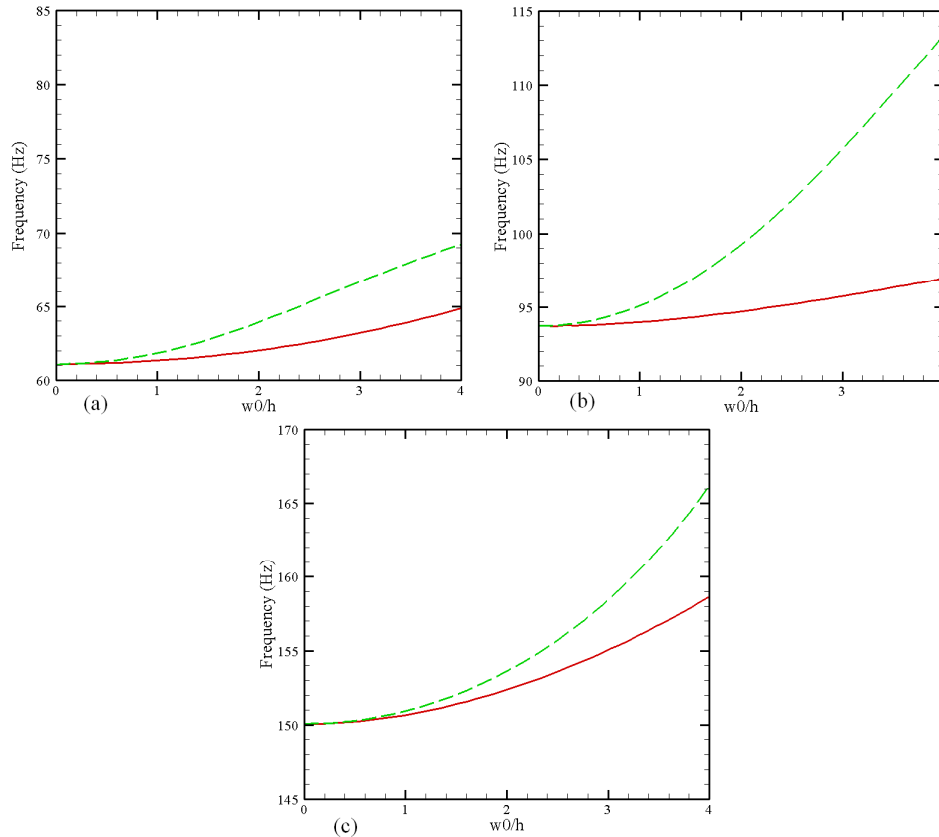


Figure 5. 2. The nonlinear frequencies of the backward (solid lines) and forward (broken lines) traveling waves of (a) (0,2), (b) (0,3), and (c) (0,4) modes of the stationary disk

Figure 5. 3 shows the particular part of the stress function (ϕ^p) and the resulting radial and hoop stresses in the normalized radial direction for three different angular directions when $w_0/h = 4$

If the lateral displacement is small compared to the disk thickness then the induced stress due to middle plane stretching is small and the nonlinear stiffness is negligible with respect to the linear stiffness. It may be noted from Figure 5. 2 that when w_0/h is less than 0.3, the difference between the nonlinear frequencies of the backward and forward traveling waves is negligible.

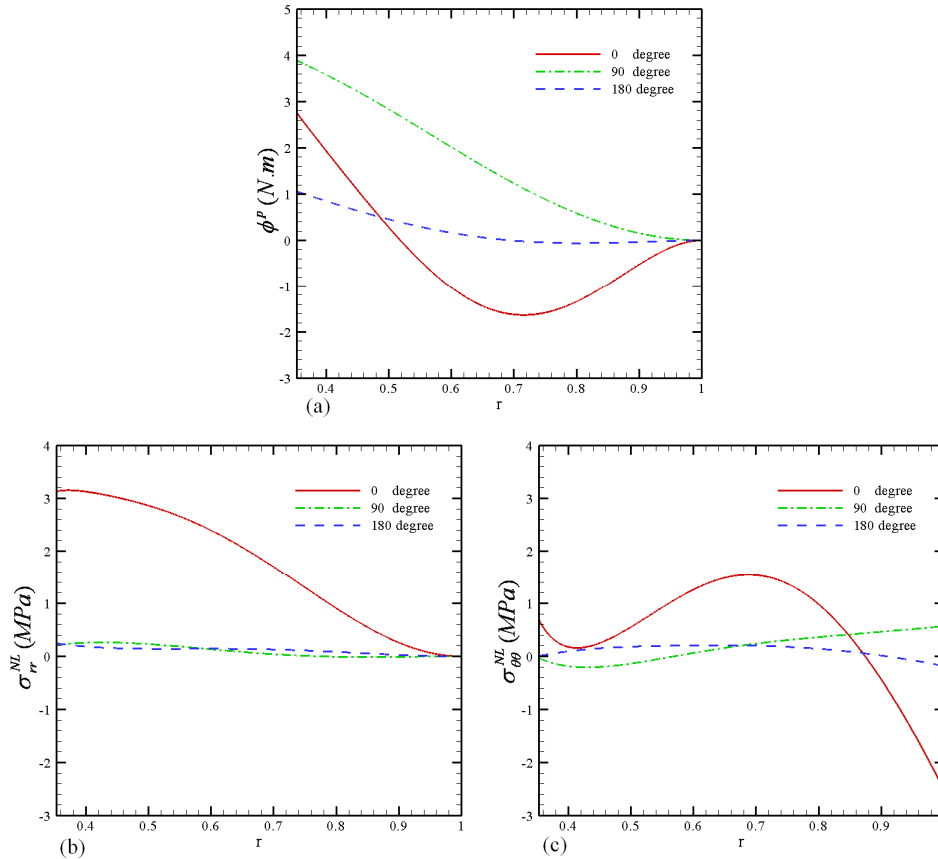


Figure 5. 3. (a) The particular part of the stress function, (b) the nonlinear radial stress and (c) the nonlinear hoop stress along the normalized radial direction for three different angular directions when $w_0/h = 4$

5.4.2. Spinning Disk

In the experimental results presented in Chapter 4, it was seen that the magnitude of disk deformation has a significant effect upon the frequency characteristics of a rotating disc. In this section of the paper the ability of the developed analysis to predict these characteristics is examined.

In the comparison of the analysis and the experiment results there are a number of specific issues that need to be considered. Analysis is, of course, an idealized exercise which may or may not represent the behaviour of the real system. In this particular study the discs used were typical of those used in the wood cutting industry of Canada (the major motivation of this work being the development of high speed saws).

- a) As such the residual stresses in the discs were unknown although likely to be small.

- b) The clamping arrangement used was unlikely to provide the level of fixity assumed in the analysis (i.e. the assumption of zero slope at the inner boundary was not exactly true)
- c) No attempt was made to include effects due to run out, unbalance, aerodynamic interaction, disc imperfections or stresses induced by the clamping process. The effect of runout on the frequency behavior of spinning disks has been previously studied by Khorasany and Hutton [16].

As will be seen in the results presented later there were discrepancies between the computed natural frequencies at zero speed and those calculated. These were likely primarily due to incorrect clamp stiffness modeling and unknown internal stresses.

Given that the purpose of the present work was to explore the effects of speed and geometric nonlinearity, the analysis was formulated to allow for the input of measured zero speed frequencies. In this way the zero speed characteristics were accurately modeled and resulting predictions relied upon speed and nonlinear effects not upon zero speed characteristics.

Analytical calculations are presented for the disc with a thickness of 0.050" and for a number of different levels of nonlinearity. The case with a low level of nonlinearity, $w_0/h = 0.1$, is considered first. Figure 5. 4 compares the numerical and the experimental results for the disc frequencies as a function of blade speed. Figure 5. 4a shows the analytical predictions assuming the inner boundary to be fully clamped. The broken and solid lines show the linear and nonlinear predictions, respectively. Figure 5. 4b presents the experimental results found in Chapter 4 of this thesis for this same disc. There is not good agreement between the calculated and measure zero speed frequencies due to reasons previously mentioned. This disagreement then propagates through the analysis to give inaccurate critical speeds. In general the response characteristics are representative of a linear system.

From Figure 5. 4a it may be noted that the first critical speed corresponds to that of the (0,3) mode and occurs at approximately 2400 RPM. It may be seen that starting at a speed in the region of this first critical speed, the predicted nonlinear frequency of all the backward traveling waves veer from their linear paths to follow an almost constant path

before collapsing back on to the predicted values for the linear case. This behaviour is repeated at a total of three different speeds in the region of the three lowest critical speeds. A similar phenomenon may be noted with the reflected waves. In this case the frequencies level off then jump up back to their linear path. These effects are not reflected in the measured data. In Figure 5. 4b, the frequency jumps and drops are illustrated by vertical arrow pointing upward and downward, respectively. Also, the speed ranges at which the measured frequencies do not change are shown by horizontal lines.

Figure 5. 5 compares the associated measured and computed dc deflections at the location where the external force was applied. The dc amplitude is calculated from the disk deflected position after the application of the space fixed external force. It can be seen that the configuration of the stationary wave existing due to the applied force is further developed at speeds in the region of the critical speeds of the three lowest modes. As the predicted critical speeds do not coincide with the measured values, the speeds at which stationary waves appear do not agree with the measured values. Since the level of nonlinearity is relatively small, the developed stationary waves cannot be sustained over a significant speed range. From this figure it can be seen that the predicted speeds for the arising of the stationary waves are consistent with the speeds at which the predicted nonlinear frequencies of the backward traveling waves veer to a constant level.

In the numerical results it is seen that when a stationary wave is developed, the calculated frequencies tend to maintain a constant level. From Figure 5. 5, it may be seen that in the experiment, the first stationary wave is developed from 2800 RPM to 3200 RPM.

From the experimental results presented in Figure 5. 4b, a lock-in phenomena (as previously noted by DAngelo and Mote [17]) in the measured frequencies of the backward traveling waves of the (0,5) and (0,6) modes are evident. After the collapse of the stationary wave at 3200 RPM shown in Figure 5. 5, drops in the measured frequencies of these two modes can be discerned. From the experimental results shown in Figure 5. 5, it can be seen that after the collapse of the first stationary wave, another stationary wave is developed at around 3400 RPM and collapses at 3800 RPM. From the experimental results illustrated in Figure 5. 4b it can be seen that the measured frequency

of the (0,0) mode jumps at 3200, due to the collapse of the first stationary wave. Another jump in the measured frequency of this mode is notable at almost 3800 RPM at which the second stationary wave collapses.

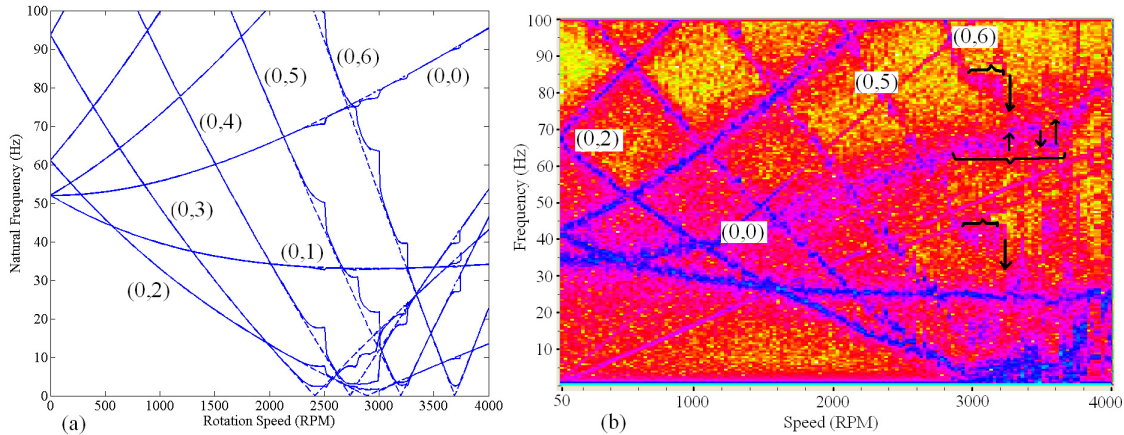


Figure 5. 4. Nonlinear frequencies of the spinning 0.05 in.-thick disk when $w_0/h = 0.1$, (a) numerical results (broken and solid lines show the linear and nonlinear results, respectively), (b) experimental results (run-up case)

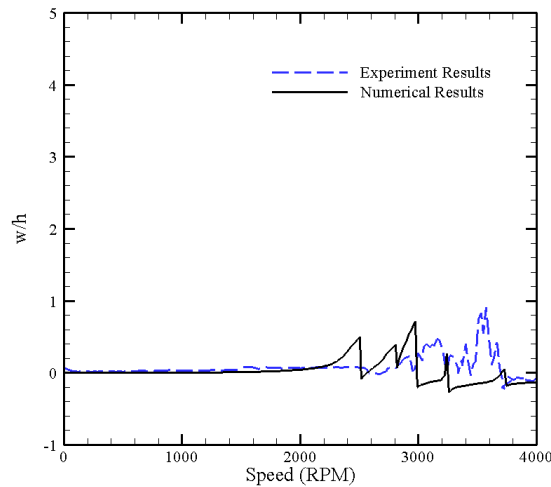


Figure 5. 5. A comparison between the numerical and experimental results (run-up case) for the dc amplitude of oscillations when $w_0/h = 0.1$ at the location of the applied external force

To see how the numerical results compare with the experimental ones when the level of nonlinearity is higher, the case with $w_0/h = 0.6$ is considered. In Figure 5. 6, the numerical and experimental results for the nonlinear frequencies are presented. In Figure

5. 7a comparison between the dc amplitude of oscillations for the numerical and experimental results is presented.

In this case the analysis is conducted using the frequency values of the stationary disc measured in the experimental work. As may be seen there is very good agreement between the predicted and measured frequency values, and the dc displacements, at all speeds. It may thus be concluded that the modeling of the speed and geometric non linear displacement effects is appropriate.

A further observation from the experimental results shown in Figure 5. 6b is the splitting of the forward and backward travelling waves at zero speed which is particularly noticeable for the (0,2) mode. This behaviour is also reflected in the analytical results.

From Figure 5. 7 it may be seen both that the predicted dc displacements corresponds closely to the measured values and that a stationary wave arises at a speed in the region of 2800RPM. From Figure 5. 6a,b it may also be seen that the backward travelling waves depart from their linear behaviour and take up values that are constant with speed (so called “frequency locking” [17]) starting in this same speed region. Thus the change in frequency can be attributed to the development of the new equilibrium configuration. It is not clear as to why the frequency maintains a constant value for increasing speed. Further, the analytical and experimental results indicate that there is a curve veering between the nonlinear frequencies of the backward traveling waves of the (0,2) and (0,3) modes before they maintain a constant level.

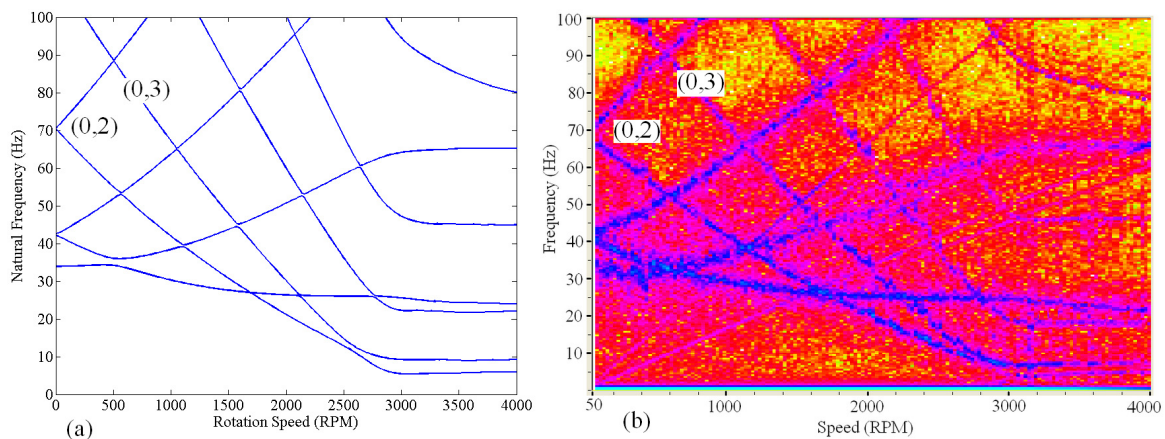


Figure 5. 6. Nonlinear frequencies of the spinning disk when $w_0/h = 0.6$, (a) numerical results
(b) experimental results (run-up case)

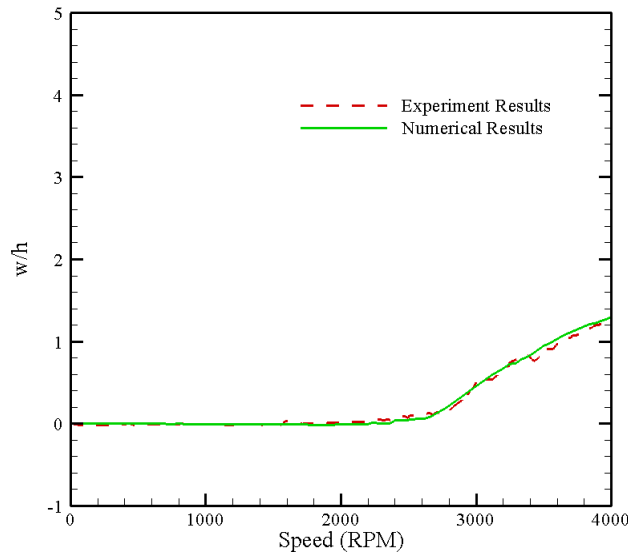


Figure 5. 7. A comparison between the numerical and experimental results (run-up case) for the dc amplitude of oscillations when $w_0/h = 0.6$

To study the disk nonlinear frequency behavior under an even higher level of nonlinearity, the case with $w_0/h = 2.0$ is considered. Figure 5. 8 and Figure 5. 9 show the calculated frequency and dc amplitude (measured at the force location) behavior of the disk, respectively, under this condition. It should be noted that the dc amplitude is calculated from the deflected disk position after application of the space fixed external force. Therefore, to find the actual dc deflection we have to add $w_0/h = 2.0$ to the calculated results. Again, in Figure 5. 8 the broken and solid lines show the linear and nonlinear calculated frequencies, respectively.

As expected, it can be seen that in this case, there is a notable split between the nonlinear frequencies of the backward and forward traveling waves of the stationary disk. It may also be noted that in this case, even at subcritical speeds, there is a significant difference between the linear and nonlinear frequencies. The curve veering that was notable at high speeds in the previous cases exists at subcritical speeds in this case. It can also be seen that, starting at a speed in the region of the lowest critical speed, the predicted nonlinear frequencies veer off and take up constant values as the speed further increases. Although the initial deflection of the disk is more than three times larger than

the previous case shown in Figure 5. 6, there is not a significant difference in the calculated nonlinear frequencies at very high speeds.

From Figure 5. 9 it may also be noted for this high level of nonlinearity the the predicted stationary wave is initiated at a speed below the lowest critical speed. This result is also consistent with the experimental results presented by Tobias and Arnold [15].

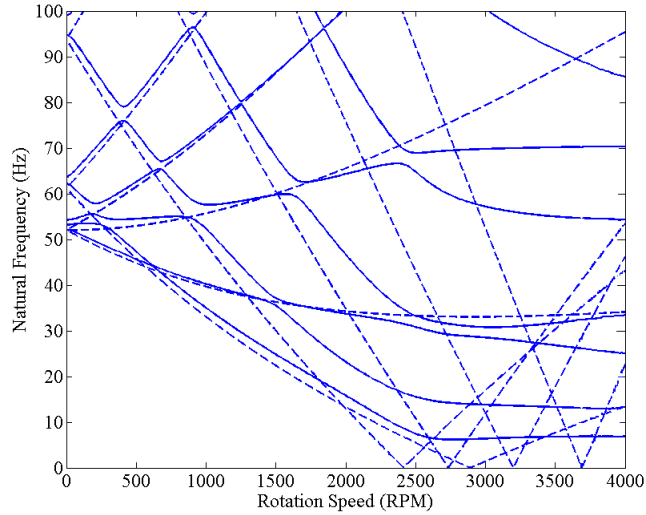


Figure 5. 8. Calculated linear (broken lines) and nonlinear frequencies (solid lines) of the spinning disk when $w_0/h = 2.0$

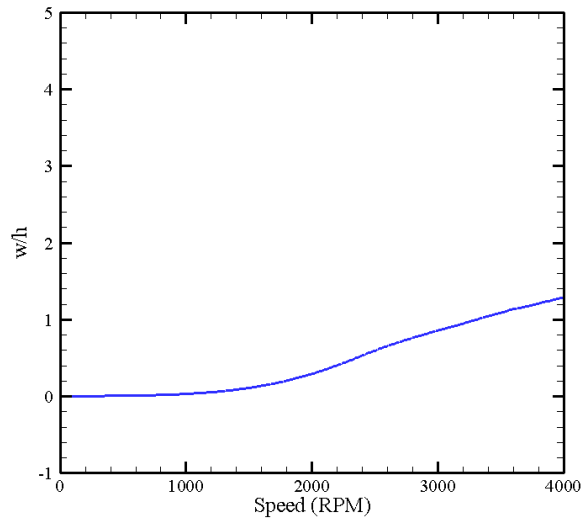


Figure 5. 9. Dc amplitude of oscillation when $w_0/h = 2.0$

5.5. Conclusions

An analysis of the frequency and amplitude response of rotating thin discs when subjected to geometric non linear displacements has been presented, and the results obtained have been shown to agree well with experimental observations.

For a stationary disk under the application of a space fixed external lateral point force large displacements result in in-plane stresses in the disk. Since the loading is not symmetric, this stress distribution is not symmetric. As a result of this lack of symmetry the frequencies of the forward and backward traveling waves of the preferential modes of the stationary disk do not coincide. Numerical results were presented that quantified this effect.

Numerical results were compared with experimental predictions for the case of a spinning disk subjected to a space-fixed point force. It was shown numerically that, for sufficiently high degrees of nonlinearity, the existing force induced stationary wave is significantly further developed starting in the region of the linear critical speed. Above this speed the calculated (and measured) frequencies diverge significantly from the paths predicted by linear theory. It was shown that the resulting frequencies then maintain an essentially constant value in the speed range considered. This nonlinear behaviour was also clearly evident in the experimental results. These results give rise to the following observations for displacement levels where non linear effects are sufficiently high:

- d) Unlike the linear case, there is no speed for which any of the backward travelling waves have zero frequency. Thus no critical speed (in the linear sense) exists.
- e) There are no reflected waves as predicted by linear analysis.
- f) No low frequency crossings occur between backward and forward travelling waves for speeds above the lowest (linear) critical speed.
- g) At speeds above the linear critical speed the computed and measured frequencies are independent of speed. So called “frequency lock-in” occurs

For low levels of nonlinearity, stationary waves form and collapse within a small speed band. At the collapse of such waves, a drop in the frequencies of the backward

traveling waves and a jump in those of the forward and reflected traveling waves were evident in the predicted results. Again this effect was not seen in the experimental results.

5.6. References

- [1] Lamb, H., and Southwell, R.V., 1921, "The Vibration of Spinning Disk," Proc R Soc Lond, 99, pp. 272-280.
- [2] Mote, C.D., 1965, "Free Vibration of Initially Stressed Circular Plates," Journal of Engineering for Industry, 87, pp. 258-264.
- [3] Hutton, S.G., Chonan, S., and Lehmann, B.F., 1987, "Dynamic Response of a Guided Circular Saw," Journal of Sound and Vibration, 112, pp. 527-539.
- [4] Chen, J.S. and Bogy, D.B., 1992, "Effects of Load Parameters on the Natural Frequencies and Stability of a Flexible Spinning Disk with a Stationary Load System", Journal of Applied Mechanics, 59, pp. S230-S235.
- [5] Tian, J.F. and Hutton, S.G., 2001, "Cutting Induced Vibration in Circular Saws," Journal of Sound and Vibration, 242 (5), pp. 907-922.
- [6] Nowinski, J.L., 1964, "Nonlinear Transverse Vibrations of a Spinning disk," Journal of Applied Mechanics, 31, pp. 72-78.
- [7] Tobias, S.A., 1957, "Free Undamped Non-linear Vibrations of Imperfect Circular Disks," Institution of Mechanical Engineers, Proceedings, 171, pp. 691-701.
- [8] Jana, A., and Raman, A., 2005, "Nonlinear Dynamics of a Flexible Spinning Disc Coupled to a Precompressed Spring," Nonlinear Dynamics, 40, pp. 1-20.
- [9] Nayfeh, A. H., Jilani, A., and P. Manzione, 2001, "Transverse Vibrations of a Centrally Clamped Rotating Circular Disk," Nonlinear Dynamics, 26, pp. 163-178.
- [10] Chen, J.S., 2001, "On the Internal Resonance of a Spinning Disk Under Space-Fixed Pulsating Edge Loads," Journal of Applied Mechanics, 68, pp. 854-859.
- [11] Touze, C., Thomas, O., and Chaigne, A., 2002, "Asymmetric Non-linear Forced Vibrations of Free-Edge Circular Plates. Part 1: Theory," Journal of Sound and Vibration, 258, pp. 649-676.
- [12] Yang, L., and Hutton, S.G., 1998, "Nonlinear Vibrations of Elastically-Constrained Rotating Discs," Journal of Vibration and Acoustics, 120, pp. 475-483.
- [13] Luo, A.C.J., and Mote, C.D., 2000, "Nonlinear Vibration of Rotating Thin Disks", Journal of Vibration and Acoustics, 122, pp. 376-383.

- [14] Khorasany, R.M.H., and Hutton, S.G., 2010, "Vibration Characteristics of Rotating Thin Discs, Part I: Experimental Results", submitted to ASME Journal of Applied Mechanics.
- [15] Tobias, S.A., and Arnold, R.N., 1957, "The Influence of Dynamical Imperfections on the Vibration of Rotating Disks," Institution of Mechanical Engineers, Proceedings, 171, pp. 669-690.
- [16] Khorasany, R.M.H., and Hutton, S.G., 2010, "The Effect of Axisymmetric Non-Flatness on the Oscillation Frequencies of a Rotating Disk," Journal of Vibration and Acoustics, in press.
- [17] D'Angelo, C., and Mote, C.D., 1993, "Aerodynamically Excited Vibration and Flutter of a Thin Disk Rotating at Supercritical Speed," Journal of Sound and Vibration 168, pp. 15-30.

Chapter 6- Summary and Conclusions

6.1. Summary and Conclusions

The main contributions in this thesis can be summarized as follows:

- 1) An analytical approach has been taken to investigate the stability characteristics of an elastically constrained spinning disk having rigid body translational degree of freedom.

Using a two-mode approximation, the stability characteristics of an elastically constrained spinning disk were investigated. It has been assumed that the disk under consideration was constrained with a one space fixed spring. At first it was shown that the divergence instability does not occur at the speed corresponding to the linear critical speed of the unconstrained spinning disk. In fact, it was shown that at the critical speeds of an elastically constrained spinning disk with one spring, having a rigid body translational degree of freedom is the same as that of the unguided disk [1].

Using an analytical technique, the stability characteristics of an elastically constrained disk with a rigid body translational degree of freedom at the location of the interaction of the rigid body mode with a forward, backward, and reflected travelling wave was studied. It was shown that the interaction between a forward or backward travelling wave with the rigid body translational mode does not produce instability.

Furthermore it was shown that the interaction between a forward or backward travelling wave with the rigid body translational mode does not induce flutter type instability. When the rigid body translational mode interacts with a reflected travelling wave, the flutter type instability may be induced. It was also shown that, depending on the mode and speed characteristics, the region of flutter type instability may move to higher speeds.

- 2) The effect of initial runout on the frequency and critical speed behavior of spinning disks was investigated.

The nonlinear equations of motion for non-flat spinning disks based on Von Karman's plate theory were used. It was assumed that the initial runout is axisymmetric. It was also assumed that the initial runout could be written as the summation of the mode shapes with zero nodal diameters. After substituting the pre-assumed shape for the initial non-flatness, neglecting nonlinear terms, and using Galerkin's method, a set of coupled linearized equations of motion were obtained. Using these equations, the effect of the initial lack of flatness on the frequency behaviour of spinning disks was studied [2].

It was found that the interaction of the initial runout and the bending deflection induces an in-plane stress in the disk. In general, it was found that the initial runout increases the natural frequencies of the stationary disk. The natural frequencies of some of the modes of the stationary disk were found to be less sensitive to some of the forms of initial runout compared to other modes. This is due to the induced in-plane stresses in the disk where in these cases have less effect on the modal stiffness in these modes. It was also found that due to assuming the form of the initial non-flatness as axisymmetric, the calculated frequencies for the backward and forward travelling waves of a given preferential mode were the same at zero speed.

It also was found that in the assumption of an initial non-flatness for a spinning disk, the critical speed is changed. It was determined that the lack of flatness increases the critical speeds, though the critical speeds of some of the modes were less sensitive to some of the forms of the initial lack of flatness compared to those of the other modes. Generally, the more complicated the shape of the initial runout, the greater its effect on the critical speeds of the disk.

- 3) Experimental studies were conducted in order to measure the frequency response characteristics for rotating disks both in an idling mode as well as when subjected to a space fixed lateral force. The applied lateral force (produced by an air jet) was such as to produce displacements large enough that non-linear geometric effects were important for the determination of the disk frequencies. Experiments were conducted on thin annular disks of different thicknesses and with the inner radius clamped to the driving arbor.

The experimental results showed that in the cases where the level of nonlinearity was relatively low, several stationary waves were developed. Since the level of nonlinearity was relatively low, the stationary waves were not sustained over a large speed range. It was noticed that at the speeds corresponding to the formation of the stationary waves, the backward travelling waves veered from their linear path to one where the frequency remained constant with speed. This behaviour was also evident for the forward travelling waves. It was observed that when the stationary waves collapse, a sudden drop in the measured frequencies of the backward travelling waves and a sudden jump in those of the forward and reflected travelling waves occur.

It was seen that when the level of nonlinearity was large enough, stationary waves were developed and they were stable up to the maximum speed attainable for the experiments. Furthermore, in these cases the measured frequencies of the backward and forward travelling waves veered from their linear paths and maintained an almost constant level. Therefore, the effect of large deformations was to modify the lowest backward travelling waves such that they do not experience a zero natural frequency. As such, the pure standing wave predicted based on the linear theory of vibrations does not exist in these cases. In other words, the critical speed that was predicted on the basis of a linear analysis does not exist in the presence of nonlinearity.

Since the applied external force due to the application of an air jet was not axisymmetric, the induced in-plane stresses were also not axisymmetric. As a result, a separation in the measured frequencies of the stationary disk for the preferential modes was noticeable. The level of separation increases by increasing the level of initial nonlinearity.

- 4) The effects of geometrical nonlinear terms on the frequency characteristics of a spinning disk under the application of a space fixed external force were studied. The governing equations were based on the Von Karman plate theory. After discretizing the nonlinear equations of motion, the equilibrium solution was found. The nonlinear equations of motion were linearized around the equilibrium solution and a set of coupled linear equations of motion were obtained. Using these equations, the

effect of large deformation on the oscillation frequencies of a spinning disk was studied.

It was found that due to the application of a space fixed point force, a non-symmetric in-plane stress is induced in the disk. This stress distribution causes a separation in the calculated nonlinear frequencies of the backward and forward travelling waves of a given preferential mode. It was found that this separation increases with the increase in the level of nonlinearity.

Numerical results were compared to the experimental results. It was seen that when the level of nonlinearity is relatively small, several stationary waves develop and then collapse. At the speed corresponding to the collapse of a stationary wave, a sudden drop and jump in the calculated frequencies of the backward and forward travelling waves, respectively, was noticeable. In this case, these drops and jumps were not seen in the experimental results.

When the level of nonlinearity was relatively large, a stationary wave was developed that was sustained over the speed range considered in this work. It was noticed that at the speed in which the stationary wave begins to develop, the calculated frequencies of the backward and forward travelling waves diverge from the paths predicted by the linear theory. It was shown that the resulting frequencies then maintain an essentially constant value in the speed range considered. Therefore, the numerical analysis based on the large deformation assumption predicts that there is no such speed at which the backward travelling waves of the preferential modes experience zero natural frequency. It was also predicted that for a sufficiently higher level of nonlinearity there would not be any reflected waves.

The experimental results were compared with the numerical results. It was seen that due to initial stresses, lack of flatness, and boundary conditions, there was no good comparison between the measured frequencies and the calculated frequencies for the stationary disk. Thus to conduct a better comparison, the measured frequencies for the stationary disk were used in the analytical solution. In doing so, it was seen that a very good agreement exists between the calculated frequencies and the mean deflection of the spinning disk.

6.2. Recommendations for Future Work

To increase our understanding of the dynamics of spinning disks, it is suggested that future works should be concerned with the following aspects:

- To study the effect of unsymmetrical lack of flatness on the dynamics of spinning disks. In Chapter 3 it was assumed that the lack of flatness is axisymmetric. This assumption may not be valid in all of the spinning disk applications.
- To study the effect of the lack of flatness on the cutting performance of circular saws. Since the lack of flatness changes the modal characteristics of spinning disks, it can also affect the cutting performance of spinning disks, too.
- To study the effect of geometrical nonlinear terms on the cutting performance of spinning disks. It was seen that the geometrical nonlinear terms can change the dynamics of spinning disks at supercritical speeds. Thus, the cutting performance of circular saws can change with the level of nonlinearity.
- To study the effect of an elastic constraint on the nonlinear frequencies of spinning disks. At first, this problem can be looked at experimentally. Then, by finding a good model for the constraint and considering the effect of geometrical nonlinear terms, the experimental results can be compared with numerical results.

6.3. References

- [1] Khorasany, R.M.H. and Hutton, S.G., 2010, “An Analytical Study on the Effect of Rigid Body Translational Degree of Freedom on the Vibration Characteristics of Elastically Constrained Rotating Disks,” *International Journal of Mechanical Sciences*, 52, pp. 1186-1192.
- [2] Khorasany, R.M.H. and Hutton, S.G., 2010, “The effect of axisymmetric non-flatness on the frequency response of a spinning disk”, *ASME Journal of Vibration and Acoustics*, 132, 051012, pp.1-8.

Appendix A.

$$\begin{aligned}
LWP_{1(mn)(pq)(uv)} &= \left[\int_{\eta}^1 \frac{\partial^2 R_{mn}^w(\lambda_{mn}^w r)}{\partial r^2} \left(\frac{1}{r} \frac{\partial R_{pq}^{\phi}(\lambda_{pq}^{\phi} r)}{\partial r} + \frac{-(p)^2}{r^2} R_{pq}^{\phi}(\lambda_{pq}^{\phi} r) \right) R_{uv}^w(\lambda_{uv}^w r) r dr + \right. \\
&\quad \left. \int_{\eta}^1 \frac{\partial^2 R_{pq}^{\phi}(\lambda_{pq}^{\phi} r)}{\partial r^2} \left(\frac{1}{r} \frac{\partial R_{mn}^w(\lambda_{mn}^w r)}{\partial r} + \frac{-(m)^2}{r^2} R_{mn}^w(\lambda_{mn}^w r) \right) R_{uv}^w(\lambda_{uv}^w r) r dr \right] \\
LWP_{2(mn)(pq)(uv)} &= -2mp \left[\int_{\eta}^1 \left(\left(\frac{1}{r} \frac{\partial R_{mn}^w(\lambda_{mn}^w r)}{\partial r} - \frac{1}{r^2} R_{mn}^w(\lambda_{mn}^w r) \right) \left(\frac{1}{r} \frac{\partial R_{pq}^{\phi}(\lambda_{pq}^{\phi} r)}{\partial r} - \frac{1}{r^2} R_{pq}^{\phi}(\lambda_{pq}^{\phi} r) \right) \right) R_{uv}^w(\lambda_{uv}^w r) r dr \right] \\
LWW_{1(mn)(pq)(uv)} &= \left[\int_{\eta}^1 2 \frac{\partial^2 R_{mn}^w(\lambda_{mn}^w r)}{\partial r^2} \left(\frac{1}{r} \frac{\partial R_{pq}^w(\lambda_{pq}^w r)}{\partial r} + \frac{-(p)^2}{r^2} R_{pq}^w(\lambda_{pq}^w r) \right) R_{uv}^{\phi}(\lambda_{uv}^{\phi} r) r dr \right] \\
LWW_{2(mn)(pq)(uv)} &= -2mp \left[\int_{\eta}^1 \left(\left(\frac{1}{r} \frac{\partial R_{mn}^w(\lambda_{mn}^w r)}{\partial r} - \frac{1}{r^2} R_{mn}^w(\lambda_{mn}^w r) \right) \left(\frac{1}{r} \frac{\partial R_{pq}^w(\lambda_{pq}^w r)}{\partial r} - \frac{1}{r^2} R_{pq}^w(\lambda_{pq}^w r) \right) \right) R_{uv}^{\phi}(\lambda_{uv}^{\phi} r) r dr \right] \\
Lwh_{(mn)(pq)} &= \delta_{mp} \pi \int_{\eta}^1 \left[\frac{\partial^2 R_{mn}^w(\lambda_{mn}^w r)}{\partial r^2} \frac{\partial \phi^h}{r \partial r} + \frac{\partial^2 \phi^h}{\partial r^2} \left(\frac{\partial R_{mn}^w(\lambda_{mn}^w r)}{r \partial r} - \frac{(m)^2}{r^2} R_{mn}^w(\lambda_{mn}^w r) \right) \right] R_{pq}^w(\lambda_{pq}^w r) r dr \\
Lwd_{(mn)(pq)} &= -\delta_{mp} \pi \Omega^2 \int_{\eta}^1 \frac{r^2}{2} \left[\frac{\partial^2 R_{mn}^w(\lambda_{mn}^w r)}{\partial r^2} + \frac{3}{r} \frac{\partial R_{mn}^w(\lambda_{mn}^w r)}{\partial r} - \frac{m^2}{r^2} R_{mn}^w(\lambda_{mn}^w r) \right] \\
I_{1mpu} &= \int_0^{2\pi} \sin(m\theta) \sin(p\theta) \sin(u\theta) d\theta & I_{2mpu} &= \int_0^{2\pi} \sin(m\theta) \cos(p\theta) \sin(u\theta) d\theta \\
I_{3mpu} &= \int_0^{2\pi} \cos(m\theta) \sin(p\theta) \sin(u\theta) d\theta & I_{4mpu} &= \int_0^{2\pi} \cos(m\theta) \cos(p\theta) \sin(u\theta) d\theta \\
I_{5mpu} &= \int_0^{2\pi} \sin(m\theta) \sin(p\theta) \cos(u\theta) d\theta & I_{6mpu} &= \int_0^{2\pi} \sin(m\theta) \cos(p\theta) \cos(u\theta) d\theta \\
I_{7mpu} &= \int_0^{2\pi} \cos(m\theta) \sin(p\theta) \cos(u\theta) d\theta & I_{8mpu} &= \int_0^{2\pi} \cos(m\theta) \cos(p\theta) \cos(u\theta) d\theta
\end{aligned}$$